The Orange Book

Dutch Neutron and
Muon Science 2000-2003

Colophon

Editorial for The Orange Book "Dutch Neutron and Muon Science 2000-2003"

What have Dutch scientists done with the neutrons that they have bought or begged over the past three years?

Rather more than just the pure physics that you might at first expect from what sounds a rather specialist technique. Indeed, this book illustrates that the range of science now being addressed with neutrons has become very broad: soft-condensed matter, solid-state physics, superconductivity, magnetism, materials science, chemistry, biology, and engineering. This work is not only of fundamental interest, but has applications in batteries, devices, recording materials, steel production, plastics, food, and energy for the future.

The contributions in this book are those in which neutron scattering (or muons) was the principle research tool, involving work by Dutch laboratories in the period 2000 to 2003. It should be remembered that neutron scattering often provides a vital supporting role in studies using other techniques, but that would be another book. It is a credit to Dutch scientists that six of the contributions in this book also appeared as highlights in the year-books of either ILL or ISIS.

Why use neutrons?

The advantage of neutron scattering, whether diffraction or spectroscopy, stems from three main characteristics. Perhaps the most obvious is that the neutron has a spin and can therefore be used to study structure and dynamics of magnetic materials. Structure and dynamics are unique with neutrons because at the wavelength corresponding to interatomic spacings, the neutron energy corresponds to thermal vibrations so that we can get the "structure of the dynamics". Unlike x-rays, the scattering cross-section of nuclei for neutrons varies almost randomly with atomic mass so that we can usually arrange to see light elements in the presence of heavy elements. Further, H and D have very different scattering cross-sections so that different parts of a system can be highlighted or suppressed. We give examples of these characteristics in this book.

Where do all these neutrons come from?

There are two approximately comparable world-top neutron sources, both of which are in Europe: ISIS in the UK and ILL in France. Dutch scientists bid for beam-time on the various instruments at these sources, and typically obtain a total of around 60 beam-days per year (even though we have no formal right of access to ILL). Many countries have a smaller national neutron source (Germany has four) that are often generally available through the Framework Programme 5 European initiative, although most mainly serve their national community. In the Netherlands, the de facto neutron scattering centre is at IRI, TUD.

What of the future?

Although the European Spallation Source has been delayed, the immediate future of neutron scattering is still bright with 150M€ being invested in a new target station at ISIS, a major instrument upgrade plan at ILL, and around 1500 M€ being invested in the USA and Japan on their new national neutron sources. Despite the modest size of our country, Dutch neutron scatterers already play an important role in these developments. The most recent instrumental development, spin-echo small-angle neutron scattering (SESANS) was devised and built at IRI using funds from the FOM. A version of this will be used for reflection at the new target at ISIS, and the Americans are also looking closely at the advantages of this machine.

How about muons?

Muons are available as a spin-off of the neutron production process ISIS (UK) and PSI (Switzerland) and for completion we include two highlights from muon work in this book. Muons not only provide the most sensitive magnetic probe available but can also be implanted in electron-rich regions of molecular systems to gain information on the dynamics of neighbouring species. A good example of this is provided in the diffusion of lithium in electrode materials as illustrated in this book.

DONUTS

NEUTRON-BAKERY

NEUTRON-BAKERY

COFFEE & DONUTS

RESTAURANT

CUISINE

-4020

HONG-FU

RES

FOO

020

Neutron scatterers buying from the neutron bakery

Contents

R.H. Tromp, NIZO
C.G. de Kruif, UU-FCC, NIZO

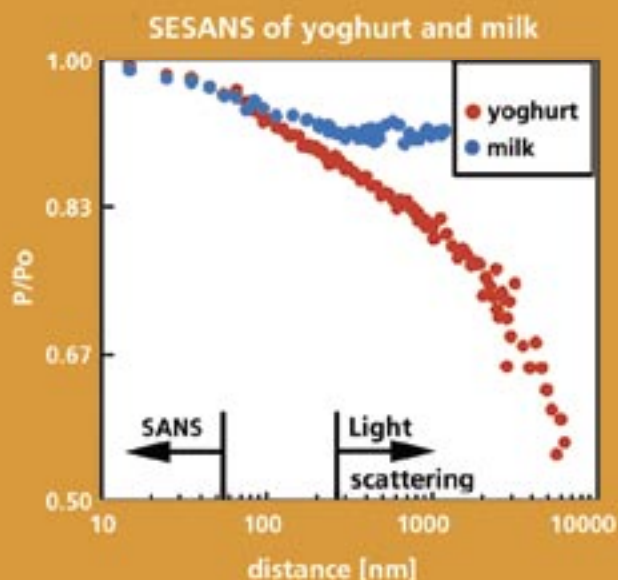# Neutron scattering in food research – some highlights

Figure 1
Preliminary result of SESANS (Spin-Echo SANS) applied on milk and yoghurt. The decline of the yoghurt signal up to long distances as compared to the levelling of of the milk data indicates structure in yoghurt which is absent in milk.
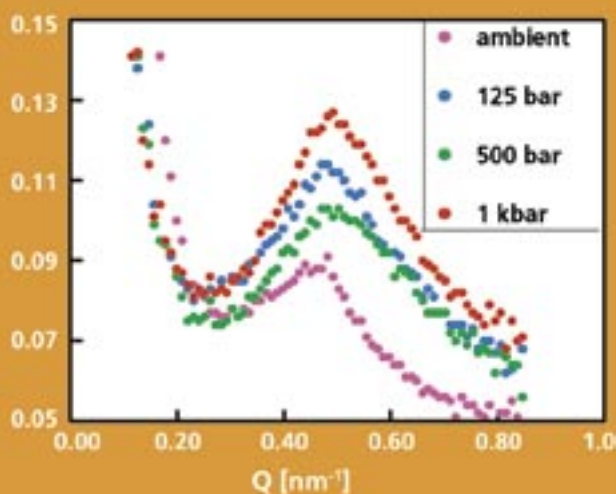

Figure 2
SANS of a 2% xanthan solution in D_2O at different pressures.

Macroscopic properties of foodstuffs, such as smearability and mouthfeel, are linked to the the structure on a nanometre to micron length scale. This length scale is accessible by small-angle neutron scattering. Here we will discus three examples. First, the structural difference between milk and yoghurt. Then, the structure of the thickener and stabiliser xanthan. And finally, the inner structure of a casein micelle, that contains the major part of protein (casein) and nearly all calcium in milk

What is the purpose of neutrons in food research? In general, the aim of SANS, the technique most commonly used, on food systems (for example milk, milk protein dispersions, thickeners and stabilisers) is to determine how different ingredients interact, and to find out the way they form structure on a nanometre and micron scale. This structure is important for macroscopic properties, such as pourability, smearability and mouthfeel (texture). Structuring mechanisms are for instance aggregation of proteins and complexation or segregation (phase separation) of proteins and polysaccharides.

In food research neutron scattering is of particular importance because of the high optical density of most food stuffs. This high optical density makes light scattering experiments unfeasible. Another reason for the use of neutron scattering, and in particular of SANS and SESANS, is the range of distances over which structural information can be obtained. SANS probes structural elements can be seen that are important for functionality and which are too small to be observable with light scattering. Examples are short helical strands and molecular proteins. SESANS is a very promising new development in small angle neutron scattering because the distance scale it probes overlaps with that of light scattering, and also cover the gap between classical SANS and light scattering (see Figure 1).

Below, two examples are treated of cases in which unique SANS properties were successfully applied on food systems: a food ingredient (xanthan) under high pressure and the substructure of casein micelles.

SANS, and in general neutron scattering is more than any other scattering technique suited to study systems under high pressure. This is because neutrons can penetrate the thick walls of the sample containers that are needed for high pressure experiments.

High pressure is an issue in food research because it offers an alternative for killing germs by heating. Pressurising in stead of heating is reported to result in fewer negative effects on taste. However, both the life supporting biomolecules of germs and food ingredients (polysaccharides and proteins) are biopolymers. Both

are therefore affected by high pressure. The texture, i.e. the degree of phase separation or aggregation may change on pressurising. An example of the effect of pressures up to 1000 bar (at which bacteria will start to suffer) on a xanthan solution is in Figure 2. Xanthan is a thickener and stabiliser often used in dressings. It forms extended (up to 1 micron) double helical stretches when the temperature is low enough and the salt concentration high enough. It turns out that also increased pressure enhances helix formation. Helix formation is indicated in this case by a scattering peak at about 0.5 nm^{-1}. This peak is associated with ordering of stiff, double-helical stretches. Macroscopically, increased helix formation will cause a higher viscosity of the product.

The major part of protein (casein) and nearly all calcium in milk is found in casein micelles. Casein micelles probably consist of submi-celles and calcium phosphate particles, kept together by physical forces. Figure 3 is an artist's impression.

The existence of an inner structure has long been a matter of debate. Neutron scattering combined with H/D substitution has brought a rather clear picture. Figure 4 shows the neutron scatter-ing pattern of casein micelles close to matching conditions (50% D_2O, match point 41% D_2O) Being close to the matching point of solvent and micelles renders the scattering very sensitive to fluctua-tions in the scattering density within the micelle. The feature at 0.35 nm^{-1} suggests a sub micelle size of about 20 nm. This is a clear example of the power of neutron scattering to reveal hidden structures, inaccessible to other (direct) techniques.

References:
[1] C. Holt, C.G. de Kruif, R. Tuinier, P.A. Timmins, Colloids and Surfaces A: Physicochem. Eng. Aspects **213**, 275 (2003).

1.1 BIOLOGY

Figure 3
Schematic drawing of a casein micelle.
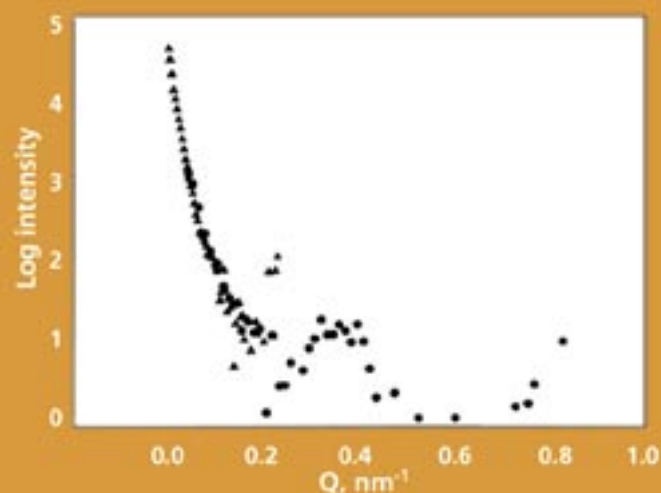**Diameter 50 to 200 nm.**

Figure 4
Scattering pattern of casein micelles close to conditions of index matching of solvent (water) and micelle [1].

**J.R.C. van der Maarel, S.S. Zakharova,
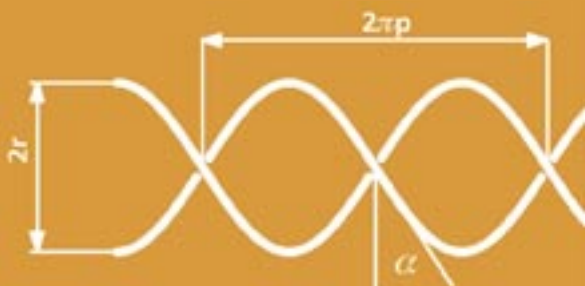W. Jesse, C. Backendorf, UL-LIC
S.U. Egelhaaf,   UE
A. Lapp, LLB**

Plectonemic structure of topologically constrained, supercoiled DNA

Figure 1
**Plectonemic helix with length *L*, radius *r*,
pitch *p* and opening angle α.**
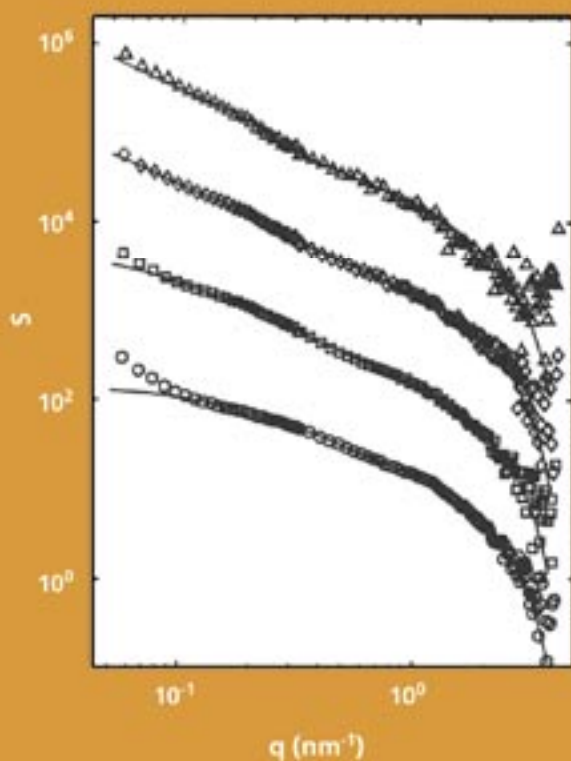
Figure 2
**Structure factor S vs momentum transfer q for 3
(▲), 6 (♦), 11 (■) and 27 (●) g DNA/dm^3 in 0.05 M
NaCl.**

Closed circular DNA usually exists in a supercoiled configuration, in which the duplex is wound around another part of the same molecule to form a higher order helix. Supercoiling is utilised in many cellular mechanisms. Here, we explore the extent to which supercoiling controls the compaction of pUC18 bacterial plasmid (2686 base pairs) in a liquid crystal [1,2]. For this purpose, the configuration of the superhelix is monitored with SANS through the phase transition.

The topological constraint is characterised by the linking number deficit ΔLk, which is the number of turns the duplex is turned before closure to form a ring. ΔLk is conserved and is distributed among writhe *Wr* and excess twist ΔTw exerted on the duplex according to $\Delta Lk = Wr + \Delta Tw$. For a right-handed, regular supercoil without end loops, *Wr* is proportional to the number of crossings *n* when viewed perpendicular to the superhelical axis $Wr = -n\sin\alpha$, with the pitch angle α as in Figure 1. It is convenient to define the normalized length *2L/l*, with *l* being the length of the DNA molecule. From integration along the contour and by neglecting the end loops one can derive that the local structure of the superhelix is fully characterised by *p* and *r*. These parameters determine α, *Wr* and *2L/l*.

In our experiments, the range of momentum transfer *q* exceeds L^{-1} by at least an order of magnitude. In this high *q*-range, the scattering is sensitive to interference over an extent of the order of *r* and *p* and effects of overall flexibility and/or branching of the supercoil are beyond observation. We can accordingly use the high-*q* approximate form of the form factor of a regular superhelix [1] which is sensitive to the DNA density per unit length projected on the superhelical axis L^{-1}. However, for $qr \gg 1$ and $qp \ll 1$ the scattering is essentially given by a single strand of the superhelix, which is proportional to the density per unit contour length l^{-1}. In both regimes, the form factor displays the characteristic q^{-1} scaling for rodlike particles, but the prefactor drops from L^{-1} to l^{-1}. Our data (Figure 2) however do not comply with such idealised structure as depicted in Figure 1. Accordingly, we have assumed a Gaussian distribution in *r* with standard deviation σ_r. It is also assumed that α is constant, which implies that *p* is proportional to *r*. Interactions among supercoils are accounted for in the second virial approximation and the total scattering function takes hence depends on *N* the number of bases, A_2 the second virial coefficient and ρ the DNA density.

Due to the presence of a significant distribution in r and p, the structure factors do not exhibit strong oscillatory behaviour. They do show however, the anticipated q^{-1} scaling and the drop in prefactor from L^{-1} to l^{-1} with increasing q.

The plectonemic structure is most clearly demonstrated in Figure 3, where the structure factors are normalised in a way that they go to unity at high q. The normalised structure factor extrapolates to $2l/L$ for $q \rightarrow 0$ and in the absence of interactions. In the fit procedure, we have optimized r, its distribution width σ_r, α and A_2. Results are given in Table 1. The other parameters are derived with their topological constraints mentioned above and standard variance propagation. Note that the margins are not related to error, but rather to variation in molecular shape.

With increasing concentration through the phase transition, r and p are seen to decrease significantly. Because of the (near) constancy of α, Wr decreases and the number of superhelical turns increases ($Wr = -n\sin\alpha$). According to the fact that the sum of the excess twist and the writhe are conserved, this decrease in Wr should be compensated by a positive twist exerted on the duplex if ΔLk is conserved. Apart from the change in physical size of the supercoil, the associated increase in molecular free energy is of great importance in controlling the phase boundaries.

References:
[1] S.S. Zakharova , W. Jesse, C. Backendorf, S.U. Egelhaaf, A. Lapp, J.R.C. van der Maarel, Biophys. J. **83**, 1106 (2002).
[2] S.S. Zakharova, W. Jesse, C. Backendorf, J.R.C. van der Maarel, Biophys. J. **83**, 1119 (2002).

1.2 BIOLOGY
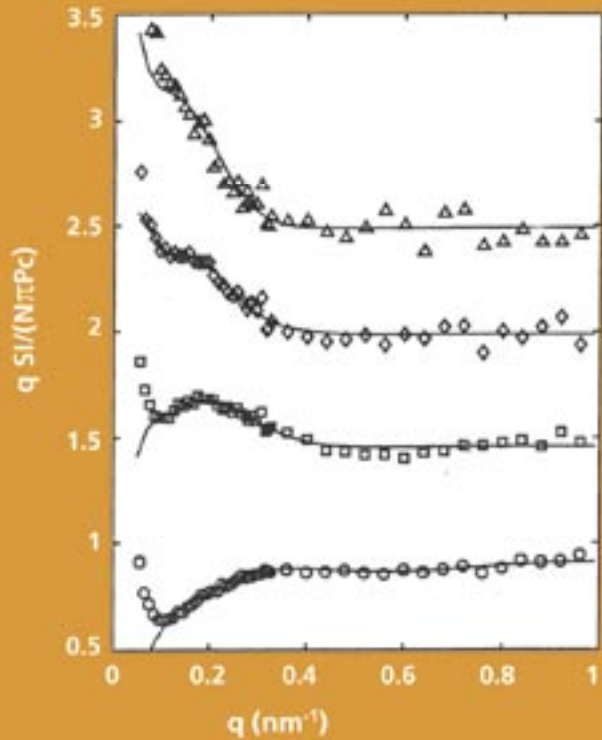
Figure 3
As in Figure 2, but for the normalised structure factor. Lines represent a fit with parameters in table 1. To avoid overlap the data are shifted along the y-axis.

c (g/dm^3)	r (nm)	p (nm)	α (°)	$2L/l$	Wr	A_2 (10^6 nm^3)
3	10±4	21±9	65	0.91	-6±3	–
6	9±5	14±7	57	0.84	-7±4	0.55
11	8±4	13±7	59	0.86	-9±5	1.22
27	5±3	6±4	52	0.79	-14±10	1.92

Table 1
Parameters resulting from the fit of the structure factor to the scattering data. Note that the margins are related to a variation in molecular shape.

H.J. Snijder, CUT
B.W. Dijkstra, RUG-BIOSON

Detergent organisation in crystals of a membrane protein
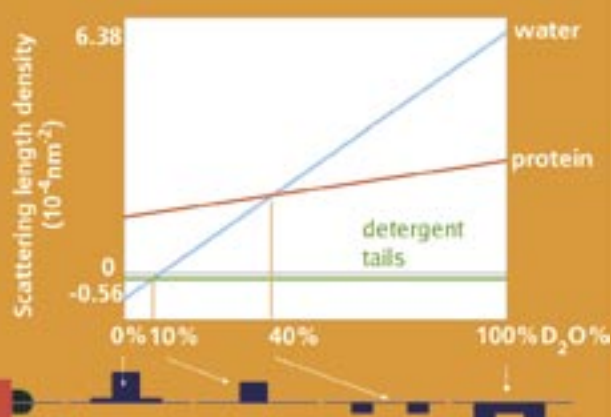
Figure 1
Representation of contrast variation in a system containing water, protein and hydrophobic detergent regions. The upper part shows the scattering length density as a function of the D_2O content of the surrounding solvent. The lower part illustrates the effect of contrast variation on scattering length density maps. From left to right, schematic views are presented of a protein surrounded by an idealised detergent micelle, and scattering length density maps at 0%, 10%, 40% and 100% D_2O, respectively. The scattering of the detergent equals that of the solvent at 10% D_2O and only protein regions can be observed. At 40% D_2O, scattering of the protein is matched out and only the detergent regions have contrast, albeit negative. Finally, at 100% D_2O, both protein and detergent have negative contrast with respect to the solvent.

Membrane proteins present one of the major current challenges for structural biology. In particular, obtaining well diffracting crystals of such proteins is often a formidable problem. This is caused by the amphiphilic nature of the surface of a membrane protein, which dictates the need for detergents to dissolve the protein. In turn, these detergents need to be accommodated in the crystal lattice without adversely affecting the packing of the protein molecules in the crystal lattice. To understand the factors that govern membrane protein crystallisation, we determined the structure of the detergent micelle in crystals of outer membrane phospholipase A by neutron diffraction contrast variation. The hydrophobic surface of the protein molecules is covered by a ring-shaped detergent micelle, which is fused to neighbouring rings to form a continuous phase throughout the crystal. These results indicate a crucial role for detergent coalescence during crystal formation. In addition, our findings shed light on the interaction between membrane proteins and their amphiphilic environment.

The world-wide effort put into membrane protein research contrasts sharply with the number of membrane proteins whose structures have successfully been determined to near-atomic resolution. This lack of structural information is at least partly related to difficulties in obtaining suitable crystals of membrane proteins. For structural studies, detergents are generally required to dissolve membrane proteins from their natural membranes. The detergent-protein complexes are subjected to crystallisation and both protein and detergent need to be accommodated in the crystal lattice. However, the detergent surface supplies few specific interactions that may lead to crystal contacts. Analyses of packing of detergent and membrane proteins in crystals can contribute to the understanding of the factors that govern membrane protein crystallisation and thus may help to rationalise the quest for diffraction quality crystals. Additionally, since the amphiphilic detergent micelles mimic the lipid membrane, elucidation of the detergent organisation can give clues on the interaction of the membrane protein with its natural environment.

The system that we study, Outer Membrane Phospholipase A (OMPLA), is an integral membrane enzyme, which is activated by dimerisation under the influence of membrane perturbations. The amino acid residues essential for dimerisation, activity and catalysis are surface located [1]. The extent to which these residues are exposed to aqueous solvent or hydrophobic detergent can, however, not be determined without knowledge of the detergent organization. Protein X-ray crystallography is an unsuitable technique to establish the detergent organisation, owing to the fluidity of the detergent molecules and their low X-ray contrast. On the contrary, neutron diffraction combined with D_2O/H_2O contrast variation

allows the study of such partially ordered systems [2,3]. Therefore, single crystal neutron diffraction experiments were carried out on DB21 at ILL, Grenoble to elucidate the organisation of the β-octylglucoside (β-OG) detergent phase in crystals of monomeric OMPLA [4].

The different chemical composition of the components in the crystal (e.g. protein, solvent and detergent) causes specific scattering-length density variations for each component in a specific way (Figure 1). These variations can be exploited to obtain structural information on each of these components, including the detergent region. Large single crystals of OMPLA were soaked in stabilising solutions containing different D_2O/H_2O ratios. Diffraction data were collected for five contrast ratios (0, 14.5, 33.0, 46.8, and 61.2% D_2O) to a resolution of approximately 1.2 nm. Figure 2 shows the neutron scattering density map at 40% D_2O contoured to highlight the detergent. The detergent occupies approximately 10% of the volume and forms a band that encircles the protein covering the exposed hydrophobic outer surface of the β-barrel. The detergent ring is intimately connected to neighbouring rings thus forming a continuous network of detergent that extends throughout the whole crystal. The thickness of the ring parallel to the protein barrel varies considerably from 1.5 – 2.0 nm to regions as thin as 0.7 – 0.8 nm, considerably smaller than the thickness of the hydrophobic region in a typical lipid bilayer. The functional dimerisation interface is covered by a large disc-like detergent region, which corroborates that OMPLA may be accommodated in the membrane as a monomeric unit. However, the detergent density is particularly weak near an exposed polar patch on the (further mostly hydrophobic) dimerisation interface indicating that burying this patch in an enzyme dimer may be favourable. In the crystal the protein molecules are packed in an intricate three-dimensional lattice formed by both hydrophobic and polar contacts. The continuous detergent network and the hydrophobic crystal contacts suggest that during crystallisation OMPLA molecules approach each other closely and that merging of their detergent belts occurs. The formation of polar crystal contacts may drive the crystallisation and induce the merging of micelles after which detergent molecules are expelled to allow hydrophobic crystal contacts. The polar crystal contacts can not drive the fusion of micelles in this particular case, which suggests that the detergent belts themselves have a tendency to coalesce.

In summary, we have succeeded in elucidating the structure of the detergent associated with a membrane protein, showing crucial roles for detergent in crystal packing and formation. Moreover, knowledge of detergent micelles sheds light on the interaction of membrane proteins with their membrane environment, which is instrumental for understanding membrane protein function.

References:
[1] H.J. Snijder, I. Ubarretxena-Belandia, M. Blaauw, K.H. Kalk, H.M. Verheij, M.R. Egmond, N. Dekker, B.W. Dijkstra, Nature **401**, 717 (1999)

[2] M. Roth, A. Lewit-Bentley, H. Michel, J. Deisenhofer, R. Huber, D. Oesterhelt, Nature **340**, 659 (1989)

[3] P.A. Timmins, E. Pebay-Peyroula, W. Welte, Biophys. Chem. **53**, 27 (1994)

[4] H.J. Snijder, P.A. Timmins, K.H. Kalk, B.W. Dijkstra, J. Struct. Biol. **141**, 122 (2003)

1.3 BIOLOGY

Figure 2
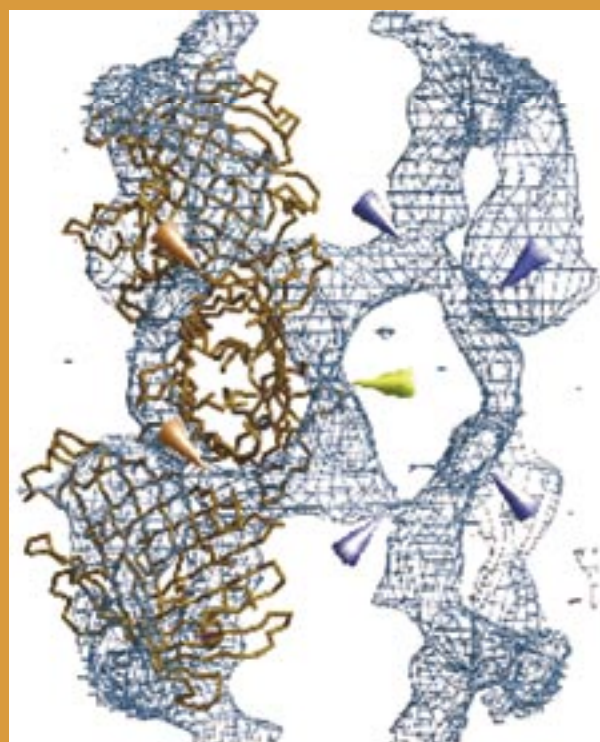**Detergent structure in OMPLA crystals. The final neutron scattering length map is contoured to highlight the 10% volume occupied by the hydrophobic parts of the detergent. Three protein molecules are displayed as C_{alpha} traces. Arrows highlight the dimerization face (yellow), hydrophobic crystal contacts (orange) and regions where detergent rings are fused to form a continuous network (violet).**
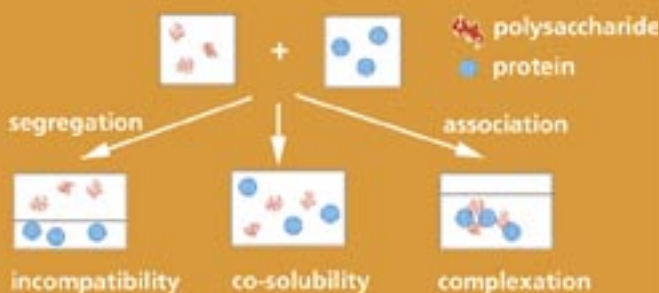
R. Tuinier, FZ Jülich
C.G. de Kruif, NIZO/UU-FCC

Figure 1
**Main trends in the behavior of protein/
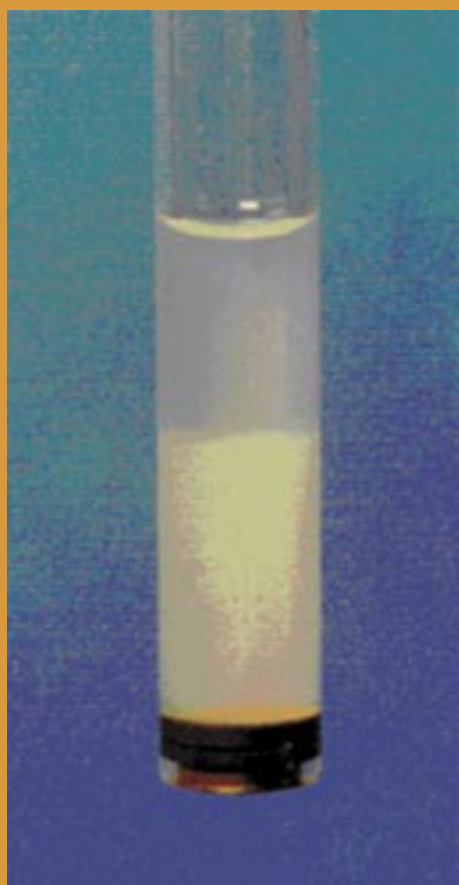polysaccharide mixtures.**

Figure 2
**A phase separated EPS/whey protein
mixture.**

Segregative interaction in a whey protein/ exocellular polysaccharide dispersion as measured with SANS

**Using small-angle neutron scattering (SANS) we measured the
effects of a depletion interaction between aggregated whey
protein colloids (AWCs) as induced by non-adsorbing exocellular
polysaccharides (EPSs). We present the phase diagram of EPS/AWC
mixtures and discuss the measured scattered intensities in compari-
son with theoretical predictions. SANS provides an excellent way to
analyse colloidal interactions in a concentrated biocolloidal system.**

Many systems in our daily life and in biology such as food
and the living cell consist of liquid dispersions crowded with
biopolymers [1,2]. When globular protein particles are mixed with
polysaccharides the interaction between them is either segregative
(the biopolymers repel each other and are denoted as incompatible)
or associative (the biopolymers attract one another) [3]. In case
of associative interaction, oppositely charged biopolymers form
complexes due to electrostatic interaction. When the polysaccha-
rides are uncharged or above the isolectric pH of the proteins, the
proteins and polysaccharides tend to segregate [1,2]. In the case of
segregative interaction also a phase separation occurs but now the
biopolymers are concentrated in separate phases, due to depletion
interaction [4]. Exceeding a certain polymer concentration leads to
a phase separation into a protein-enriched and a polysaccharide-
enriched phase. The main trends of mixing polysaccharides and
proteins are (highly) schematically illustrated in Figure 1.

Yogurt, but notably also other fermented milk products, consist of
a dispersion of aggregated casein micelles, and contain exocellular
polysaccharides (EPS) produced by a range of (food grade) micro-
organisms, such as lactic acid bacteria. The EPSs have a significant
influence on the rheological properties of fermented milk
products [5,6]. As such the mixtures of EPS and milk proteins makes
the product a natural example of a biopolymer mixture containing
polysaccharides and proteins. In several studies we have shown that
segregative or depletion interaction leads to an effective attraction
between casein micelles, whey protein particles [7], and oil droplets
covered with whey proteins, as induced by an exocellular polysac-
charide produced by the lactic acid bacterium *Lactococcus lactis*
subsp. *cremoris* strain NIZO B40 [8].
Here we show how SANS experiments helped us to measure deple-
tion interaction between (aggregated) whey protein colloids (AWCs)
and the EPS. The EPS used can be described as a random coil polymer
with a radius of gyration of 86 nm and a small polydispersity [8]. The
AWC particles can be viewed as hard sphere colloids. Upon increas-
ing either the EPS or the AWC concentration phase separation will
occur, see Figure 2. The observed phase diagram of EPS/AWC mix-
tures in aqueous solutions with 0.10 M salt is given in Figure 3. The
EPS concentration c is normalised with the overlap concentration c*
being 0.92 g/L [8]. The protein content is given as the effective AWC

volume fraction. Just above the phase boundary we recognised a two-phase system [7]. This phase diagram is relatively difficult to describe theoretically in a quantitative fashion. Even when neglecting the effects of charges on EPS and protein particles (they are supposed to be largely screened at 0.1 M salt) one deals with a polymer-colloid mixtures where the effective segment size (17 nm) is significant compared to the sphere radius (30 nm). Moreover, EPS B40 behaves as a chain with an excluded volume in a good solvent. The critical point of the phase diagram is estimated from the relative phase volumes. The location of the critical point at ϕ=0.235, as well as the value of the polymer concentration of the binodal curve are consistent with recent computer simulation results of the full many body system of hard spheres and self-avoiding polymer chains [9] (compare with q=3.86 in Figure 2 [9]). This confirms the idea that a depletion interaction was responsible for demixing of the EPS/AWC mixture. Using SANS it is possible to show whether attractive or repulsive interactions occur in colloidal dispersions. Classical light scattering could not be used because the solutions are far too turbid. Experimental results for ϕ_{AWC}=0.21 are plotted in Figure 4. The quantity $I_0(Q)$ refers to the scattered intensity of the AWCs (without EPS) and $I(Q)$ is the scattered intensity of the mixture of AWCs and EPS. The scattering of the AWCs was found to be more than a magnitude larger than the scattering of the EPSs. Therefore the total scattered intensity could be approximated as being the scattered intensity of the AWCs but with an additional interaction due to the presence of the EPSs. Since the scattering intensity $I(Q)/I_0(Q)$ equals $S(Q)/S_0(Q)$ (where $S_0(Q)$ is the structure factor of AWC without EPS). In the limit $Q{\to}0$, the structure factor $S(Q)$ is directly related to the osmotic compressibility $\partial\rho/\partial\prod$, where ρ is the number of particles per volume and $\prod$ is the osmotic pressure. In the case of increasing attraction, $\partial\rho/\partial\prod$ decreases and vanishes at the spinodal. Hence an increase in $S(0)$, reflects an increase in attraction. The quantity $I(Q)/I_0(Q){\approx}S(Q)/S_0(Q)$ thus only deviates from unity due to interactions between the proteins induced by the added EPSs. Indeed from the curves in Figure 4 we observe at small Q an increase of the structure factor with increasing EPS concentration. The full curves are a theoretical description of the data [7]. Mixing aggregated whey protein colloids (AWCs) with exocellular polysaccharides leads to a segregative interaction. Upon exceeding a certain concentration of both components the system phase separates.

References:

[1] V.Ya. Grinberg, Tolstoguzov, V.B., Food Hydrocoll **11**, 145, (1997).

[2] J.-L. Doublier, Garnier C., Renard, C., Sanchez, C., Curr. Opin. Coll. Int. Sci. **5**, 184, (2000).

[3] H. G. Bungenberg de Jong, In *Colloid Science*; ed. Kruyt, H. R., **Vol. 2.** (1949).

[4] D. Frenkel, Physica A **313**, 1 (2002).

[5] M.E. Marle, van, van den Ende, D., de Kruif, C.G., Mellema, J., J. Rheology, **43**, 1643, (1999).

[6] P. Ruas-Madiedo, Tuinier, R., Kanning, M., Zoon, P., Int. Dairy J. **12**, 689 (2002).

[7] R. Tuinier, Dhont, J.K.G., de Kruif, C.G., Langmuir **16**, 1497 (2000).

[8] R. Tuinier, 'An exocellular polysaccharide and its interaction with proteins', Ph.D. thesis Wageningen University (1999)

[9] P.G. Bolhuis, Louis, A.A., Meijer, E.J., Phys. Rev. Lett. **90**, 068304 (2003).

1.4 BIOLOGY
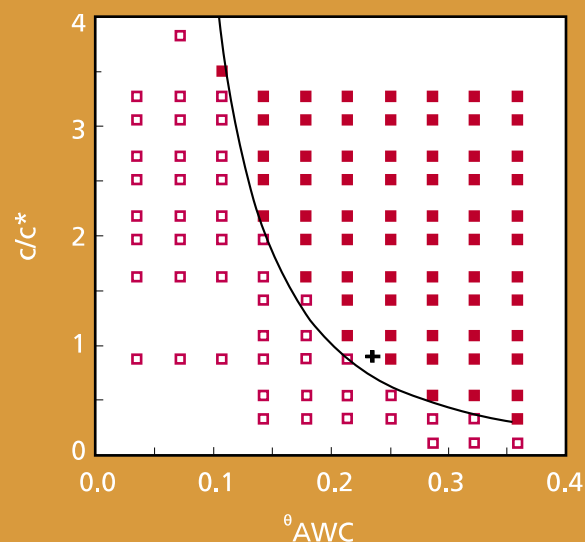
Figure 3
Phase diagram as obtained from visual observation. The polymer concentration c/c* is given as a function of the AWC volume fraction. The drawn line sketches the binodal curve based on the experimental data points; open symbols refer to stable mixtures and closed symbols phase separated systems. The estimated critical point is indicated as the cross.
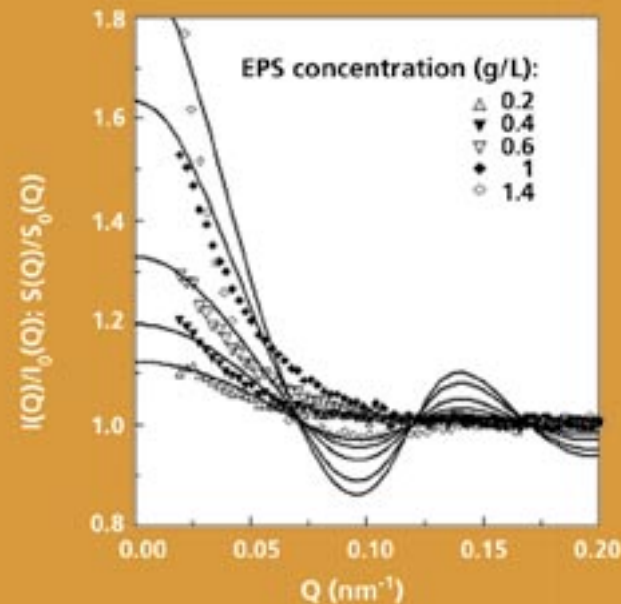
Figure 4
The relative scattered intensity $I(Q)/I_0(Q)$ as measured by SANS for ϕ=0.21 (30 g/L) AWC. Results are given for EPS concentrations of 0.2, 0.4, 0.6, 1.0 and 1.4 g/L. The full curves are theoretical predictions as described in reference 7.

C. Ohms, A.G. Youtsos, JRC

Measurements of residual stresses by neutron diffraction
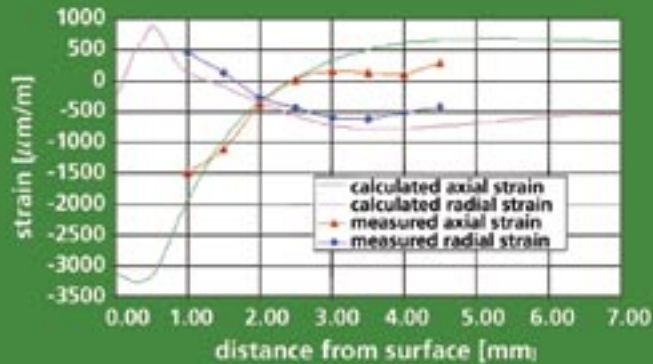
Figure 1
Radial and axial strains in a deep rolled and induction hardened crankshaft section; experimental results obtained at the HFR, numerical data courtesy of Volkswagen AG.

Figure 2
Component set-up for measurements in the hoop.

At the High Flux Reactor in Petten neutron scattering is used to measure residual stresses in industrial components and composite materials. The method is applicable to a wide range of engineering problems. We will present examples in the field of surface treatment, welding and cladding.

At the High Flux Reactor (HFR) of the Joint Research Centre of the European Commission in Petten neutron scattering is used to measure residual stresses in industrial components and composite materials. This engineering application of neutron diffraction is based on Bragg scattering. Hereby changes in lattice spacing, caused by the stresses under investigation, are determined through measuring the corresponding changes in the neutron scattering angle. Two facilities are av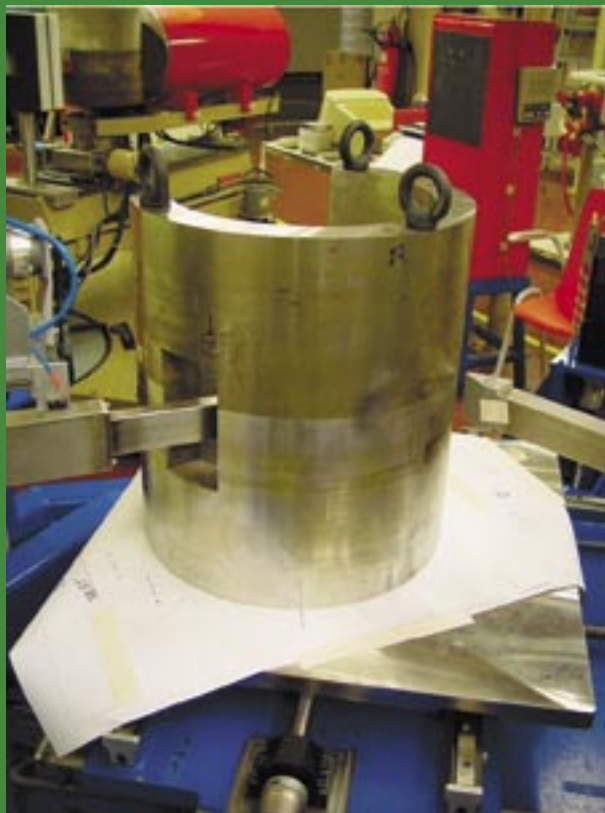ailable for residual stress measurements, and one of these facilities is capable of mapping residual stresses in heavy industrial components of up to 1000 kg.

The method is applicable to a wide range of problems, which include for instance residual stresses due to welding, thermal or mechanical treatments, mismatch of thermo-mechanical properties of the constituents of composite materials, clad or coated components or dissimilar metal welds. At the HFR the focus of the investigations has recently been on welding residual stresses in components relevant to power production systems, but automotive and aerospace applications and certain composite materials have been studied as well. Some examples will be presented.

For many mechanical applications it is desirable that components or particular parts of them exhibit compressive residual stresses in the surface region. Such stresses would prevent surface cracks from opening further or counteract tensile stresses eventually applied to a component by normal service loads.

There are a number of methods for introducing such compressive stresses into surfaces, e.g. shot peening, rolling, induction hardening or thermal methods, like shock quenching. Stresses are introduced through different mechanisms, like plastic deformation, chemical composition or microstructure gradients close to the surface.

The impact of such treatments is given here through the example of a crankshaft section that had been treated by localised rolling and induction hardening. Due to the particular shape and size of the test piece measurements could be obtained in the specimen

radial and axial directions at the HFR, based on a $2 \times 2 \times 2$ mm^3 gauge volume. Figure 1 shows the residual strains measured in these two directions compared against numerical results provided by Volkswagen AG – Central Laboratories. A very good agreement between the neutron scattering measurements and theoretical predictions has been achieved.

An application of relevance to nuclear power production is dissimilar metal welding, by which – for example – a pressure vessel of a power plant, made from ferritic steel, is connected to the primary piping system, made from austenitic steel. Apart from welding stresses, which can to a significant degree be relieved through thermal treatments, in this case there is the mismatch of the thermo-mechanical properties causing residual stresses.

The example given here is a full-scale mock-up of such an application, which constituted a tube of 453 mm diameter and 51 mm wall thickness. The component weighed about 250 kg. Stresses have been mapped throughout the weld pool and the heat affected zones of the ferritic and austenitic materials. Figure 2 shows the test set-up for measurements in the component hoop direction, and in Figure 3 hoop residual stresses derived are shown together with numerical results obtained at JRC based on a simplified model. In the case shown, the agreement of measurement and prediction is excellent. This agreement has not yet been achieved for all available data. More detailed simulations are ongoing.

Another problem investigated at the HFR facilities were residual stresses in a ferritic steel block clad by three welded layers of austenitic steel totaling 10 mm in thickness. This would be a typical application in a reactor pressure vessel, made from ferritic steel and protected against corrosion by an austenitic cladding.

This component had to be reduced to 25 mm in thickness at the test location in order to make 3-dimensional measurements by neutron diffraction, using a small gauge volume, feasible. Stresses were then measured along a line across the cladding substrate interface. In this case it became clear that the cutting of the component altered the original residual stress field. Investigations performed by the Helsinki University of Technology and the University of Bristol based on the original component yielded a different stress distribution in particular in the ferritic part.

Figure 4 shows the welding longitudinal stresses derived from the measurement. A sharp transition from tensile (cladding) to compressive (substrate) stresses at the interface is apparent.

References:

[1]   A.G. Youstos, C. Ohms, ECRS5, Proceedings of the fifth European Conference on Residual Stresses Materials Science Forum **347**, 524 (2000).

[2]   C.Ohms, A.g. Youstos, P. van der Idsert and T. Timke, ECRS5, Proceedings of the fifth European Conference on Residual Stresses Materials Science Forum **347**, 658 (2000).

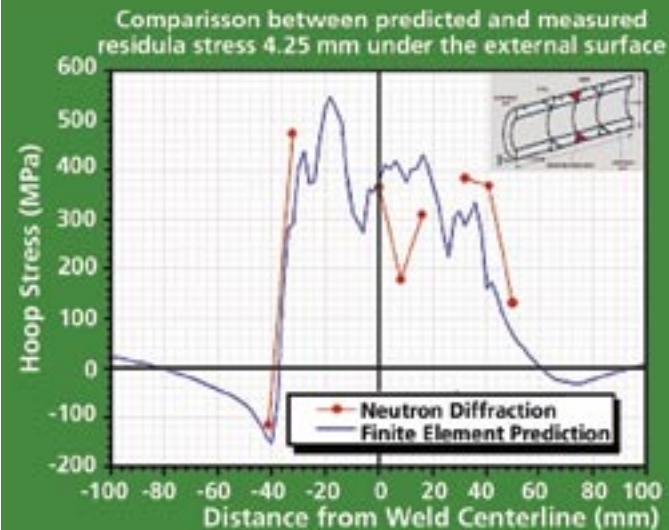## 2.1 ENGINEERING

Figure 3
Numerically and experimentally determined hoop residual stresses close to components.
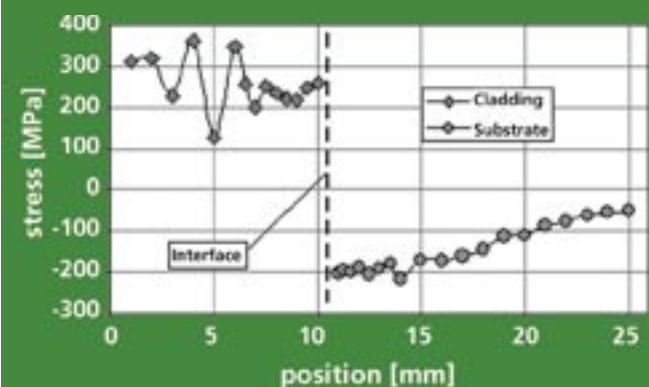

Figure 4
Welding longitudinal stresses measured at the HFR in cladding and substrate of a clad steel component.

3.1 INSTRUMENTATION

W.G. Bouwman, T.V. Krouglov, J. Plomp, S.V. Grigoriev, W.H. Kraan and M.Th. Rekveldt, IRI-TUD

Development of a novel high resolution scattering technique: Spin-echo small-angle neutron scattering

Figure 1
A schematic side view of the centre of the SESANS-setup. The areas shaded in grey indicate the regions where the neutron polarisation precesses. Each foil, indicated with a white bar, effectively reverses the precession direction. So the light and dark areas indicate the sign of the precession. In the diagram the sample is positioned in the centre of the set-up. In practice it is sometimes also set between the last two magnets to scan the spin-echo length z. Then the distance between the sample and the centre of the last precession device determines the spin-echo length. In the centre of the set-up the magnetic fields reverse to create a spin-echo situation. Unscattered neutrons experience spin-echo, independent of the incoming angle, since it is equal to that of the outgoing angle. Scattered neutrons, indicated with the dotted arrow, will experience a nett precession that is linearly dependent on the vertical scattering angle θ.

Spin-echo small-angle neutron scattering (SESANS) is a new efficient method to measure particle sizes in real space. It uses Larmor precession of polarised neutrons and the spin-echo principle to achieve a high resolution without the usual loss of intensity. The structure can be determined over three orders of magnitude in length scale, from 10 nm to 10 μm, which is a order of magnitude larger than conventional small-angle neutron scattering (SANS). These properties make SESANS a new powerful tool in the study of structural properties of materials.

Traditional small-angle neutrons scattering (SANS) using pin-hole geometry has proved itself to be a versatile and efficient tool for measuring the form factors of dilute suspensions of mesoscopic particles. Among the very few disadvantages of traditional SANS is the fact that scattering from large particles tends to be indistinguishable from the neutron beam that passes through the experimental sample without being deviated. To separate the two requires the use of small samples, high resolution 2-D detectors and long neutron flight paths, each of which decreases the measured neutron intensity. Spin-echo SANS (SESANS) has been invented [1-3] as a means to overcome this disadvantage. The technique uses the usual principles of neutron spin echo to code the scattering angle of the neutron in a way that is independent of the collimation of the neutron beam, thus breaking the inverse relationship between measured intensity and resolution that plagues conventional SANS. The method is based on the Larmor precession of polarised neutrons in magnetic fields with inclined faces. The precession encodes the direction of the neutron trajectory. Finally, the measured polarisation is a Fourier transform of the scattering cross-section and thus closely related to the scattering length density correlation function [1,4]. This facilitates the direct interpretation of measurements. In Delft we have built the first dedicated SESANS-instrument that can measure up to length scales of 10 nm to 10 μm.

The basic principle of SESANS and related Larmor techniques to measure elastic scattering is to create precession in regions with tilted interfaces [2]. The polarisation of neutrons in a magnetic field process proportional to the wavelength, magnetic field and path length through this field. This way it is possible to obtain a direct relation between the vertical component of the wave vector momentum transfer and the precession angle. The sensitivity can be tuned with the applied magnetic field, the wavelength, the length of the setup and the tilt angle of the interfaces. All these parameters can be combined into a single parameter, the spin-echo length z, which is on the one hand an experimental scan parameter and on the other hand the length cord between two scattering volumes in the sample. This is the parameter that is shown in SESANS measurements on the horizontal axis.

A schematic view of the main part of the setup is depicted in Figure 1. A very effective method to build such precession devices like these is using π-flipping foils which effectively reverse the precession direction [5]. Therefore the precession in the magnetic field before and behind the foil have opposite signs. These foils have some great advantages in building the setup: Inhomogeneities at one side of a magnet is directly compensated at the other side, leading to a higher polarisation. The other advantage is that the interface tilt angle is rather large, yielding a very high spin echo length at moderate magnetic fields and length of the setup. This has greatly extended our application range compared to earlier setups [6]. This way spin-echo length's up to 10 μm can be measured.

In practice one can not measure the precession angle directly, but one measures the polarisation P of the beam, normalised with the polarisation of the instrument without a sample P0, which is a cosine of the precession angle which has to be averaged with the differential scattering cross section which gives the so-called SESANS correlation function. This SESANS correlation function is a projection of density autocorrelation function along the axis parallel to the neutron beam [4]. This allows us to calculate the SESANS correlation function directly from the real space and vice versa.

The first quantitative calibration of the method was a measurement on a dilute dispersion of well characterised polystyrene spheres, which showed that the method indeed measures in the way it was calculated [3]. Both the amount of scattering and the shape of the signal fitted the calculation based on the composition of the sample. The measurement illustrates that the signal is what you would expect for the autocorrelation function of a sphere with a maximum length of 200 nm.

The first applications of SESANS in colloid science and food science are in other contributions in this edition by Krouglov and Tromp, respectively. We expect many more applications for the technique in colloidal science, food materials, polymers, composite materials and metals.

References:

[1] M.Th. Rekveldt, Nucl. Instr. & Methods in Phys. Res. B **114**, 366 (1996).

[2] M.Th. Rekveldt, W. G. Bouwman, W. H. Kraan, O. Uca, S. Grigoriev, S.Habicht, T. Keller, Neutron Spin Echo, Vol. **601** of Lecture Notes in Physics, Springer, Berlin, 87-99 (2003).

[3] W. G. Bouwman, O. Uca, S. V. Grigoriev, W. H. Kraan, J. Plomp, M.Th. Rekveldt, J. Appl. Phys. A **74**, S115 (2002).

[4] T. Krouglov, I. M. de Schepper, W. G. Bouwman, M. T. Rekveldt, Journal of Applied Crystallography **36**, 117 (2003).

[5] W. H. Kraan, J. Plomp, T. V. Krouglov, W. G. Bouwman, M. Rekveldt, Physica B **335**, 247 (2003).

[6] M.Th. Rekveldt, W. Bouwman, W. Kraan, O. Uca, S. Grigoriev, R. Kreuger, Neutron Spin Echo, Vol. **60**1 of Lecture Notes in Physics, Springer, Berlin, 100-115 (2003).

3.1 INSTRUMENTATION

Figure 2
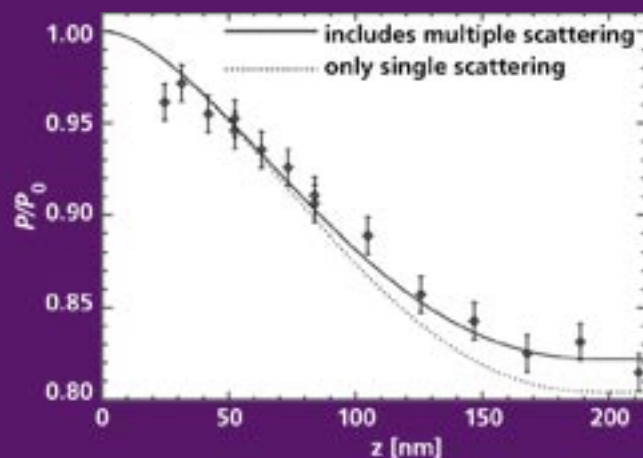**Photograph of the SESANS instrument built in Delft.**

Figure 3
The symbols present the SESANS-signal of a dilute suspension of mono-disperse polystyrene spheres with a radius of 100 nm. The drawn line is the calculated signal including multiple scattering with the known composition of the solution. The dotted line was calculated assuming only single scattering.

**C.W.E. van Eijk, A. Bessière,
C.M. Combes, P. Dorenbos,
J.T.M. de Haas, R.W. Hollander,
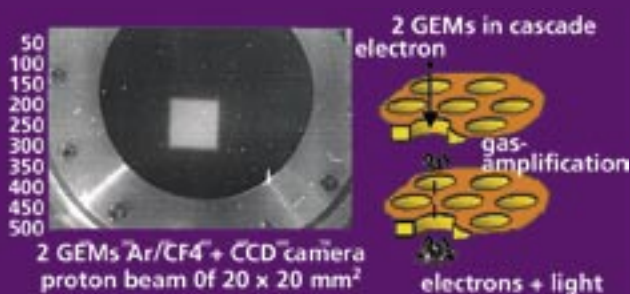R. Kreuger, T. van Vuure,
IRI-TUD**

Figure 1
Application of GEMs (schematic right) in combination with a CCD camera (not shown) to observe a proton beam (photo left, cross section 20 x 20 mm^2) through a detector window. The beam is coming towards the viewer. In fact we look at the bottom of the GEMs on the right. The same method can be employed for neutron detection.
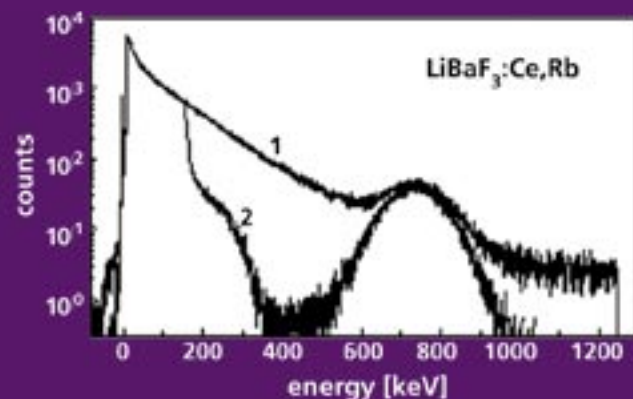

Figure 2
Pulse height spectrum of a mixed neutron-gamma field emitted by a Pu-Be source shielded with paraffine and 6 cm of lead, recorded with a LiBaF$_3$:Ce,Rb scintillation crystal. #1 shows the spectrum of the mixed field with a gamma continuum and a neutron bump on top at ~ 750 keV. #2 shows the same spectrum, however with pulse shape discrimination on, i.e. requiring absence of CVL. The neutron peak at 750 keV gamma-equivalent energy is almost free from gamma background. Thus excellent thermal neutron sensitivity can be obtained with full gamma-ray background suppression.

Thermal neutron detection – novel concepts

Innovative development in thermal-neutron detection in necessary to meet the ever increasing demands concerning count rate, spatial resolution and costs. Three novel concepts developed at the Delft University of Technology are briefly reviewed: Gas Electron Multipliers, inorganic scintillators, and scintillator-silicon well detectors.

For neutron detection in neutron scattering experiments at the intense neutron spallation sources that are under construction, i.e. SNS (Oak Ridge, USA) and JSNS, the Japanese spallation source, new detector concepts have to be developed. Furthermore, for neutron detection in experiments at neutron sources currently in operation, such as ISIS and ILL, improvement of efficiency and position resolution is required. At present neutron detection relies mainly on two principles: detection in gas proportional counters (^{3}He tubes, multi-wire proportional counters and micro-strip gas chambers) and detection in scintillators. New concepts are based on the introduction of new proportional counter methods [1], new scintillators [2] and light-readout schemes [3], and new converter principles, such as boron coating inside a proportional counter [4] and gadolinium foils coupled to a silicon detector [5]. For a review see [6]. We will address some of the novel concepts, studied at TUD.

One new concept is shown in Figure 1. In a gas electron multiplier (GEM), electrons are gas-amplified in a counting gas in the strong electric field created inside small holes (with diameter ~70 µm) in a thin (50 µm) foil by applying a voltage difference across the thin conducting layers on both sides [1]. In the amplification process light is emitted as well.

Employing two GEMs in cascade, gas amplification can be made high enough to observe this light through a detector window by means of a CCD camera. In Figure 1 on the left, the thus observed cross section of a proton beam, crossing the GEMs perpendicularly, is shown. The same method can be used for neutron imaging if ^{3}He is used as detector gas, mixed with a stopping gas. Actually even individual reactions can be recorded [7].

New scintillators like LiBaF$_3$:Ce,Rb have scintillation mechanisms that respond differently to on the one hand products of the reaction n(^{6}Li,^{4}He)^{3}H and on the other hand gamma rays [8]. Scintillation due to the dopant Ce luminescence centre is emitted upon neutron absorption as well as gamma-ray interaction. The very fast intrinsic ~ 1 ns response, due to so called core valence luminescence (CVL), does only manifest itself upon gamma-ray detection. This offers an excellent possibility to discriminate between neutrons and gamma rays (Figure 2).

Another new scintillator developed in Delft, Cs_2LiYCl_6:Ce, has the very high light yield of 70,000 photons per neutron [9]. This is only beaten by LiF/ZnS:Ag. A pulse height spectrum is shown in Figure 3. The neutron response at channel 9,000 corresponds with 70,000 scintillation photons. The new scintillator offers the possibility of pulse shape discrimination, using CVL as in Figure 2, and in addition pulse height discrimination, simply by selecting the neutron peak in the pulse height spectrum. Note the neutron peak position relative to the 480 and 662 keV gamma peaks.

A new concept, scintillator-silicon well detector [10], to realize a pixelated neutron detector is shown in Figure 4. Deep wells are etched in a 500 µm silicon wafer. Diodes are made in the thin bottom (10 µm thick) for light detection. The wells are filled with grains of a new scintillator, $^6Li_6{}^{158}Gd(BO_3)_3$:Ce^{3+}, mixed with a wavelength shifter for efficient light detection. The scintillator was developed by Photogenics, USA. MESA, Twente, and DIMES, Delft processed the silicon. In Figure 4 a pulse height spectrum of one pixel is presented showing the neutron response from the reaction with ^{6}Li.

References:

[1]   R. Bouclier *et al.*, Nucl. Instr. Meth. **A386**, 531 (1997).
[2]   C.W.E. van Eijk, Nucl. Instr. Meth. **A460**, 1 (2001).
[3]   D.P. Hutchinson *et al.*, Proc. Int. Workshop on Position Sensitive Neutron Detectors, June 28-30, 2001, Berlin, HMI. Vol. **1**,195 (2002).
[4]   M. Klein *et al.*, ibid, Vol. **2**, 453 (2002).
[5]   C. Petrillo *et al.*, J. Neutron Res. **4(1-4)**, 65 (1996).
[6]   C.W.E. van Eijk, Nucl. Instr. Meth. **A477**, 383 (2002).
[7]   F.A.F. Fraga *et al.*, Nucl. Instr. Meth. **A471**, 125 (2001).
[8]   C.M. Combes *et al.*, Nucl. Instr. Meth. **A416**, 364 (1998).
[9]   A. Bessiere *et al.*, Proc. SCINT2003, Valencia, Spain, tbp in Nucl. Instr. Meth. A.
[10] C.P. Allier *et al.*, Proc. Sensor Technology Conference 2001, Enschede, The Netherlands, 14-15 May, 2001, Ed. M. Elwenspoek, Kluwer Ac. Publ. 191 (2001).

3.2 INSTRUMENTATION

Figure 3
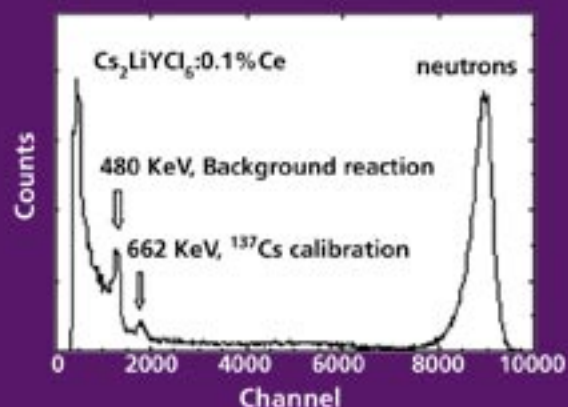**Pulse height spectrum of neutrons from a beam of the IRI reactor, under simultaneous irradiation of the scintillator with 662 keV gamma rays from a ^{137}Cs source, recorded with Cs_2LiYCl_6:Ce scintillator coupled to a Photo Multiplier Tube. The light yield is 70,000 photons per neutron.**
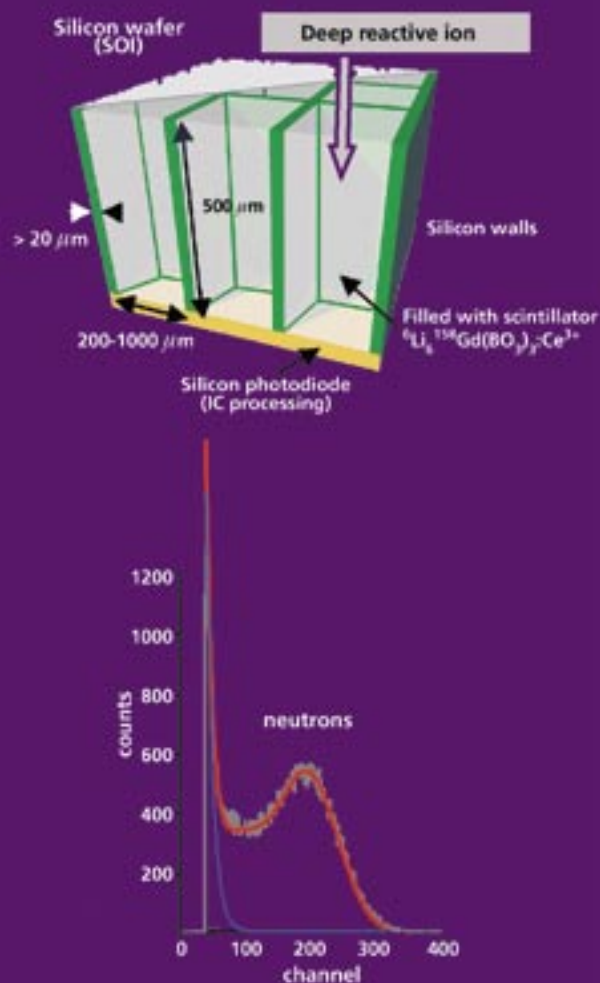

Figure 4
Scintillator-silicon well neutron detector concept (top) and pulse height spectrum (bottom).

**M.Th. Rekveldt, W.H. Kraan,
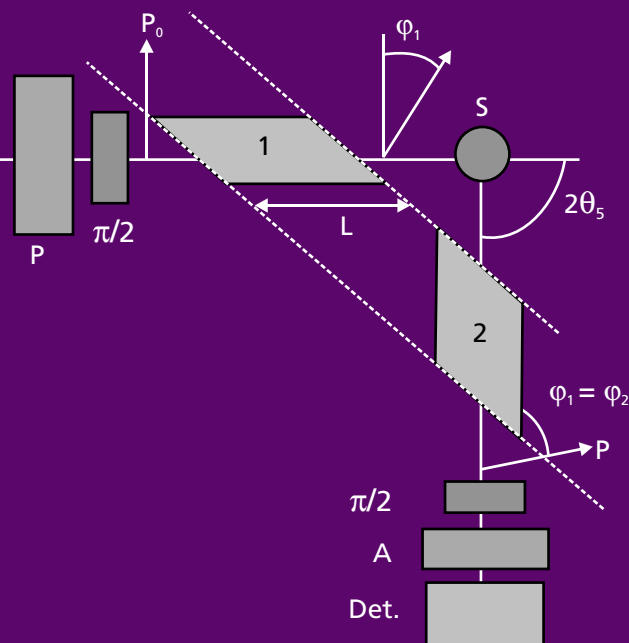W.G. Bouwman, IRI-TUD
T. Keller, HMI**

High resolution diffraction using Larmor precession of polarised neutrons

Figure 1
Sketch of Larmor set-up with two precession devices with inclined front and end face indicated by the numbers 1 and 2.

A new Larmor precession device, consisting of two separate precession modules, is introduced. It operates as a high-resolution neutron diffractometer, without the need of a highly collimated beam, necessary in conventional high-resolution neutron diffraction. The same instrument operates in different modes as an effective small angle scattering device or accurately determines the line profile, the lattice plane orientation or the angular spread in crystal orientations. A dramatic intensity gain can be obtained in all applications discussed, compared with the conventional analogues, owing to the possibility to use a relaxed wavelength and angular resolution. Experiments in the high-resolution diffraction mode on silicon and aluminum are discussed.

In the following the principles of the high-resolution mode will be explained and some first experiments in the high resolution diffraction mode demonstrate the possibilities of this new technique. A sketch of the proposed set-up is given in Figure 1. The polarisation of the incident beam precesses in device 1 in front of the sample and in device 2 after being scattered by the sample. The measured polarisation is a cosine average over all precession angles of the polarisation in precession devices 1 and 2 of all scattered neutrons at the sample S. The precession angles are proportional to the travel times. By choosing the inclination angles of the precession devices about parallel with the average diffraction plane of the sample, it appears that the measured average precession angle is just inversely proportional to the wave vector transfer at the sample. Because the precession angle can be measured with a relative accuracy of 10^{-6}, the same accuracy can be achieved in absolute sense in the wave vector transfer or in the lattice spacing. The damping of the polarisation vector or depolarisation is a direct measure of the line width of that specific reflection. The results are independent on beam divergence or wavelength resolution of the neutron beam used.

We have carried out diffraction experiments on annealed pure aluminium and aluminium strongly deformed in a vice to demonstrate the sensitivity of this diffraction method in analysing the variation of lattice spacing by the deformation (Figure 2). The damping of the polarisation as function of the precession angle ϕ_t in devices 1 and 2 determines the line widths of the Bragg reflection considered.

Figure 3 shows the temperature dependence of the normalised polarisation of the (111) reflection of aluminium.

The lattice spacing can be determined in an absolute way, without needing to know the precise neutron wavelength. The technique could find its strength in the study of a single diffraction line, e.g. in stress studies or temperature dependences of lattice spacings. The use of a rough monochromator or pulsed beam, e.g. of a spallation source may be useful and advantageous.

For more information on these developments see references 1-4.

References:

[1] M.Th. Rekveldt, W.H., Kraan, J. Neutron Research **8**, 53 (1999).

[2] M.Th. Rekveldt, Materials Science Forum **321-324**, 258 (2000).

[3] M.Th. Rekveldt, Th. Keller, R. Golub, Europhysics Letters, **54** 342 (2001).

[4] M.Th. Rekveldt, W.H., Kraan, Th. Keller, J. of Appl. Cryst. **35** 28 (2002).

3.3 INSTRUMENTATION
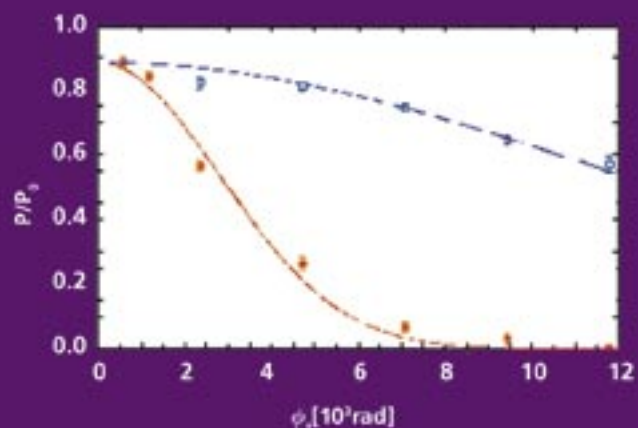
Figure 2
Measured amplitudes as a function of precession angle for deformed and annealed aluminium.
The lines through the points are fits corresponding to Gaussian line widths of half width at half maximum $\varepsilon_{1/2}$ = (6.9±0.2)×10^{-5} and (2.97±0.07)×10^{-4} respectively.
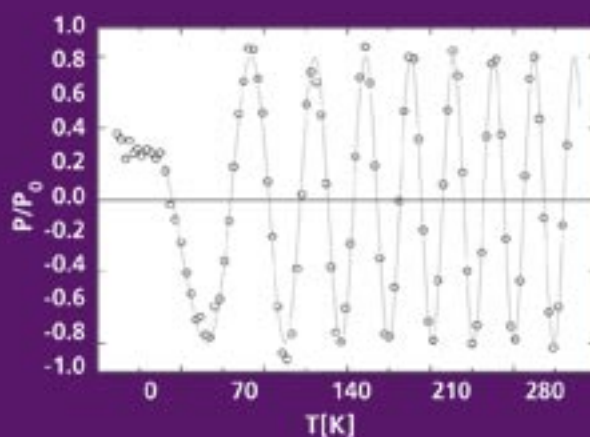
Figure 3
Normalised polarisation as a function of temperature measured on annealed polycrystalline aluminium, showing the sensitivity of the Larmor phase for small changes of the lattice constant. One period in phase corresponds to a relative change of 1 in 10^4 in lattice constant.

R.W.E. van de Kruijs, H. Fredrikze,
M.Th. Rekveldt, IRI-TUD
V.A. Ul'yanov, N.K. Pleshanov,
V.M. Pusenkov, A.F. Schebetov,
V.G. Syromyatnikov, PNPI
S. Langridge, ISIS

Correlated magnetic domains and roughness at interfaces within a multilayer system
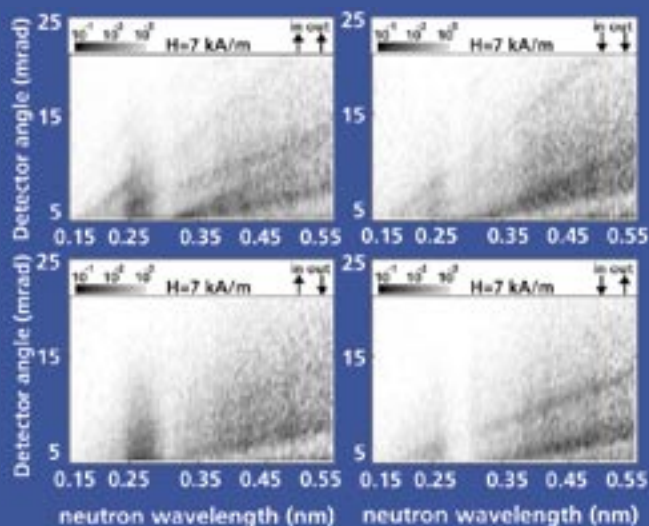
Figure 1
Off-specular reflectivity spectra taken close to the coercive field. The polarization direction of the incident beam ('in') and the direction of polarization analysis after scattering ('out') are marked by arrows indicating parallel (↑) and anti-parallel (↓) alignment with the applied field direction.
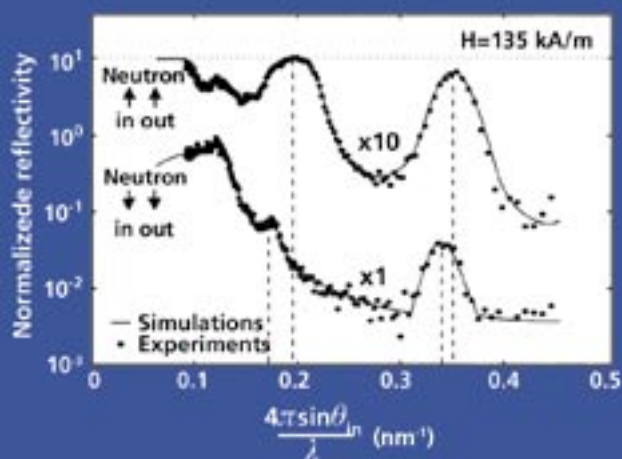
Figure 2
Experimental and simulated specular reflectivity curves at saturation. Model parameters are discussed in the text.

Specular neutron reflectivity is a powerful tool for determining the magnetic or composition profile near the surface of thin films. Changes in this profile are measured via the scattering-length density profile for neutrons perpendicular to the surface (or surfaces for multilayers). There may also be lateral fluctuations in this density, which arise from magnetic domains and/or rough interfaces between layers, and these can be studied by the off-specular scattering of neutrons. Neutron reflectometry has the unique ability to see, and distinguish between, magnetic and compositional variations. By using polarisation analysis of off-specular neutron reflection we can determine the average domain size, and elucidate the role played by conventional roughness of interfaces within the multilayer system. These questions are not only of fundamental interest, but are also relevant to the development of sensors. The ROG reflectometer at IRI was useful for much of the preliminary work, but the detailed work presented here required the use of the CRISP machine at the ISIS neutron source in the UK.

We have recently observed relatively high intensity off-specular neutron scattering from FeCoV/TiZr multilayers, which we attributed to the presence of magnetic domains and rough interfaces. Here we describe experiments that focus on the polarisation analysis of the off-specular scattering from which we obtain the orientations of the domains and the orientations of the interfacial moments, that is: magnetic roughness. We present specular and off-specular polarised neutron reflection (PNR) experiments on [FeCoV/TiZr] multilayers together with model simulations. The experiments shown here were carried out close to the coercive field and at saturation.

At an applied field of H=7 kA/m, close to the coercive field observed in the hysteresis loop, the non-spin-flipped specular reflectivity curves for both incident beam polarisation directions are similar and no spin-flipped reflectivities were detected. This occurs because neutrons effectively probe a structure with net magnetisation close to zero.

The off-specular reflectivity shown in Figure 1 consists mainly of a diffuse band without pronounced Bragg enhancements. Such enhancements are expected for multilayers with a strong coupling between magnetic layers through a non-magnetic interlayer, whereby correlations in the domain orientations are introduced. The resulting multilayered domain structure gives rise to specific Bragg enhancements. In the present case the large TiZr interlayer thickness (30 nm) prevents strong magnetic coupling between the FeCoV layers and thus domain correlations as evidenced by the diffuse nature of the domain scattering.

A polarisation analysis of the diffuse scattering reveals a complete depolarisation for all neutron wavelengths. If the domains were oriented along the easy axis, the neutron spin would always be either parallel or anti-parallel to the magnetic moments and only non-spin-flipped scattering would result. The observed depolarisation of the neutron beam is explained by an isotropic distribution of domain orientations, where the neutron spin precesses in subsequent local magnetic domain orientations and becomes depolarised.

Figure 2 illustrates the specular reflectivity curves obtained for a field in which the hysteresis loop was completely saturated (H=135 kA/m). The absence of spin-flip, together with the absence of the diffuse scattering from domains (see Figure 3), confirms that all layer magnetisations are parallel at saturation. We analysed the data by fitting reflectivity calculations, obtained from a standard matrix formalism, to the experimental data. We were unable to obtain satisfactory agreement with experiment, within the constraint that the shapes for the FeCoV/TiZr and TiZr/FeCoV intermixing regions be equal. The calculations shown in Figure 2 (solid lines) were obtained by using a more detailed description of the intermixing regions in the model calculations, including a nonmagnetic interfacial layer of approximately 1.0 nm and unequal r.m.s. heights of the intermixing regions: σ (FeCoV/TiZr) = 3.0 nm, σ (TiZr/FeCoV) = 2.0 nm.

Although the transversal dimensions of the intermixing regions are readily obtained by fitting the specular reflectivities, no information is obtained about the lateral properties of the interfaces. By studying the off-specular scattering of neutrons, information about the in-plane correlation lengths and fractal dimensionalities of the rough interfaces becomes available.

Figure 3 shows the off-specular spectra for the saturated sample, for which lines of enhanced scattering are clearly visible. The ↑↑ and ↓↓ spectra can be reproduced by model calculations of interfacial scattering using a Distorted Wave Born Approximation, including dynamic multilayer effects. Figure 4(a) shows simulations using a Gaussian surface roughness (fractal dimensionality = 0.5) and an in-plane correlation length of 5 μm. The thickness, roughness and scattering length density of all layers were taken from the analysis of the specular data. The roughness of all layers is assumed to be correlated by a perfect vertical reproduction. An uncorrelated roughness (Figure 4(b)) shows no distinct lines of enhanced scattering in the model calculations.

Polarisation analysis of the spectra at saturation revealed that spin-flipped off-specular scattering is still present at saturation. The non-zero spin-flip scattering indicates the presence of magnetic moments that are not fully aligned with the applied field. Because spin-flip scattering is enhanced along the lines identified with interfacial scattering, it seems likely that the unaligned moments are situated at the chemically rough interfaces and that their orientations are correlated throughout the multilayer stacking. The in-plane correlation length of this magnetic roughness is comparable in size to that of the chemical roughness.
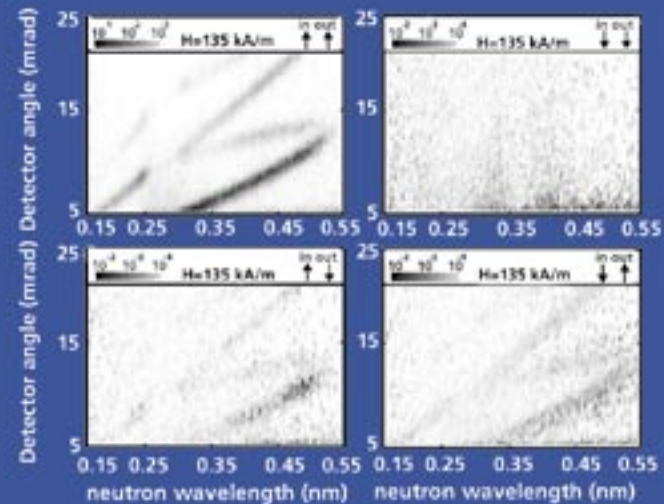
4.1 MAGNETISM

Figure 3
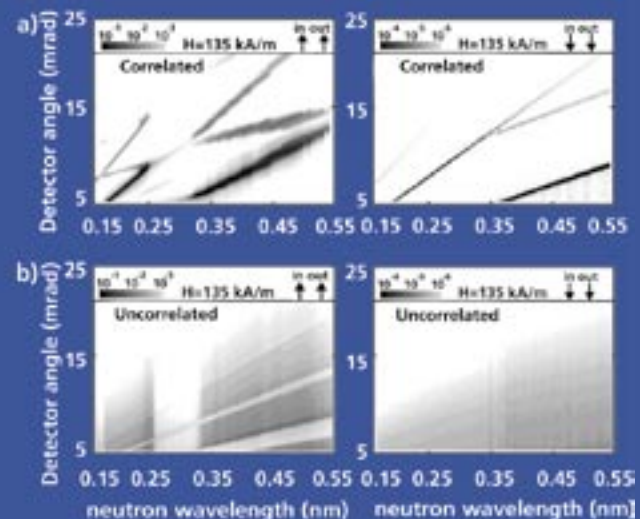**Off-specular neutron reflectivity spectra for the saturated multilayer.**

Figure 4
Model calculations of off-specular neutron reflectometry from correlated (a) and uncorrelated (b) interfaces.

E. Brück (UvA)

Small-angle neutron-scattering study on Fe-Pt based alloys

Model	Porod law		Mono- and polydisperse		
State	K_P $(10^{-9}$ nm$^{-1-\alpha})$	α	D_{max} (nm)	R_{max} (nm)	I_0 $(10^4$ cm$^{-1})$
virgin	350 ± 60	2.94 ± 0.11	105		5.6 ± 0.1
field	160 ± 40	2.94 ± 0.17		125	14.2 ± 0.1
remanent	510 ± 40	2.48 ± 0.05		106	13.4 ± 0.1

Table 1
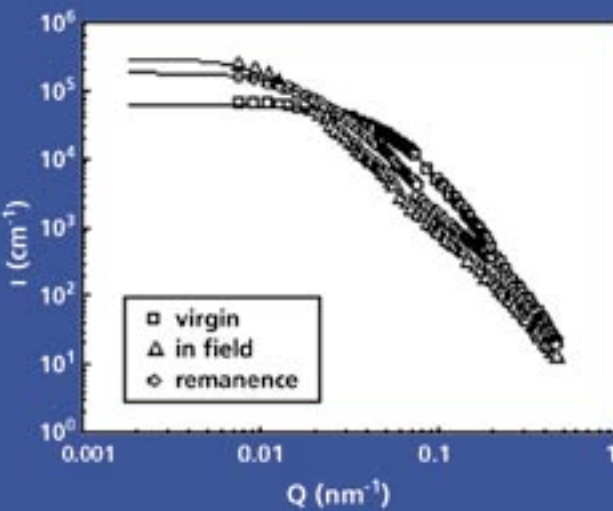**Fitting parameters obtained from the Porod law, the monodisperse and polydisperse models.**

Figure 1
Symbols: experimental SANS results for Fe$_{59.7}$Pt$_{39.8}$Nb$_{0.5}$; lines: model calculations (monodisperse for virgin state and polydisperse for in-field and remanence state)

To understand the mechanism responsible for the high-performance magnetic properties of Fe-Pt alloys a detailed analysis of the microstructure is important. We present SANS experiments from which we determine both the size of the particles and the magnetic domains of the different phases of the sample.

In Fe-Pt alloys the prominent hard-magnetic properties are intimately connected with the face-centered cubic (fcc) to face-centered tetragonal (fct) structural phase-transition [1]. To understand the mechanism responsible for the high-performance magnetic properties a detailed analysis of the microstructure is important. Using small-angle neutron scattering (SANS) one can investigate the microstructure of nanostructured systems within the bulk of the material. Additionally, SANS data include both structural and magnetic contributions to the scattering from nano-scale particles. Therefore, by analysing the SANS data, one can obtain information on the size of the particles and the magnetic domains of the different phases in the sample.

Fe$_{59.7}$Pt$_{39.8}$Nb$_{0.5}$ was prepared into disk-shape for the SANS measurements. The samples were annealed at 1325 °C under Ar, followed by an ageing at 625 °C. The SANS experiments were carried out at room temperature in an applied transverse magnetic field of up to 1.2 T, perpendicular to the neutron-beam direction on the instrument D11 at the ILL. The neutron wavelength was λ = 1 nm with a wavelength spread of $\Delta\lambda/\lambda$ = 10 % and the wave-vector transfer was Q = 0.006 - 0.5 nm^{-1}. The SANS data were collected in three different states: before applying the magnetic field (virgin state), in the magnetic field (field state), and after removing the magnetic field (remanent state). In the high-Q region of the magnetic scattering intensity $I(Q)$ the Porod law can be used for a two-phase system of particles in a matrix $I(Q) = K_P Q^{-\alpha}$, where K_P is the Porod constant and α an exponent which usually equals 4 [2]. For an ensemble of randomly distributed scattering objects, the indirect Fourier transform is most widely used to fit the $I(Q)$ curve [3]. If a system can be considered as monodisperse, the distance distribution function $p(r)$ can be determined. The maximum correlation distance D_{max} in $p(r)$ is then related to the magnetic domain size. In the case of a polydisperse system, where particles may have different shapes or sizes, the volume distribution function $D(R)$ can be determined. The average particle size is then derived from the obtained $D(R)$ curve. Alternatively, the average radius R of spherical particles can be estimated from $R = (3/\pi)(Q_P/K_P)$, where the Porod invariant Q_P is given by $Q_P = \int I(Q)Q^2 \, dQ$.

For the considered Fe-Pt alloys we observed that, in the field and remanent states, the magnetic SANS intensities are significantly smaller than in the virgin state. Therefore, in the virgin state the scattering contribution from randomly oriented magnetic domains is dominant. However, the SANS data in the field state are characterised by an inhomogeneous magnetisation. Thus, in this state, the scattering from particles with different magnetisation becomes the main contribution. To analyse the SANS data, we therefore propose that the monodisperse model is suitable for the Fe-Pt alloys in the virgin state. For the field state, and maybe for the remanent state, a polydisperse model is required. In Figure 1 the SANS data are presented as a function of the wave-vector transfer Q for $(Fe-Pt)Nb_{0.5}$. The Porod law was applied in the high-Q region of the $I(Q)$ curves. The parameters obtained from the Porod fitting are listed in Table 1. The fitting results based on the monodisperse and polydisperse models are also presented in Figure 1. The parameters obtained from these fits are given in Table 1. The function within one particle in a monodisperse model, $p(r)$, is plotted in Figure 2. From the value of D_{max} the average magnetic-domain size is derived to be about 100 nm.

The size-distribution function in a polydisperse model, $D(R)$, is plotted in Figure 3. The main peak at about 6 nm correlate with the fine fct nano-particles with average size of 3 - 8 nm as observed by TEM. Additionally, by integrating the $I(Q)$ curve, we obtain the value of $Q_P = 325 \times 10^{-9}$ nm$^{-\alpha}$ for the field state, which indicates an average fct particle size of 4 nm. This average size is also consistent with the result obtained by TEM.

Summarising, the Porod law is valid for exponent values smaller than 4. This suggests the presence of rough interfaces for the particles, which may be connected with lattice defects or an inhomogeneous distribution of the elements [4]. The monodisperse model was applied to fit the SANS data in the virgin state. The obtained magnetic domain size is in the range of a few hundred nanometres in agreement with previously reported results for the Fe-Pt alloy [5]. To determine the average fct particle size, the polydisperse model was used for the SANS data in the field state. Furthermore, the particle size was also estimated from the Porod invariant. The results are in agreement with the TEM analysis.

References:

[1] K. Watanabe, Trans. Jpn. Inst. Met. **51**, 91 (1987).
[2] G. Porod, Z. Kolloid **125**, 51 (1952).
[3] O. Glatter, J. Appl. Cryst. **10**, 415 (1977): J. Appl. Cryst. **13**, 7 (1980).
[4] V.M. Nadutov, N.A. Bulavin, V.M. Garamus, Mater. Sci. and Engin. A **264**, 286 (1999).
[5] T. Klemmer *et a*l., Scr. Metall. Mater. **33**, 1525 (1995).

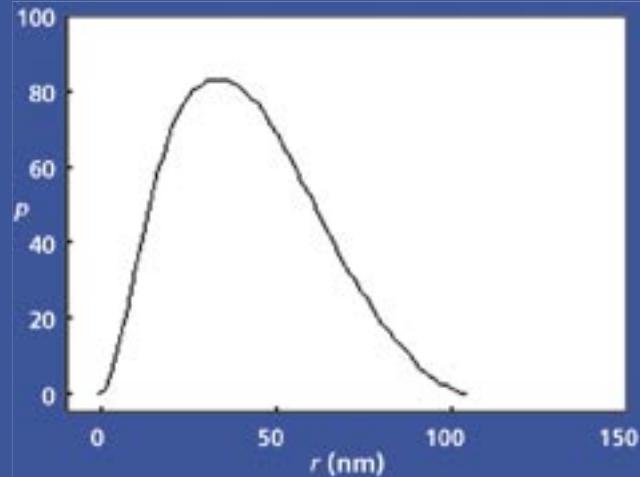## 4.2 MAGNETISM

Figure 2
Distance distribution p(r) for Fe$_{59.7}$Pt$_{39.8}$Nb$_{0.5}$ in the virgin state, obtained from a monodisperse model.
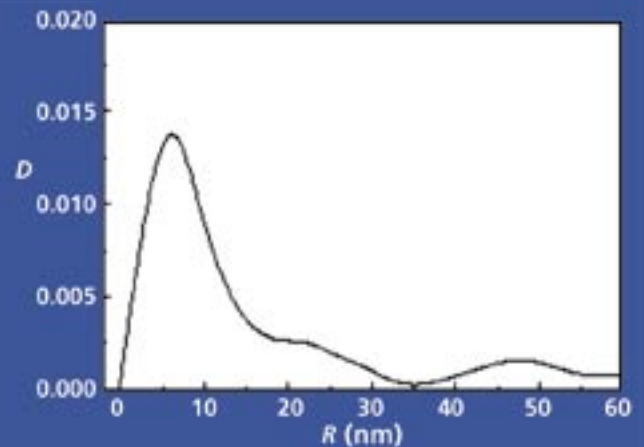

Figure 3
Particle-size distribution function D(R) for Fe$_{59.7}$Pt$_{39.8}$Nb$_{0.5}$ in the field state, obtained 8from a polydisperse model.

**F. Galli, R.W.A. Hendrikx,
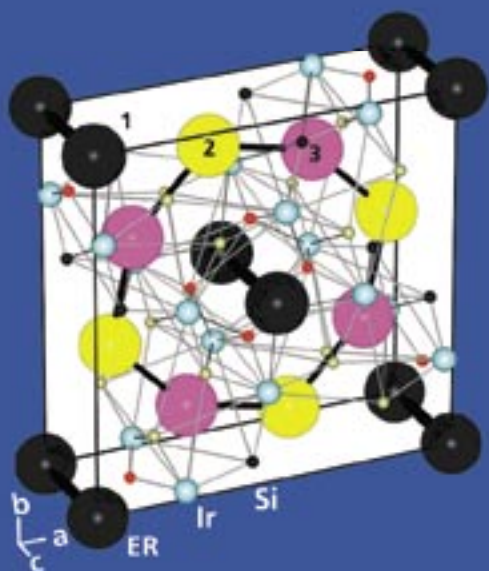G.J. Nieuwenhuys, UL-KO
R. Feyerherm, HMI**

Magnetic structure of Er^{3+} moments in the charge-density-wave compound $Er_5Ir_4Si_{10}$

Figure 1
Crystal structure of $Er_5Ir_4Si_{10}$. Note the three inequivalent Er sites.

The structural and magnetic properties of the intermetallic compound $Er_5Ir_4Si_{10}$ have been studied by neutron and X-ray synchrotron scattering experiments. A complex intermediate incommensurate nuclear structure has been found which locks into a commensurate superstructure at low temperatures. The resulting antiferromagnetic structure shows different moments for each crystallographically different Er ion. The magnetic order parameter is not coupled to the structural distortion.

The intermetallic compound $Er_5Ir_4Si_{10}$ is a remarkable system, showing a number of phase transitions. A detailed study has been reported in [1]. $Er_5Ir_4Si_{10}$ crystallises in the *P4/mbm* space group and the unit cell contains three inequivalent rare-earth sites. The crystal structure is depicted in Figure 1. The structure is tetragonal and thereby significantly anisotropic. It has been shown by Galli *et al.* [2] that the compound shows a structural phase transition at 155 K. Below this temperaure, the structure of $Er_5Ir_4Si_{10}$ is described by a-typical incommensurate charge density wave (CDW), which locks-in commensurately at 55 K. The CDW is located along the c axis, with a displacement vector $q = (0,0,¼±\delta)$ below 155 K and $q = (0,0,¼)$ below 55 K.

Besides this charge density wave or periodic lattice distortion, the Er^{3+} ions have a magnetic moment and order antiferromagnetically at the Neél temperature $T_N = 2.8$ K. Then the interesting question arises whether there is an interplay between the CDW and the AF order, or whether these orderparameters simply coexist in the material. It is known for the isostructural material $Lu_5Ir_4Si_{10}$ that super-conductivity and the CDW coexist below 4 K. The CDW in $Lu_5Ir_4Si_{10}$ can be suppressed via the application of external pressure resulting in an increase of the superconductivity transition temperature from 4 K to 8 K [3].

The magnetic structure of $Er_5Ir_4Si_{10}$ was determined by means of powder as well as single crystal neutron scattering. These diffraction experiments were carried out at the neutron facility (BENSC) of the Hahn-Meitner Institute, Berlin on the spectrometers E2 and E6. Because of the fact that the magnetic susceptibility measurements indicated an antiferromagnetic order at $T_N = 2.8$ K, neutron powder diffractograms were collected at 1.7 K and at 3.5 K. The 1.7 K diffraction data showed a number of extra 'magnetic Bragg' reflections, see Figure 2. Almost all reflections could be indexed as $(h/2,k/2,0)$; h, k = odd, which corresponds to a magnetic vector $k = (½,½,0)$. In order to improve the statistical quality of the data we subsequently performed single crystal measurements.

The single-crystal samples for these experiments were grown in a tri-arc crystalpuller using the Czochralski technique [4]. The quality of the samples was verified using electron-probe micro-analysis (EPMA) and Laue diffraction.

From the single-crystal neutron diffraction data we deduced the following:

- The magnetic structure can be represented in a cell which is rotated by 45° with respect to the original crystallographic cell with cell parameters $a' = b' = a\sqrt{2}$. This magnetic unit cell contains 20 Er ions.
- All Er-ions are located in common planes perpendicular to k. If all the magnetic moments of the Er ions are assumed to be of equal magnitude, this would result in ferromagnetic sheets stacked along k.
- However, the presence of the reflections of type ($h/2,k/2,0$) shows that the magnetic moments are not parallel to k, i.e. not perpendicular to the sheets.
- The relatively small intensity of the reflections of type ($h/2,k/2,1$) with small h,k observed in powder data indicates that the moments are oriented parallel to c.

These observations lead to a magnetic structure which can be described by the magnetic space group *Pm'mm*, resulting in a magnetic structure model with only three free parameters: the magnetic moments on Er1, Er2b and Er3b ions. The Er2a and Er3a are located on perpendicular mirror planes and therefore carry no ordered moment. The resulting magnetic structure is depicted in Figure 3.

Experiments on the same single crystal, combining simultaneously high intensity x-ray diffraction to follow the charge density wave and magnetic x-ray diffraction to follow the magnetic order, proved that the the CDW and the antiferromagnetism coexist without coupling between their order parameters [5].

References:

[1] F. Galli, Ph.D. thesis Leiden University (2002).
[2] F. Galli *et al.* Phys. Rev. Lett. **85** (2000).
[3] R.N. Shelton, *et al.* Phys. Rev. **B 34**, 4590 (1986).
[4] A.A. Menovsky, J.J.M. Franse, J. Crys. Growth **65**, 286 (1983).
[5] F. Galli, *et al.* J. Phys. Condens. Matter **14**, 5067 (2002).

4.3 MAGNETISM
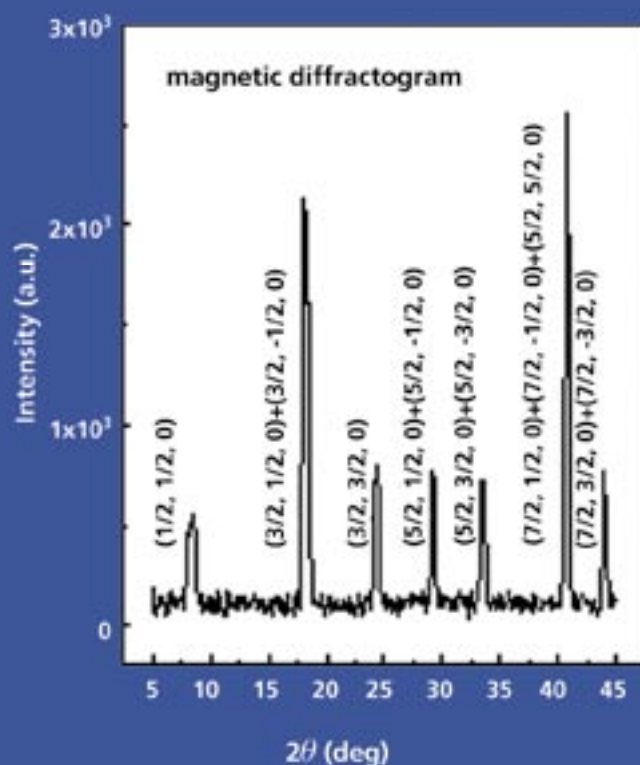
Figure 2
Difference between the diffractogram at 2 K (antiferromagnetic state) and at 4 K (paramagnetic state). Only Bragg reflection of magnetic origin remain.
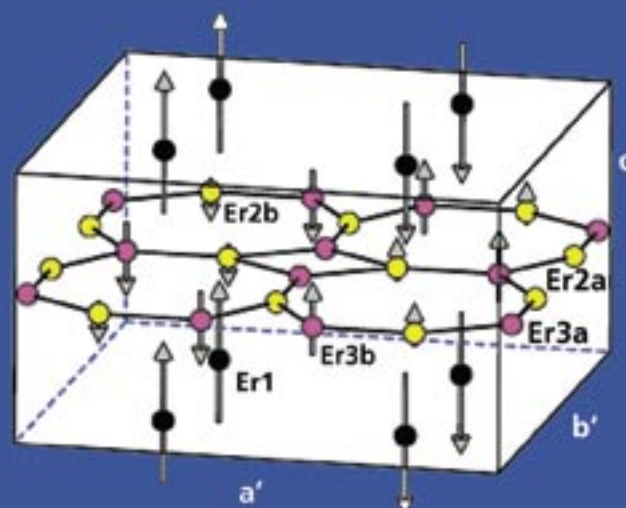

Figure 3
Magnetic unit cell. Only Er atoms are shown, with the new five inequivalent positions. The ordered moments are different from site to site, and for symmetry reasons are zero on the Er2a and Er3a sites. For clarity the c axis is expanded by a factor of two.

**T.T.M. Palstra, Y. Ren,
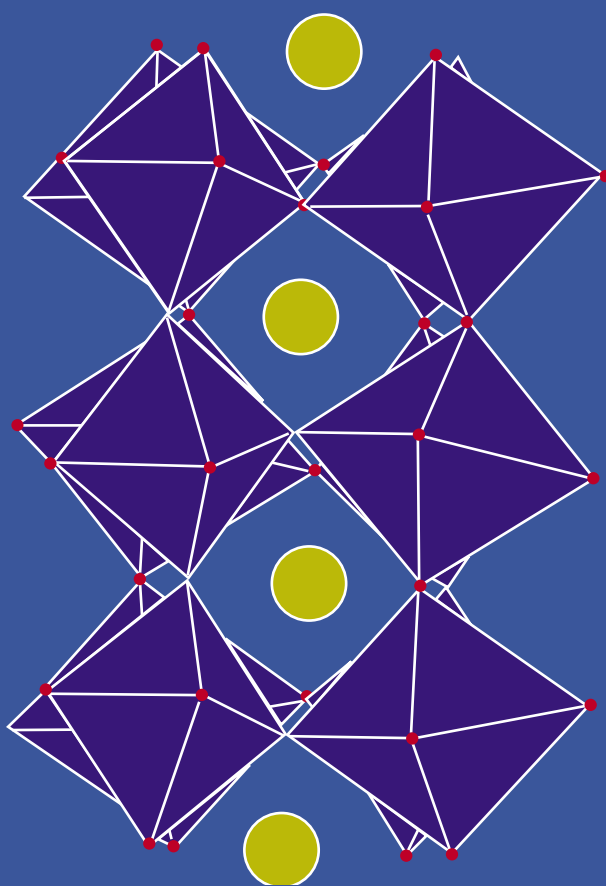G. R. Blake, A. Nugroho,
RUG-MSC**

Orbital ordering induced phenomena in perovskites

Figure 1
Representation of a Jahn-Teller distorted perovskite with Pbnm symmetry. The circles represent R, the octahedra O, and the M is located at the center of the octahedron.

The relation between crystal structure, orbital and spin ordering is investigated in a series of RMO_3 perovskites. Neutron diffraction measurements were carried out on YVO_3 using the Polaris diffractometer (ISIS) in order to investigate the interplay between spin and orbital degrees of freedom. An increase in octahedral tilting on cooling leads to a transition between orbital orderings at 77 K which in turn induces a change in magnetic structure.

The transition metal perovskites RMO_3 form the basis for many interesting physical phenomena, such as high temperature superconductivity, ferro-electricity, and colossal magneto-resistance. Such properties are relevant for technological applications in the electronics industry. Despite these materials being the subject of intense study, in many cases their crystal structures have not been investigated in detail. Nevertheless, structural data form the basis for our understanding of the complex relationships between the spin, orbital, and charge degrees of freedom. The perovskites form an interesting class of materials, because this relatively simple 3d-network of corner-shared octahedra , Figure 1, yields a dazzling multitude of spin / orbital orderings often intimately coupled to each other, resulting in for instance metallicity or superconductivity.

Our group has intensely studied RMO_3 compounds with R a rare earth element, and M a cation with orbital degeneracy, such as Ti^{3+}, V^{3+}, Mn^{3+}, and Co^{3+}. While it is commonly accepted that the spin and charge state determine the electronic properties, it has become of recent interest to study the consequences of orbital degeneracy on physical properties. For insulating materials long-range ordering of degenerate d-orbitals is expected to take place below a transition temperature and will be accompanied by a Jahn-Teller distortion, which corresponds to an elongation of one of the two-fold axes of the octahedron, Figure 2. This orbital ordering can have pronounced and hitherto unrecognised effects on physical properties, such as the insulator-to-metal transition and charge ordering. Unfortunately, it is not yet routinely possible to interpret scattering experiments that scatter selectively on the 3d-electron system. Therefore, we utilise neutron scattering to determine accurately the atomic positions of the coordinating oxygen positions. From this we infer the nature of the orbital ordering. The high neutron cross section of oxygen makes neutron scattering preferable above X-ray scattering techniques, which is hampered by a relatively small oxygen form factor.

The anti-symmetrisation of the total wavefunction leads in the case of the perovskites to a distinct number of possible spin and orbital orderings. Rietveld refinement of powder neutron diffraction data often cannot differentiate between these different symmetries, because the refinement is not always most sensitive to the differ-

ences in symmetry. Furthermore, alternation of the bond lengths due to an alternation of orbital occupation (e.g. d_{xz} and d_{yz} in YVO_3) results in relatively small changes in the lattice parameters. Therefore, the space group symmetry is derived from single crystal studies using local X-ray or synchrotron based facilities. The symmetry of the crystals can alternatively be studied using optical techniques such as IR absorption or Raman spectroscopy.

We studied extensively RVO_3, notably R=Y, in which orbital ordering takes place due to a degeneracy of the d^2 state for the three t_{2g} orbitals, d_{xy}, d_{yz}, d_{xz}. YVO_3 received considerable interest because of a succession of magnetization reversals at 77 and 95K [1,2]. The magnetisation reversals are associated with the canting of the anti-ferromagnetically coupled spins, resulting in a magnetic moment of ~0.01 μ_B. We found that the orbital ordering takes place at considerably higher temperature, $T_o = 200$ K, than the magnetic ordering $T_N = 117$ K. From careful symmetry measurements we learned that the low temperature state, T < 77 K has orthorhombic *Pbnm* symmetry, whereas the intermediate state, 77 K < T < 200 K, has monoclinic symmetry with the loss of the mirror plane perpendicular to the c-axis [3,4]. From the oxygen distortion pattern we infer that in both states the orbital ordering consists of alternating occupation of d_{xz} and d_{yz} orbitals in the basal plane. However, the low temperature state has a different stacking sequence of the orbitals than the intermediate temperature range, as shown in Figure 3, determined by our Polaris data. The anti-symmetric state of the spin plus orbital part of the total electronic wavefunction necessitates that the easy axis of the spin state must change completely between the high and low temperature phases. Indeed the transition involves not only the easy axis, but also a reversal of the magnetic moment, a change in the magnetic symmetry, and is of first order. We associate this transition with the degree of octahedral tilting in YVO_3. For R with a larger ionic radius, the ground state corresponds with the high temperature state of YVO_3, whereas for smaller rare earth ions, the low temperature state is observed. The transition is linked to the degree of R-O covalency, of the hybridisation between the rare earth ion, d-orbitals and the oxygen ion 2p orbitals.

Thus, YVO_3 seems to be unique among the perovskites in displaying a double magnetisation reversal alongside two types of orbital and antiferromagnetic ordering. The degree of octahedral tilting and covalency, resulting in an R site-shift, should be an important factor in determining the most stable orbital ordering configuration and the accompanying magnetic structure. It would also be worthwhile to study this relationship between degree of octahedral tilting, R site-shift, orbital ordering and electronic properties for other RMO_3 perovskites.

References:
[1] Y. Ren, T.T.M. Palstra, D.I. Khomskii, E. Pellegrin, A.A. Nugroho, A.A. Menovsky, G.A. Sawatzky, Nature, **396**, 441 (1998).
[2] Y. Ren, T.T.M. Palstra, D.I. Khomskii, A.A. Nugroho, A.A. Menovsky, G.A. Sawatzky, Phys. Rev. B **62**, 6577 (2000).
[3] G.R. Blake, T.T.M. Palstra, Y. Ren, A.A. Nugroho, A.A. Menovsky, Phys.Rev. Lett. **87**, 245501 (2001).
[4] G.R. Blake, T.T.M. Palstra, Y. Ren, A.A. Nugroho, A.A. Menovsky, Phys. Rev. B **65**, 174112 (2002).

4.4 MAGNETISM

Figure2
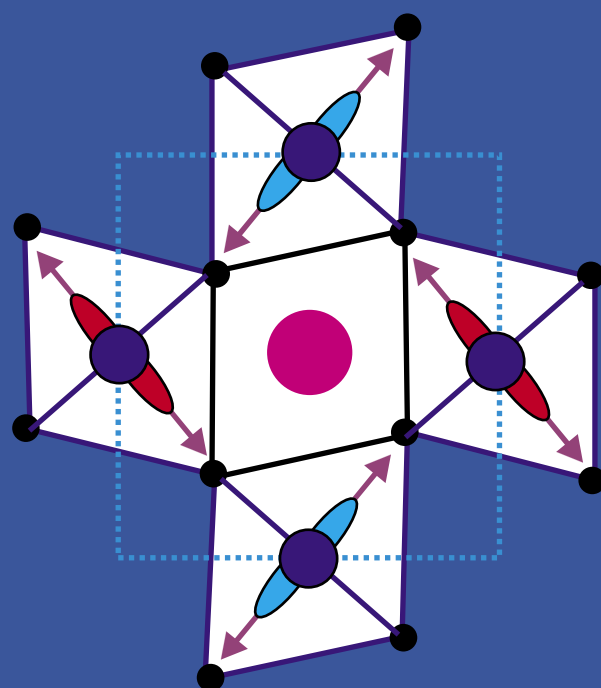**Alternate occupation of d_{xz} and d_{yz} orbitals in the basal plane of YVO_3. The direction of the distortion of the octahedron due to the Jahn-Teller effect is indicated by the red arrows.**
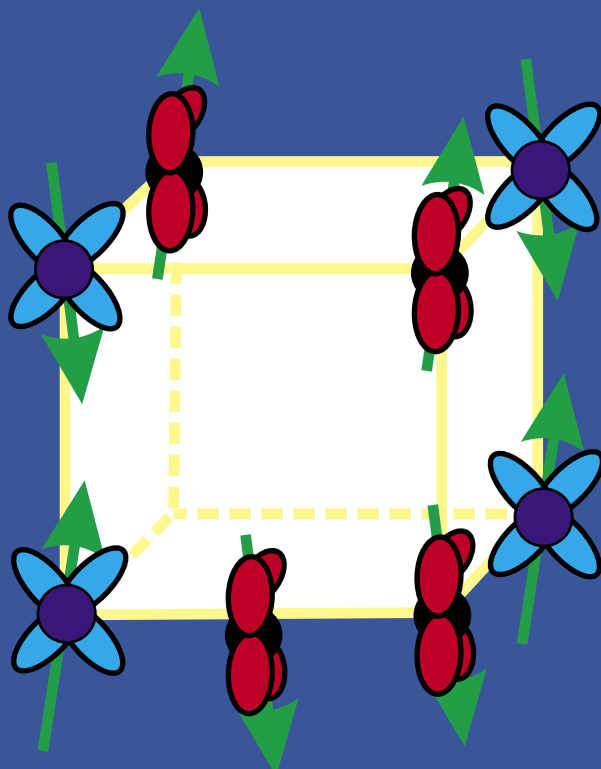

Figure 3
Represenatation of the low temperature C-type orbital ordering, G-type antiferromagnetic ordering corresponding with a d-type Jahn-Teller ordering of YVO_3.

V.P. Plakhty, E. Moskvin, PNPI
J. Kulda, ILL
D. Visser, NWO
J. Wosnitza, UK
R.K. Kremer, MPI

Figure 1
The clockwise (A) and counter-clockwise (B) chiral domains in the magnetic structure of CsMnBr$_3$.

Figure 2
Critical behaviour of the dynamical chirality (above T_N) in magnetic field applied along the scattering vector and along the hexagonal axis. Inset: the polarisation-dependent component of the energy spectra.

Chirality in CsMnBr$_3$- evidence for a new universality class of phase transitions

Using polarised neutrons we have observed spin chirality in the frustrated triangular-lattice antiferromagnet CsMnBr$_3$. We were able to determine both the critical exponent $\beta_C = 0.43(2)$ describing the average chirality in the ordered phase below the Néel temperature $T_N = 8.37$ K and the crossover exponent $\phi_C = 1.27(9)$ corresponding to the dynamical chirality above T_N. These results provide the first experimental proof of the new chiral universality class of phase transitions predicted by theory.

An important feature of phase transitions is their universality, which means that the critical behaviour of physically different systems depends only on the number of the order-parameter components and on the spatial dimensionality of the system. Each universality class has a particular set of exponents which characterises its critical behaviour. The order parameter of frustrated triangular-lattice anti-ferromagnets, as well as of helimagnets includes, in addition to the ordinary spin variables, S_R, the spin chirality, $C = [S_{R1} \times S_{R2}]$, which describes whether the spin structure is a right- or left-handed one. According to Kawamura [1], the chirality results in new universality classes. The conventional critical exponents are modified and, more-over, two new exponents, $\beta_C \approx 0.45$ for the average chirality below the Néel temperature (T_N) and $\gamma_C \approx 0.77$ for the chiral susceptibility above T_N are expected to appear.

Since the observed values of the conventional critical exponents fit different scenarios [2,3]. Kawamura's conjecture is under consider-able discussion. However, the chiral exponents were never deter-mined experimentally, in part because of the absence of a suitable technique to produce a single-domain crystal. The original motiva-tion of the present experiment was the proposition by Maleyev [4], suggesting that above the Néel temperature the dynamical chirality, i.e., the projection of the chiral field on the sample magnetisation, results in an inelastic polarisation-dependent cross section that is odd in energy transfer. Its temperature dependence would be described by the crossover chiral exponent, $\phi_C = \beta_C + \gamma_C$.

A convenient representant of planar (XY) frustrated triangular-lat-tice antiferromagnets is CsMnBr$_3$ whose structure is displayed in Figure 1. The magnetic moments of the manganese ions lie in the hexagonal plane. The chirality is characterised by the sense of their rotation when passing from a manganese atom to the next one along one of the crystallographic axes in the basal plane. Figure 1 gives an example of domains with spin rotations in the clockwise (A) and counter-clockwise (B) sense.

The dynamical chirality has been investigated at $Q = (1/3, 1/3, 1)$ using the cold neutron three-axis spectrometer IN14, IN12 and the thermal neutron triple axis spectrometer IN20. A crystal of about
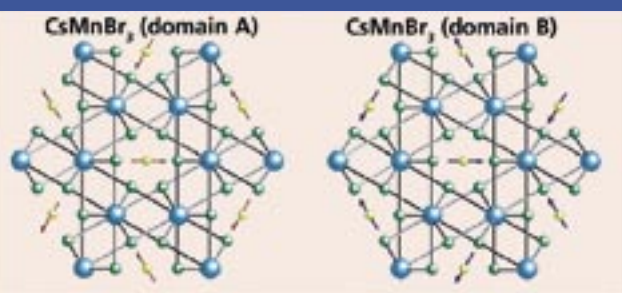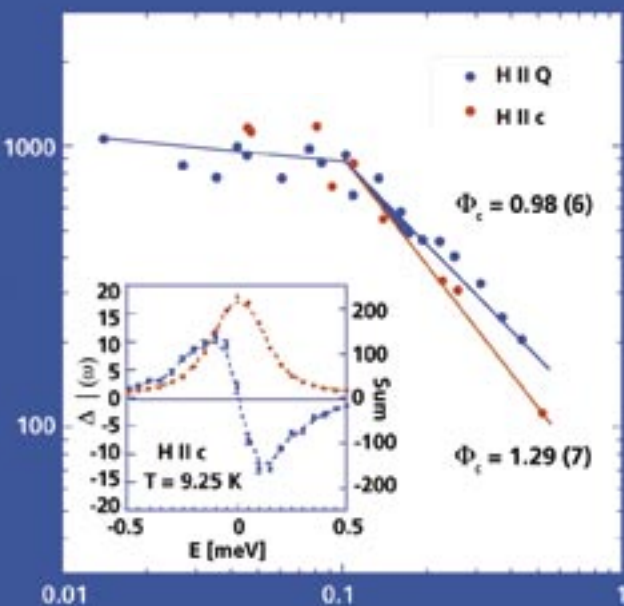
3 cm³ has been mounted in a 4 Tesla horizontal cryomagnet with field parallel to the hexagonal axis. The difference between the scattering intensities of neutrons with incident polarisation parallel and antiparallel to the applied field, $\Delta I(\omega) = I^+(\omega) - I^-(\omega)$, has then been measured. A typical spectrum exhibiting the antisymmetric variation with the energy transfer is shown in the inset of Figure 2.

An empirical function, a squared Lorentzian multiplied by the energy transfer, $\Delta I(\omega) = S\omega\Gamma^3/[\Gamma^2+(\omega-\omega_0)^2]^2$ convoluted with the resolution function has been used to fit these data. According to refence [5] the value of the chiral cross-section characterised by S should depend on: $\tau = |(T - T_N)/T_N|$ as $S = \tau^{-\phi_C}$.

A logarithmic plot of S versus τ is shown in Figure 2. From the slope at $\tau > 0.1$ one obtains the value of the chiral crossover exponent $\phi_C = 1.29\,(7)$ which is in good agreement with Kawamura's calculated value 1.22(6) for the XY model C [1]. At lower τ, the slope decreases, apparently due to the inverse correlation length becoming smaller than the resolution width. This aspect has recently been clarified by further experiments and it was found that the whole critical region down to TN can be described by a single chiral crossover exponent $\phi_C = 1.26\,(7)$ [6].

In the course of the experiment it turned out that in the ordered state, below $T_N = 8.37$ K, different populations of left- and right-handed domains can be frozen in. Their proportion depends, in a random manner, on the cooling history. In the case of unequal populations again a difference in the (1/3,1/3,1) Bragg-peak intensity is observed between the two incident neutron polarisations, parallel and antiparallel to the guide field (about 10 Gauss) along the scattering vector. This part of the study was carried out using polarised thermal neutrons on the IN20 spectrometer ($k = 2.662$ Å^{-1}, Si 111 analyser and PG filter to remove any 2nd order contamination). The sum of the scattered intensities for the two polarisations is proportional to $\tau^{2\beta}$ with the expected exponent $2\beta \approx 0.42$. The difference signal, displayed in Figure 3, provides the critical exponent $\beta_C \approx 0.43(2)$, being in excellent agreement with Kawamura's theory [1]. Combining the two measured critical exponents, β_C and ϕ_C the experimental value for the chiral susceptibility exponent, $\gamma_C \approx 0.86(9)$, can be derived [7]. Similar results have been obtained for the critical behaviour of $CsNiCl_3$ in the spinflop phase [8] and for $CsVBr_3$. All these results provide support to Kawamura's predictions of a new universality class of chiral phase transitions.

References:

[1]   H. Kawamura, J. Phys.: Condens. Matter **10**, 4707 (1998).
[2]   P. Azaria, B. Delamotte, T. Jolicoer, Phys. Rev. Lett. **64**, 3175 (1990).
[3]   S.A. Antonenko And A.I. Sokolov, Phys. Rev. B **49**, 15901, (1994).
[4]   S.V. Maleyev, Phys. Rev. Lett. **75**, 4682 (1995).
[5]   V.P. Plakhty, S.V. Maleyev, J. Kulda, J. Wosnitza, D. Visser, E. Moskvin, Europhys. Lett. **48**, 21 (1999).
[6]   V.P. Plakhty, J. Kulda, J. Wosnitza, D. Visser. Phys. Rev B (submitted) (2003).
[7]   V.P. Plakhty, J. Kulda, D. Visser, E. Moskvin ,J. Wosnitza,. Phys. Rev. Lett **85**, 3942 (2000).
[8]   V.P. Plakhty, S.V. Maleyev, J. Kulda, D. Visser, J. Wosnitza, E. V. Moskvin, Th. Brückel, R.K. Kremer, Physica B **297**, 60 (2001).
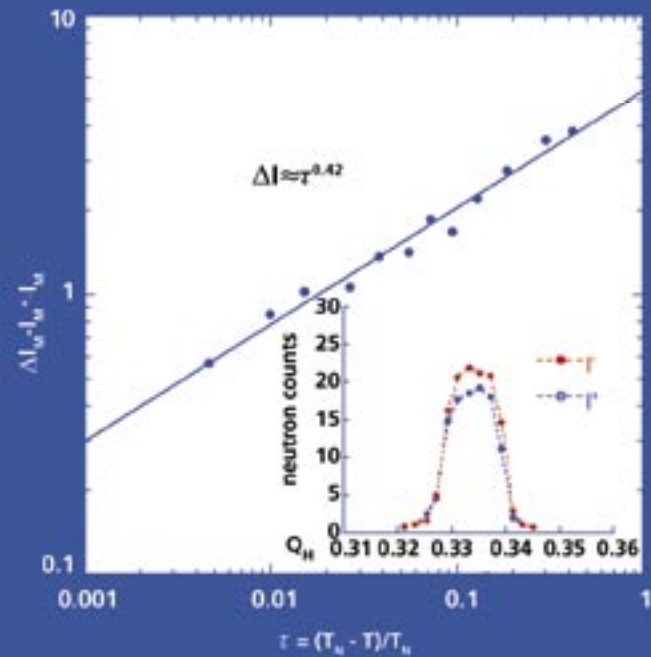
Figure 3
Critical behaviour of the average chirality below T_N. Inset: the difference in (1/3, 1/3, 1) Bragg peak intensities I$^+$, I$^-$, due to unequal chiral domain population.

**E.M.L. Chung, M.R. Lees,
G. Balakrishnan, D.McK. Paul, UW
D. Visser, NWO
G.J. McIntyre and C. Wilkinson, ILL**

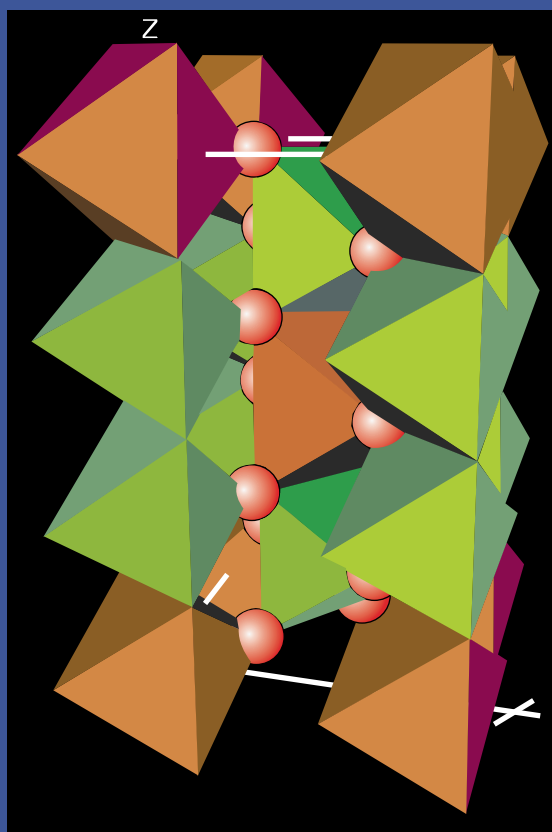# Short-range magnetic correlations in tapiolite revealed by Laue diffraction

Figure 1
Schematic of the $FeTa_2O_6$ structure. Fe and Ta are both octahedrally coordinated to O atoms at the vertices of the volumes shown. Fe is in the centre of each brown octahedron, Ta in the centre of each green.
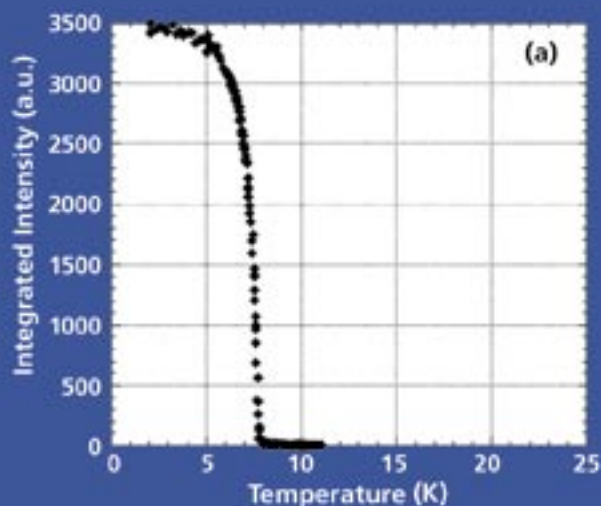

Figure 2a

Difference Laue diffraction patterns on VIVALDI, the first instrument of the Millennium Programme at ILL, Grenoble, reveal with striking clarity the 2D magnetic ordering in the mineral tapiolite. Complementary temperature-dependent monochromatic data suggest the ordering is two-stage, first to a 2D paramagnet, then to a 2D antiferromagnet.

Named after the god Tapio of Finnish mythology, tapiolite ($FeTa_2O_6$) is one of a group of naturally occurring minerals with general formula $A^{2+}B_2^{5+}O_6$. The crystal structure can be described as the conventional rutile unit cell tripled along the tetragonal c-axis. The trirutile structure arises from the ordering of the divalent and pentavalent cations, and results in each layer of Fe^{2+} cations being separated from the next by two sheets of diamagnetic Ta^{5+} ions (Figure1). This results in a highly convoluted magnetic exchange pathway, and favours 2D magnetic ordering.

Past reports of the magnetic properties of $FeTa_2O_6$ are based almost exclusively upon the analysis of polycrystalline samples. Early researchers mistakenly reported the long-range ordering temperature as coinciding with the maximum in the magnetic susceptibility at $T(\chi_{max}) \approx 14$ K. In fact, a single thermodynamic quantity is not sufficient to characterise the magnetism fully, and measurements of other properties such as the heat capacity are required to show that the true Néel temperature occurs at $T_N \approx 8.5$ K. Broadening of the susceptibility maximum above T_N arises from short-range correlations, and is now acknowledged to be a classic signature of 2D magnetic ordering. Combined interpretation of data from Mössbauer spectroscopy and neutron powder diffraction indicated that the 3D ordered phase consists of anti-ferromagnetic planes of Fe <110> moments with adjacent planes rotated by 90º, consistent with the local co-ordination of oxygen atoms. To investigate the 2D ordering we undertook magnetisation and neutron diffraction experiments on a single crystal of $FeTa_2O_6$.

Although it is possible to find natural crystals of tapiolite growing in granite pegmatites, these tend to contain impurities such as Mn^{2+} and Nb^{2+}, and exhibit a substantial reduction in cation ordering. Our sample was cut from a crystalline boule grown in an optical floating-zone furnace. Magnetisation data with the field along the <100>, <110> and <001> indicated high anisotropy between the a-b plane and the c direction. Our single-crystal data have clear points of inflection at $T_N = 8.0(1)$ K, but the ratio $T_N / T(\chi_{max})$ depends on the orientation of the crystal relative to the field, with $T_N / T(\chi_{max})$ = 0.92(3) for H along <001> and $T_N / T(\chi_{max})$ = 0.54(2) for the field along <110> or <100>; evidence that short-range order is prevalent within the a-b plane at elevated temperatures. Can we obtain more detail of the 2D ordering by neutron diffraction?

The obvious choice is monochromatic neutron diffraction on an instrument like D10, ILL. The first step was to verify the 3D ordered structure by collection of extensive diffraction data at 2 K, which confirmed the model of planes of antiferromagnetic <110> Fe moments with a 90° rotation between successive planes. Significant moments were also detected on both bridging oxygen sites, indicative of the importance of the nextnearest neighbour super-exchange.

To search for evidence of 2D order above T_N, extended scans were made around the positions of the stronger magnetic reflections of the form $h+0.5 \, k \, l+0.5$ or $h \, k+0.5 \, l+0.5$. Well-defined rods of scattering were observed extending along c*, decreasing monotonically in intensity with increasing $|l|$, characteristic of greatly reduced ordering between the antiferromagnetic planes. The evolution with temperature of the intensity and the width (in k) of the rod 0.5 0 l at l = 2.5 are superimposed on the intensity variation of the 0.5 0 1.5 magnetic reflection in Figure 2. Below 3 K the ordering is completely 3D. Between 5 K and T_N = 7.95 K there is a gradual cross-over from 3D to 2D order; the spins remain antiferromagnetically ordered within the planes but there is a reduction in correlation between planes. Between T_N and 9.5 K (the inflection in Figure 2b), there is little or no correlation between planes, but still considerable order within each plane. Above 9.5 K the structure evolves towards a 2D paramagnet where the moments remain within the a-b plane, but become more disordered and mobile. As the temperature is further increased the structure gradually changes to the 3D paramagnetic state.

While the presence of 2D order is indisputable from the mono-chromatic D10 data, we were guided by magnetisation data in our search. In the white-beam Laue method the next best thing to a point-like Bragg reflection should be a rod of scattering. What can the new thermal-neutron Laue diffractometer VIVALDI reveal? The Laue diffraction pattern at 2 K (Figure 3a) shows clearly the additional magnetic reflections between pairs or rows of structural reflections. At 10 K only the structural reflections remain (Figure 3b), but we can also see additional extended streaks radiating from the straight-through beam, as well as the triangular fans from preferred orientation in the cryostat heat shields. These additional streaks are more evident in the difference Laue diffraction pattern (Figure 3c), and are the projections of several of the 1D diffuse rods that extend along c*. Again we did know where to look for diffuse rods in the Laue experiments, but the additional 1D scattering in the Laue diffraction patterns, especially in the difference pattern, is very obvious; yet another advantage of the global view afforded by the Laue method. Modelling the scattering is complicated by chromatic overlap, nevertheless comparison of patterns above and below transitions should be routine in all studies of magnetic structures by the Laue method. This is only one of many recent experiments that show the unique importance of the neutron Laue method for exploring the whole of Q-space as a function of temperature, pressure, etc. A white beam from a continuous neutron source can provide an exceptionally high average flux on the sample, and this, combined with the very large solid angle of the detector, makes this a powerful instrument that will not easily be bettered, even on the new pulsed sources.

4.6 MAGNETISM
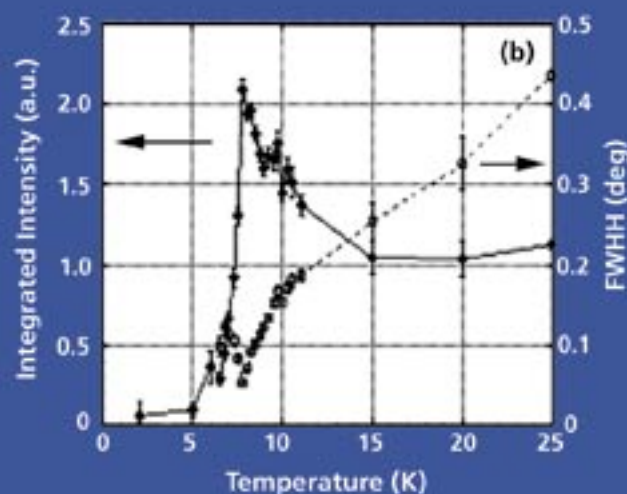
Figure 2
Temperature dependence of (a) the integrated intensity of the 0.5 0 1.5 magnetic reflection, (b) the integrated intensity and full-width-at-half-height in a scan across the 1-D rod at 0.5 0 2.5.
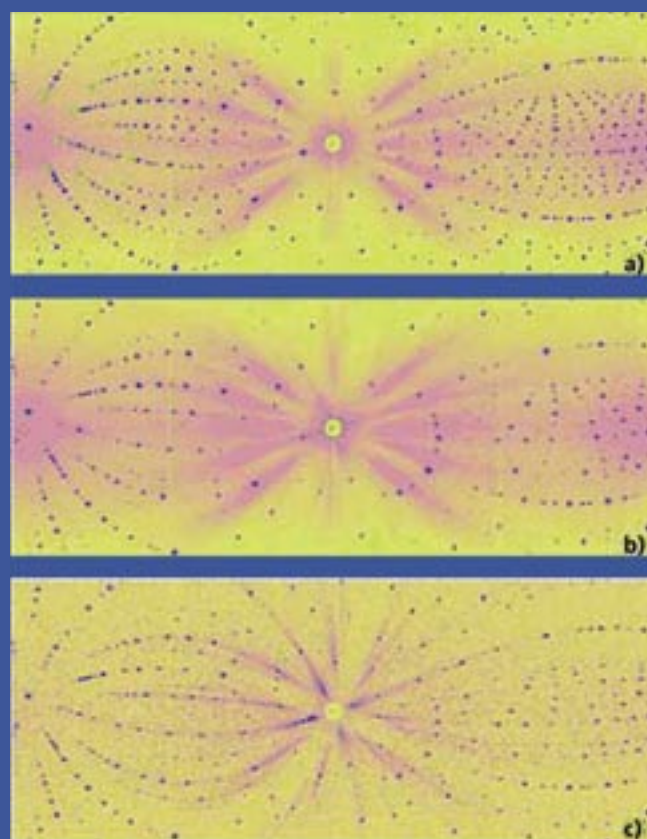
Figure 3
Laue diffraction patterns observed on VIVALDI for $FeTa_2O_6$, (a) at 2 K, with the predicted structural reflections marked by +, (b) at 10 K, with a hint of diffuse scattering at low Q and (c) the difference between the patterns at 10 K and 2 K, yielding rods of magnetic scattering along l. Neutron waveband: 0.8 – 3.5 Å.

**M. Wagemaker, G.J. Kearley,
F.M. Mulder, A.A. van Well,
IRI-TUD**

Finding multiple needles in a haystack: Li intercalated in anatase TiO$_2$

Figure 1

Li$_{0.12}$TiO$_2$ diffraction pattern measured on GEM, at 10K. Fit and difference are indicated. The inset shows the high quality of the data down to low d-spacing (or high Q).

Figure 2

Two discrete intra octahedron sites in titanate (left) and anatase (right).

Rechargeable lithium ion batteries have transition metal oxide electrodes in which lithium is (de-) intercalated during electrical (dis-)charge. In order to understand the physical properties of such material it is a prerequisite to know the accurate position(s) of Li in such oxides. Using state of the art neutron diffraction, quasielastic neutron scattering and molecular dynamics simulations it appears that there is more than meets the eye: when the oxygen cage in which the Li is located is distorted the Li appears to choose its position from several sites within the cage. Such is the case in Li intercalated anatase TiO$_2$.

Lithium intercalation in micro-crystalline TiO$_2$ anatase produces by spontaneous phase separation a nano-morphology of lithium-poor Li$_{0.01}$TiO$_2$ and lithium-rich Li$_{0.6}$TiO$_2$ domains with typical diameters of several tens of nm [1,2]. The material serves as an anode material for lithium rechargeable batteries and electro chromic devices.

In principle the approximate position of Li within the structure has been known for a long time in the Li$_{0.5}$TiO$_2$ compound. For the Li-poor anatase phase the position was unknown. Recent investigations using nuclear magnetic resonance [1] prompted us to investigate the position of the Li in both phases. Li is not a strong neutron scatterer, and the very low site occupation calls for an excellent diffractometer in order to observe it inside this two-phase system.

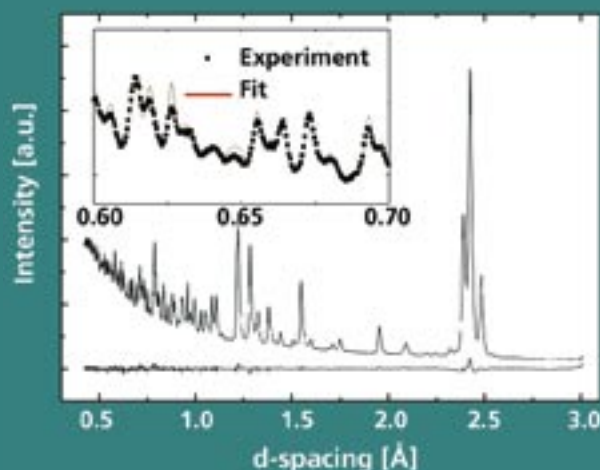The general materials diffractometer (GEM) provides us with simultaneously an unprecedented data acquisition rate, large d-spacing range and very good resolution. These factors make that Li in the Li-poor phase can be successfully located using good resolution and low-noise Fourier maps (such a map presents a real space image of the structure based on a Fourier transform of the diffraction data). Surprisingly the Fourier maps for Li-poor anatase show two Li sites inside the oxygen octahedron located at a distance of 1.8 Å apart. Apparently the distorted and elongated shape of the octahedron makes these two sites possible (Figure 3). Clearly because of Coulomb repulsion and the van der Waals radius of Li both sites in one octahedron will not be occupied simultaneously. Also the Li position in the Li-rich titanate phase appears to be a split one, albeit with a smaller separation ~0.7 Å between the two sites. Here one of the two sites appears to be occupied more than the other. For both structures the positions were checked by including the Li in Rietveld refinements, which yielded very good fits.

To the best of our knowledge the observation of multiple discrete Li sites inside one oxygen octahedral has not been done before. It appears likely, however, that this will be more common for oxides having distorted octahedra that are intercalated with small ions like Li or H. The multiple sites are observed here due to the good resolution in the diffraction patterns as well as in the Fourier maps.

Force field molecular dynamics simulations appear to reproduce the different sites very well. When the temperature is raised the simulations even show the hopping between the sites on a ps timescale (Figure 3). This hopping was also observed experimentally by quasielastic neutron scattering experiments on $Li_{0.6}TiO_2$. It appears that Li is moving on a ps time scale with an activation energy of E_A=5.7 ± 0.3 meV. This work was published in [3].

References:

[1] M. Wagemaker, R. van de Krol, A.P.M. Kentgens, A.A. van Well, F.M. Mulder; J. Am. Chem. Soc., **123** 11454 (2001).
[2] M. Wagemaker, A.P.M. Kentgens, F.M. Mulder; Nature, **418**, 397 (2002).
[3] M. Wagemaker, G.J. Kearley, A.A. van Well, H. Mutka, F.M. Mulder; J. Am. Chem. Soc. **125**, 840 (2003).

5.1 MATERIALS

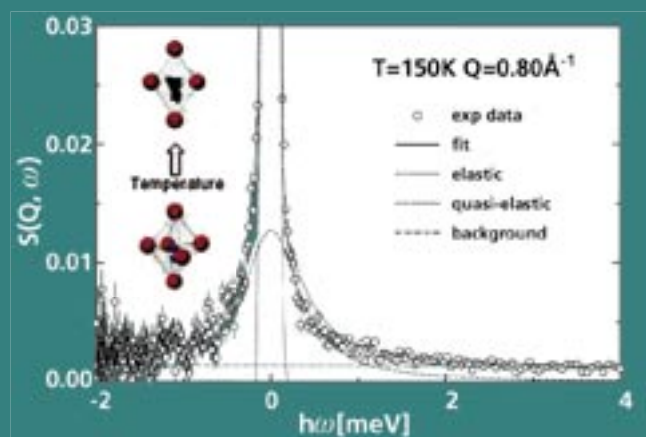**Figure 3**
Right: Quasi-elastic neutron spectrum of $Li_{0.6}TiO_2$ at 150K for momentum transfer Q = 0.8 Å.
The fitted elastic and quasi-elastic contribution are also shown. Left: Li on two positions in the oxygen octahedra. Molecular dynamics simulations reproduce the sites and show the hopping at elevated temperatures.

5.2 MATERIALS

H.G. Schimmel, G.J. Kearley,
F.M. Mulder, IRI-TUD
K.P. de Jong, UU-Debye

For hydrogen storage carbon nanotubes are just bundled rolls of graphite

Figure 1
Pressure-temperature curves for: circles: SWNT, squares: Norit AC, triangles: Fishbone nano fibres

Figure 2
Nanotubes stack in bundles as can be observed using spin-echo small-angle neutron scattering (SESANS). A hydrogen molecule is also shown. Bottom: the diameters of the tubes detemined from XRD and a hydrogen molecule compared to the inter-tube void size.

Single walled carbon nanotubes (SWNT) were reported to have record high hydrogen storage capacities at room temperature, indicating an interaction between hydrogen and carbon matrix which is stronger than known before. Here we present a study of the interaction of hydrogen with activated charcoal, carbon nanofibers and SWNT, that disproves these earlier reports, and indicates why the storage capacities are rather low.

Pressure-temperature curves were used to estimate the interaction potential, which was found to be 580 ± 60 K for SWNT and has similar values for the other materials (Figure 1). The hydrogen storage capacity of these materials correlates with the surface area of the material, with the activated charcoal having the largest. Hydrogen gas was adsorbed in amounts up to 2 wt.% at 1 Bar and only at low temperatures. The SWNT appear to have a relatively low accessible surface area due to bundling of the tubes; the hydrogen does not enter the voids between the tubes in the bundles (Figure 2).

The molecular rotations observed with inelastic neutron scattering (INS) indicate that molecular hydrogen is present, because atomic hydrogen bound to the carbon cannot show such rotations. No significant difference was found between the hydrogen molecules adsorbed in the different investigated materials. This indicates that the binding to the carbon matrix does not influence the hydrogen molecule very much. Such influence is known to occur in compounds where the hydrogen molecule is bonded more strongly to a substrate: the electron density involved in the bonds to the substrate is withdrawn from the H-H bond, which lengthens this bond. The lengthening effect has a pronounced influence on the rotational frequency, i.e. the neutron spectrum. Because the INS spectra are virtually the same there has to be only a weak interaction between hydrogen and carbon, which is in agreement with the macroscopic adsorption measurements. Results from a Density Functional Theory computer calculation show molecular hydrogen bonding to an aromatic C-C bond that is present in the materials investigated.
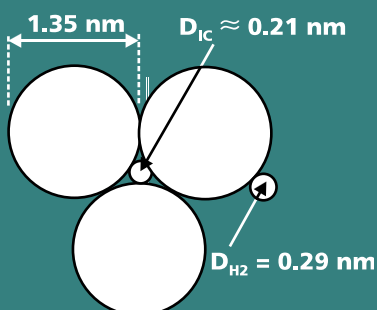
A high-resolution measurement for lower hydrogen loadings (Figure 3) shows that the environments of the hydrogen molecules slightly differ depending on the number of hydrogen molecules in the neighborhood. For low hydrogen coverages on graphite it is known that the hydrogen forms a surface layer commensurate with the carbon hexagons where the distance between the hydrogens is large, i.e. the hydrogens are not touching each other. For higher hydrogen loading the molecules form a layer incommensurate with the C structure and do touch; for even higher loadings a second monolayer will form. The change of the shape of the spectrum is related to the different regimes of hydrogen coverage.

In conclusion the interaction of hydrogen with several nano-structured carbon substrates was shown to be too small to cause large hydrogen adsorption at room temperature. The stacking of nanotubes in bundles limits the accessible surface (Figure 2), making the nanotube adsorption capacity even smaller. The claims of high storage capacities of SWNT related to their characteristic morphology are unjustified.

5.2 MATERIALS
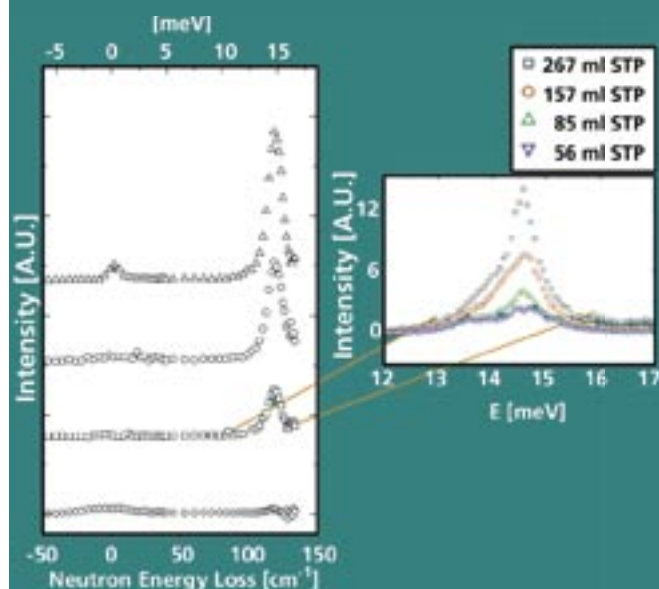
Figure 3
Left: Neutron energy loss spectra of hydrogen adsorbed in Norit AC990293 (triangles), Norit GSX (circles), single walled carbon nanotubes (squares) and graphitic nanofibers. The data are normalized on the number of incoming neutrons. Right: High resolution measurement (TOSCA, ISIS) of four different hydrogen loadings on SWNT.

G.J. Kearley, F.M. Mulder,
O.V. Kruglova, IRI-TUD
S.J. Picken, P.H.J. Kouwer, TUD-DCT
J. Stride, ILL.

Stabilising Self-Assembled Discotic Molecular Electronics

Figure 1
Liquid crystalline phases with increasing molecular order. In order of decreasing temperature:
a) Nematic discotic, b) nematic columnar,
** c) columnar hexagonal.**
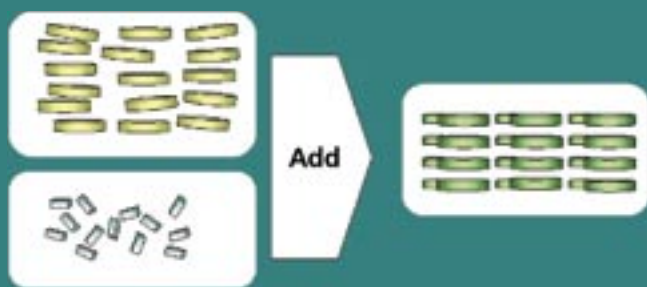
Figure 2
Indicated on the right is the proposed structure in the liquid crystalline columnar phase of the donor-acceptor complex of triphenylene and TNF.
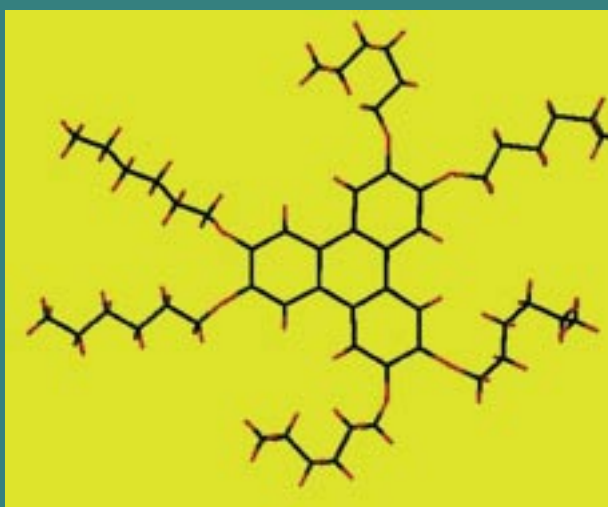
Figure 3
HAT 6 or hexakis(n-hexyloxy) triphenylene.

It is generally thought that rotation of discs is the most important motion in determining the conductivity of discotic materials. Quasielastic neutron scattering combined with molecular dynamics simulations however, shows the translational motion of the disks over each other is more important on the timescale over which the conductivity occurs.

Discotic materials are molecules with planar, disk-like poly-aromatic cores that can self- assemble into "molecular wires". Highly aniso-tropic charge transfer along the wires arises when there is sufficient intermolecular overlap of the π-orbitals of the molecular cores. Discotic materials can be applied in molecular electronics, field-effect transistors and -recently with record quantum efficiencies- photovoltaics [1]. Nevertheless, there is still an order of magnitude difference between the conductivities measured on microscopic and more macroscopic scales, the latter being much smaller. Our aim is to account for this "missing" conductivity, the suspicion being that it arises from a loss of correlation within the columns due to thermal motion of the disks. This problem, and the role of the tails plus charge-transfer inserts make a good study for quasielastic neutron scattering [2].

Materials with mesomorphic properties can be formed, depending on the nature of the hydrocarbon chains that are attached as "tails" to the aromatic cores. In addition to a crystalline phase they often display intermediate liquid crystalline phases prior to melting to the isotropic liquid (Figure 1). The liquid crystalline phases appear to have the best conductivity, while in the crystalline phase results in unwanted tilting of the cores.

Recently, it has been shown that the liquid crystalline columnar hexagonal phases can be stabilised, and tilting of the disks reduced, by adding the acceptor molecules such as TNF (2,4,7 trinitrofluoren-9-one). This extends the range in which efficient charge transfer occurs down to room temperature.

The first part of the study was of HAT6, which is about the simplest discotic system to form liquid crystalline columnar phases. Ideally, the important core motion could be studied by deuteration of the tails, but this deuteration is difficult, so we used a more indirect route: deuteration the 6 core-hydrogens and then subtraction of this spectrum from that of the fully protonated material. The quasielastic spectra revealed motion on two timescales within the range of IN6: 0.2 and 7 picoseconds. However, whilst the intensity of the slower component decreases on core-deuteration, it is too intense to arise only from the core hydrogens, which constitute only 10% of the total. In such complex systems there is motion on almost every timescale and the only reasonable route to understanding

the origin of the two motions observed on IN6 is via a molecular dynamics simulation. A rather simple model (for such a complex system) consisting of a column of 4 discotic molecules (578 atoms) was constructed from which it quickly became clear that the two observed motions are whole-molecule displacements parallel and perpendicular to the column axis.

The more rapid motion corresponds to a sliding of the discs relative to each other whilst the slower motion corresponds to a tilting of the disks out of their formal molecular plane. Interestingly, on the picosecond timescale the motions of the tails and the cores are strongly correlated, the original concept of distinct core and tail motion being incorrect. This is shown in the radial correlation function between a core carbon atom and successive carbon atoms along the alkyl chain (Figure 4). It is also interesting to note that the core-core and tail-tail interactions play an almost equal role in determining the dynamics of the disk. In fact, there is some "entanglement" between tails of successive discs, and consequently, only very limited partial rotation of the disks was seen even on the 1 nanosecond timescale.

In the second part of the study we investigated HMT which has the same triphenylene core as HAT6, but has the simplest possible, $-OCH_3$, tails that are easy to deuterate (FIgure 5). Again, motion on two timescales is found, but perhaps surprisingly, in this simpler system the signal for the slower motion disappears on deuteration of the methyl tails. A molecular dynamics simulation of 4 HMT disks also shows clearly that the slower motion seen on IN6 is associated with torsion of the whole methyl group (including the carbon) around the O-core bond. The measured core motion is about twice as fast as in HAT6, reflecting the slowing down effect of the longer tails. However, on addition of the TNF the charge-transfer complex is formed and the signal from the slow motion becomes too slow to measure on IN6. The faster core-motion slows by more than a factor of 2, to a timescale similar to that of HAT6. The molecular dynamics simulation for HMT with the charge-transfer complex has yet to be done, but it is seems likely that the motion parallel to the column has become too slow to measure, and that the sliding of the disks slows down to the value obtained with the much longer tails of HAT6. One particularly interesting aspect of HAT6 is that just above the melting point in the isotropic liquid phase the measured quasi-elastic signal is not liquid-like, even though all Bragg-peaks are absent. The measured quasi-elastic spectra are similar to those of the columnar phase, though somewhat broader. What does this mean? It transpires that our MD simulation using a single column of 4 discotic molecules agrees better with these "liquid" spectra than with the columnar liquid crystalline phase. The lack of column-column interactions and the limited size of our model seem to provide a good representation of disc-disc interactions that persist into the 'isotropic liquid' phase. This is a correlation over a limited distance and limited time, as evidenced by the lack of Bragg-peaks, and this should not be regarded as "chunks of column" floating around in the liquid.

References:

[1] L. Schmidt-Mende, *et al.*, Science 293, 1119 (2001).
[2] F.M. Mulder, J. Stride, S.J. Picken, P.H.J. Kouwer, M.P. de Haas, L.D.A. Siebbeles and G.J. Kearley, J. Am.Chem.Soc. 125, 3860 (2003).
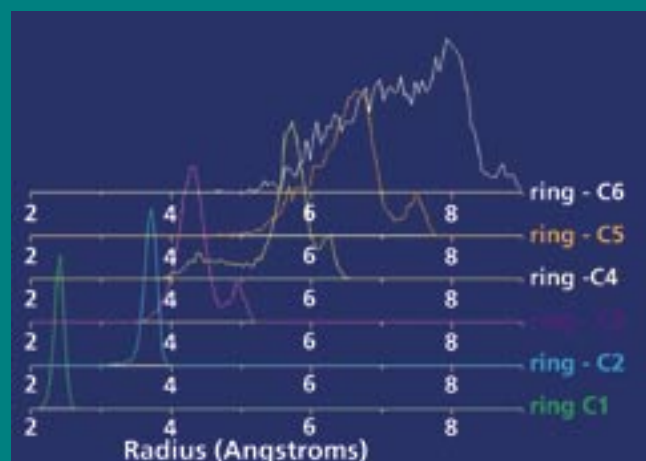
5.3 MATERIALS

Figure 4
Radial correlations between the indicated tail C atoms with the corner of the HAT6 core it is connected to.
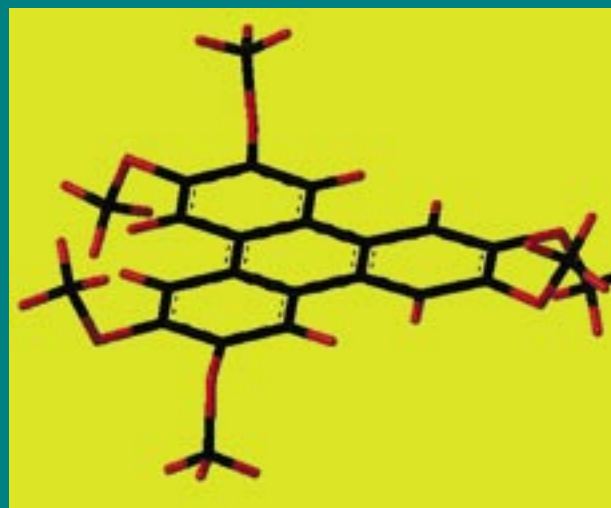

Figure 5
Molecular structure of HMT.

W.T. Fu , D.J.W. IJdo, UL-LIC
D.Visser, NWO

On the crystal structure of the ternary oxides BaTbO₃ and Sr₂SnO₄

Figure 1
A section of high-resolution back- scattering data of BaTbO₃ showing the basic (2 0 0) (~2.14 Å) and (4 0 0) (~1.07 Å) refections

Figure 2
A section of the high-resolution backscattering data of Sr₂SnO₄ at T = 200 K, showing the presence of a weak (1 3 6) superreflection as well as the line broadening of the (0 4 0) reflection. All peaks are indexed in the space group P4₂/ncm.

The resolution capacity of powder neutron diffraction at ISIS facility has been exploited in BaTbO₃ and Sr₂SnO₄ to determine their exact space groups. Diffraction patterns recorded on a high-resolution time-of-flight diffractometer have allowed the recognition of subtle difference between different octahedral tilting patterns. The results demonstrate that this technique is a powerful tool to investigate the crystal structure of oxide materials.

Many distorted perovskites (ABO₃) and the layered variants (A₂BO₄) are due to the cooperative tilting of the BO₆ octahedra. This type of distortions occurs when the ratio of the radii of the A and B-ion, r_A and r_B respectively , do not fullfil the condition of the Goldsmith tolerance factor $t = 1$: $r_{A\text{-}O}/(r_{B\text{-}O}\sqrt{2})$. As the tilting may take place singly or multiply along the different crystallographic axes, a large number of space groups may be generated.

The tilting of the octahedra gives rise not only to the splitting of the main diffraction peaks but also to the possible appearance of additional superlattice peaks due to the enlargement of the unit cell. Although the superlattice reflections may easily be revealed using the powder neutron diffraction technique, identification of the nature of octahedral tilt and, subsequently, the corresponding space group, from the peak shapes is not always straightforward due mainly to the instrument resolution. Examples are BaTbO₃ and Sr₂SnO₄. BaTbO₃ is a distorted perovskite whose structure has previously been assigned to be rhombohedral ($R\bar{3}c$) [1] and orthorhombic (*Pnma*) [2] respectively. The structure of Sr₂SnO₄ is derived from K₂NiF₄-structure, and the space groups *Bmab* and *P4₂/ncm* were reported for the room temperature and the low temperature structure, respectively [3].

In a recent study, high-resolution time-of-flight powder neutron diffraction at ISIS (HRPD) was used to investigate the structures of BaTbO₃ and Sr₂SnO₄. For BaTbO₃, the *Pnma* model could be rejected right away since no reflections resulted from the coupled in phase tilting around the pseudo cubic $[100]_p$ axis were detected. Figure 1 shows a section of high-resolution backscattering data and the comparison of three possible models corresponding to the TbO₆ tilting around the three principle cubic axes: $R\bar{3}c$ ($[111]_p$), *Imma* ($[110]_p$), and *I4/mcm* ($[111]_p$). The space group $R\bar{3}c$ is not consistent with the observed profiles, since the basic (400) ($d \approx 1.07$ Å) reflection is asymmetric due to splitting. Further, the basic (2 2 2)
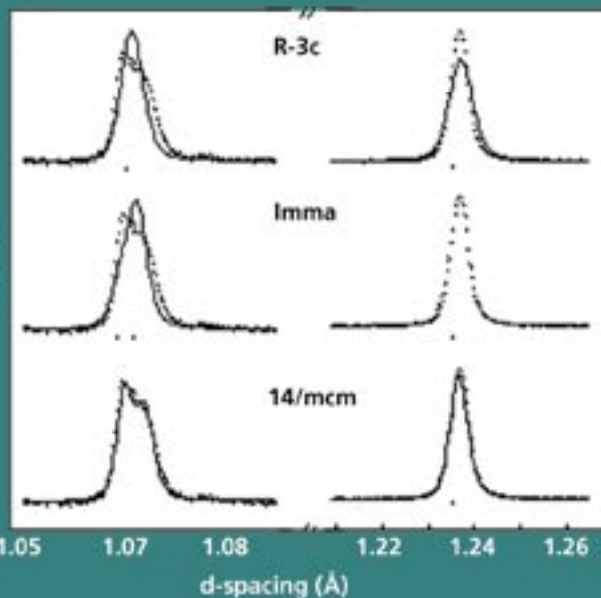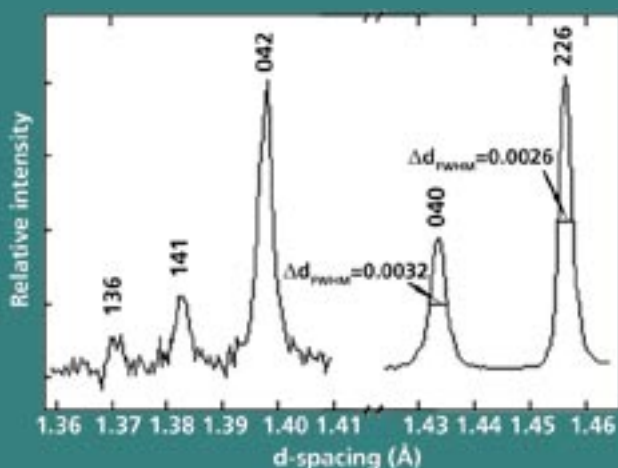
diffraction ($d \approx 1.236$ Å) does not split within the instrument resolution, suggesting a tetragonal or a pseudo-tetragonal structure. The refinements carried out in both *Imma* and *I4/mcm* models have, however, confirmed the tetragonal structure; the weighted R-values are R_{wp}(*I4/mcm*) = 4.48 % and R_{wp}(*Imma*)= 6.08 % respectively. This result supports the conclusions that the space group $R\bar{3}c$ is unlikely adopted by the $A^{2+}B^{4+}O_3$-type perovskites due to the decrease of Coulomb energy stabilization in $R\bar{3}c$ with respect to the other tilt systems, when decreasing the charge of A-cation [4].

In the case of Sr_2SnO_4, neither the space group *Bmab* nor *P4₂/ncm*, corresponding to the SnO_6 octahedral tilting around the tetragonal $[110]_T$ and $[010]_T$ axis respectively, describes correctly the observed high-resolution diffraction data recorded between 4 K and 300 K (see Figure 2). For example, a weak superreflection ($d \approx 1.37$ Å), which is indexed as (1 3 6) in *P4₂/ncm*, is present, and it is not allowed in the space group *Bmab*. On the other hand, the (0 4 0) diffraction shows a noticeable line broadening as compared to that of the (2 2 6) diffraction, indicating the presence of the orthorhombic strain. The structure of Sr_2SnO_4 was, therefore, modeled with the subgroup group *Pccn,* in which the SnO_6 tilted around both $[100]_T$ and $[010]_T$ axis with non-equal tilts. The refinements resulted in a superior fit of the neutron powder diffraction data at all measured temperatures [5].

It is worth noting that the previous refinements, using only the space groups *Bmab* and *P4₂/ncm*, do support one structure model over the other at different temperatures [3]. A first-order phase transition is thus predicted below the room temperature. This may arise from the systematic change of the tilting angles in Sr_2SnO_4. Figure 3 shows the temperature dependent tilting angles of α (around the $[100]_T$ axis) and β (around the $[010]_T$ axis) in the space group *Pccn*. As can be seen, α is quite small and remains virtually constant, but β is fairly large and increases with decreasing temperature. When the difference between α and β is relatively small, e.g. at room temperature, the *Bmab* model leads to a superior fit. At low temperature, however, the difference between α and β becomes larger. The space group *P4₂/ncm* resulted in a better fit despite the presence of orthorhombic strain. Thus, the observed apparent phase transition may well be accidental.

References:

[1]   A.J. Jacobson, B.C. Tofield, B.E.F. Fender, Acta Crystallogr., Sect. B, **28**, 956 (1972).

[2]   K. Tezuka, Y. Hinatsu, Y. Shimojo, Y. Morii, J. Phys.: Condens. Matter, **10**, 11703 (1998).

[3]   M.A. Green, K. Prassides, P. Day and J.K. Stalick. J. Chem. Soc., Faraday Trans., **92**, 2155 (1996).

[4]   W.T. Fu, D. Visser and D W. J. IJdo. J. Solid State Chem. **165**, 393 (2002).

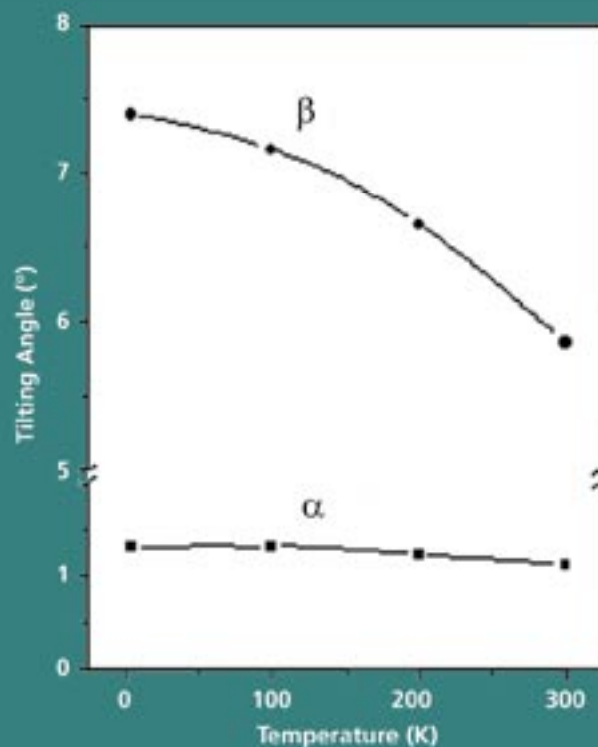[5]   W.T. Fu, D. Visser and D.W.J. IJdo. J. Solid State Chem. **169**, 208 (2002).

Figure 3
Tilting angles of α and β in Sr_2SnO_4 at different temperatures.

**A.M. Mulders, C.T. Kaiser,
P.C.M. Gubbens, IRI-TUD
A. Amato, PSI
F.N. Gygax, A. Schenck, ETH
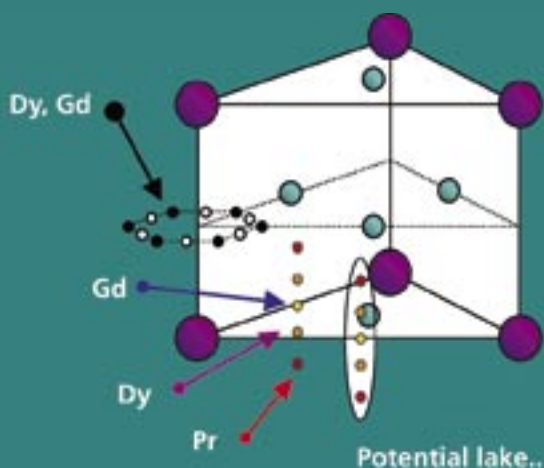P. Dalmas de Réotier, A. Yaouanc, CEA
K.H.J. Buschow, A.A. Menowsky, UvA**

Muon location and quantum hopping in GdNi$_5$ and DyNi$_5$

Figure 1
Unit cell of RNi$_5$. The muon localises at the 3f or 6i site in the whole temperature range and also below ~80 K in either the 6m (0.13, 0.26, 0.5) or 6k (0.225, 0, 0.5) sites in GdNi$_5$ and DyNi$_5$ (the potential lake). The muon occupies all latter six sites within the time range of the experiment. This result suggests that the muon forms an extended localised ring-shaped orbit (6$_{ring}$).

RNi$_5$ materials are very good as storage material for hydrogen. Moreover, this material is also the base for so-called Ni-H batteries. In GdNi$_5$ and DyNi$_5$, the hydrogen-like muon localises at the 3f (0, 0.5, 0) and 6i (0, 0.5, 0.1) interstitial sites, respectively. Below ~ 80K a second muon site becomes populated, the metastable 6$_{ring}$ site. We determine the mean residence time of the muon in this ring site and analyse its temperature dependence with a multi-phonon quantum diffusion process.

The RNi$_5$ compounds (with R a rare earth) have the hexagonal CaCu5 structure as shown in Figure 1. Its magnetic behaviour is well described by crystal field theory. Single crystals of GdNi$_5$ and DyNi$_5$ were prepared by the Czochralski method in Amsterdam from starting materials of at least 99,99% purity. The samples have been cut into a spherical shape in order to cancel the Lorentz and demagnetisation fields. The μSR spectra were taken with B$_{ext}$ = 0.6 T at temperatures between 15 K and 270 K with the a, $a*$ and c axis parallel to the external field. In addition angular scans in the $aa*$ plane and ac plane have been taken.

The muon, which is a spin ½ particle, localises at an interstitial site of the host crystal lattice. The local magnetic field it experiences, B_{loc}, causes the muon spin to precess with an angular frequency ($\omega = \gamma^{\mu} B_{loc}$, where γ^{μ} is the gyromagnetic ratio of the muon). The muon experiences a local field which is the sum of the external field and a field due to the 4f moments of the host. The relative frequency shift, $K^{\alpha}_{4f} = (B^{\alpha}_{loc} - B_{ext})/B_{ext}$, is proportional to the susceptibility of the host along the α direction. The coupling between the 4f moments in the host and the muon at its interstitial site is mainly of dipolar origin. Moreover, $K^{\alpha}_{4f} = (A^{\alpha\alpha}_{dip} + A_{con}) \chi^{\alpha}_{4f}$ with χ_{4f} the measured magnetic susceptibility in the different directions of the single crystal. By calculating the dipolar term $A^{\alpha\alpha}_{dip}$ for a wide variety of crystallographic positions the muon sites can be found. A_{con} is isotropic and the Fermi hyperfine field of the conduction electrons.

In Figure1 the muon sites at the 3f site (GdNi$_5$) [1] and the 6i sites (PrNi$_5$ [2] and DyNi$_5$ [3]) are indicated. Apparently, the difference in energy for the muon to localise at the 3f and 6i sites is not very

large. Therefore, this area in the crystal can be regarded as a potential lake as shown in Figure 1. Moreover, below T = 80 K in $GdNi_5$ and $DyNi_5$ a second metastable muon site (6_{ring}) is observed. This site shows no angular dependence, indicating a high symmetry. From dipolar calculations we find an average for the 6*m* or 6*k* sites, forming an hexagon around the (0, 0, 0.5) position as shown in Figure 1. Determination of the hydrogen sites by neutron techniques coincide partly with the muon allocations [3]. Since analysis with a simple exponential muon depolarisation fails to describe the muon occupation across the two muon sites, the transverse μSR spectra taken around and below 80 K have been reanalysed taking into account the hopping of muons from the 6_{ring} site to the 3*f* and 6*i* sites in $GdNi_5$ and $DyNi_5$, respectively. The average residence time of the muons at the 6_{ring} site, τ_{ring}, has to be taken in account [3].

As the damping rate of the 6*i* site in $DyNi_5$ increases rapidly below 100 *K* and the 6*i* signal becomes difficult to observe, the fits are not sensitive to τ_{ring} but mainly to $\lambda'_{ring} = \lambda_{ring} + 1/\tau_{ring}$, in which λ_{ring} is the relaxation rate. We introduce $\tau'_{ring} = 1/\lambda'_{ring}$ which is plotted as function of l/T in Figure 2.

The solid curve in Figure 2 is a fit to multi-phonon induced muon tunneling. Multi-phonon processes equalise for an extremely short time (10^{-13} s) at the local energy levels of the potential well where the muon is localised. When this occurs the muon can tunnel through the energy barrier between the two sites. Within the framework of the small polaron theory we use the formula shown in Figure 2, where E_a is the coincidence energy needed to equalise the energy levels of both potential wells and J the tunneling matrix element (Fermi's golden rule) which can be seen as a bandwidth. We get E_a = 400(20) K and J = 0.21(7) meV. A comparison of these values with the results obtained on $GdNi_5$ (E_a = 272(10) *K* and J = 0.11(2) meV (the dotted curve in Figure 2) show that the potential well of the 6*i* site is deeper than the 3*f* site with respect to the 6_{ring} site.

References:

[1] A.M. Mulders *et al.,* J. of Alloys and Comp.**454**, 330 (2002).

[2] R. Feyerherm *et al.,* Z. Phys. B: Cond. Matter **99**, 389 (1995).

[3] A.M. Mulders *et al.,* Phys. Rev. B **67**, 014303 (2003).

Figure 2
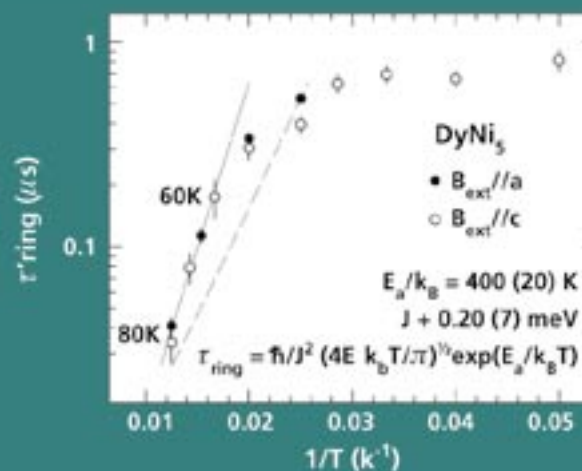τ'_{ring} as deduced with the equation described in Reference 3 from the spectra taken in the transition region. At high temperature (60 K < T < 80 K) λ_{ring} » 0 and τ_{ring} can be determined. At lower temperature the critical slowing down of the Dy moments dominates. For comparison the residence time at the 6_{ring} site in $GdNi_5$ is shown as a dotted line.

C.T. Kaiser, V.W.J. Verhoeven,
P.C.M. Gubbens, F.M. Mulder,
I.M. de Schepper, IRI-TUD
A. Yaouanc, P. Dalmas de Réotier, CEA
E.M. Kelder, J. Schoonman, TUD-DCT
S.P. Cottrell, ISIS

Li mobility in the battery cathode material $Li_x[Mn_{1.96}Li_{0.04}]O_4$: a technological application of μSR

The common use of rechargeable batteries as power supplies means that it is important for them to be cheap, light and environmental friendly, properties shown by the newly developed battery which uses $Li_x[Mn_{1.96}Li_{0.04}]O_4$ as the cathode material. We have characterised the Li^+ mobility in $Li_x[Mn_{1.96}Li_{0.04}]O_4$ with the zero-field muon spin depolarisation technique. The results suggest that the battery could be recharged more efficiently above room temperature than at room temperature as is usually done.

There is an increasing demand for new batteries with good rechargeable properties, and research into materials, which are harmless to the environment, is ongoing.

Materials of the composition $Li_x[Mn_{2-z}Li_z]O_4$ with the cubic spinel structure are very promising as cathodes for Li batteries. In combination with boronphosphate as the intermediate solid electrolyte and carbon or B_2CN as the anode, these materials form excellent solid state rechargeable batteries, fulfilling all the requirements mentioned above. They are based on the transport of Li ions, which are light and give a high power density. Since compounds of the type $Li_x[Mn_{2-z}Li_z]O_4$ are ceramics, they give access to an interesting temperature range from 320 K up to at least 380 K.

As shown in Figure 1 the flow of Li^+ ions induces a voltage difference between the anode and cathode of the battery when it is used as a power supply. The battery operates between the $x = 0.2$ ('charged') and $x = 1$ ('empty') states. The x refers to the degree of occupation of the regular Li sites. Pure $LiMn_2O_4$ ($x = 1$, $z = 0$) contains equal amounts of Mn^{3+} and Mn^{4+} ions. It undergoes a phase transition at 290K attributed to a cubic to tetragonal structural transition driven by a co-operative Jahn-Teller distortion mechanism around the Mn^{3+} cation sites, and this makes it unsuitable as a cathode because of the bad cycling performance. Small Li substitution on to Mn sites gives rise to an increase in Mn^{4+} concentration and subsequently a small decrease in Mn^{3+} concentration, leading to an increased stability of the cubic spinel structure.

$Li[Mn_{1.96}Li_{0.04}]O_4$ does not exhibit a structural phase transition, and this makes it very suitable as a cathode material. On the other hand, for efficient operation of the cathode, the amount of Li substitution, i.e. the amount of Mn^{4+} ions, must be restricted.

To optimise $Li_x[Mn_{2-z}Li_z]O_4$ for use as a cathode material, the Li^+ mobility ion for different x and z values needs to be known. Therefore we have performed a detailed investigation of the Li^+ ions behaviour with the zero-field muon spin relaxation (μSR) technique for $x = 1$ and $x = 0.2$ with $z = 0.04$ [1]. The μSR measurements
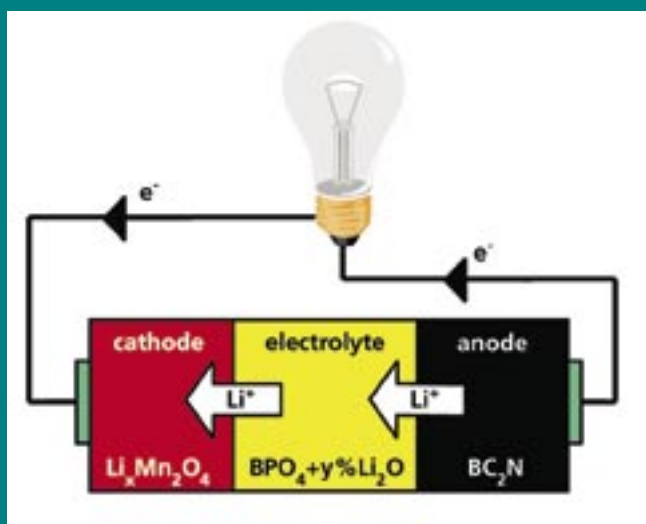

Figure 1
Principle of a battery based on the cathode material $Li_xMn_{1.96}Li_{0.04}O_4$ working as a power supply.

were done at the EMU and MuSR spectrometers of the ISIS facility. Above 100K, the muon depolarisation function could be fitted by the product of an exponential relaxation function with the so-called dynamical Kubo- Toyabe function. The exponential component is due to the relaxation on the Mn magnetic moments; it is relatively small and temperature independent. The depolarisation is mainly due to the quasi-static field distribution induced at the muon site by the nuclear magnetic moments of Li and Mn. The distribution is characterised by its variance Δ^2.

As shown in Figure 2, Δ drops by $\approx$ 35% between 230 K and 300 K for $Li[Mn_{1.96}Li_{0.04}]O_4$. For $Li_{0.2}[Mn_{1.96}Li_{0.04}]O_4$ the drop of Δ is even larger but starts at $\approx$ 300K. This thermal dependence of Δ cannot be a muon diffusion effect; in fact the muon is quasi-static for both compounds in the whole temperature range investigated. The decrease of Δ can only be understood if we suppose that some of the Li^+ ions do not contribute any longer to the depolarisation. This means that, as the temperature is raised, some of the Li^+ ions diffuse and their contribution to the muon depolarisation is motionally narrowed. A quantitative discussion of the magnitude of Δ supports our interpretation.

We performed some measurements up to 600 K. In Figure 3 we compare two spectra recorded at 300 K on $Li_{0.2}[Mn_{1.96}Li_{0.04}]O_4$. One spectrum was taken before heating the compound above 300 K. The other spectrum was recorded after the material had been heated up to 600 K. Clearly the two spectra are different. The observed irreversibility is not surprising since it is known that a structural phase transition occurs at $\approx$ 490K. We have checked that no irreversibility effect occurs if the two compounds ($x = 0.2$ and $x = 1$) are heated only up to 380 K.

In contrast to the Li^+ ion behaviour, the muon is quasi-static in the whole temperature range investigated. This rather surprising result is understood if the diffusing particle passes through a bottleneck in the transition state as for example if it has to squeeze through the lattice from one interstitial state to the next. Then the lighter particle has the higher activation energy and so may not diffuse as fast as the heavier particle.

In conclusion we have discovered that the onset of Li^+ diffusion in $Li[Mn_{1.96}Li_{0.04}]O_4$ occurs at 230 K and for $Li_{0.2}[Mn_{1.96}Li_{0.04}]O_4$ at 300 K, i.e. just above room temperature. This latter result suggests that the battery could be recharged more efficiently above 340 K than at room temperature as usually done since, according to Figure 2, the Li^+ ions start to diffuse above 300 K. However, the temperature should not be too high to avoid irreversibility effects. Quite remarkably, for our study we did not need a single crystal sample. In fact our sample was quite close to the cathode material which will be used in commercial batteries.

References:

[1] C.T. Kaiser, V.W.J. Verhoeven, P.C.M. Gubbens, F.M. Mulder, I.M. de Schepper, A. Yaouanc, P. Dalmas de Réotier, S.P. Cottrell, E.M. Kelder, J. Schoonman, Phys. Rev. B, **62**, 9236 (2000).
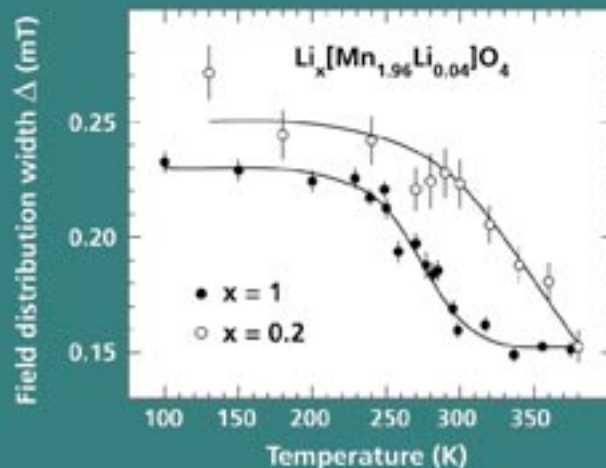
Figure 2
Kubo-Toyabe linewidth D measured up to 380K for $Li[Mn_{1.96}Li_{0.04}]O_4$ and $Li_{0.2}[Mn_{1.96}Li_{0.04}]O_4$. The solid lines are guides to the eye.
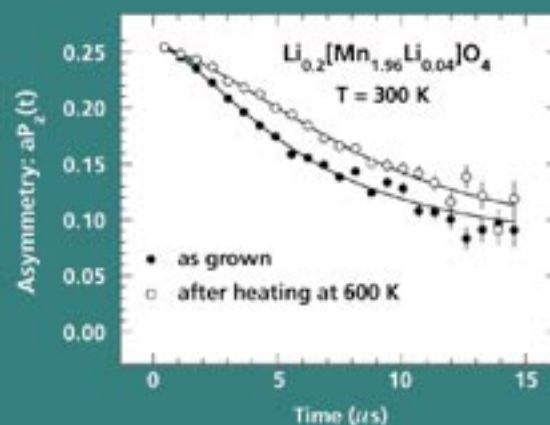
Figure 3
Comparison of two mSR spectra of $Li_{0.2}[Mn_{1.96}Li_{0.04}]O_4$ measured in zero field at 300K. The solid lines are fits to the data.

A. Ramzi, TUE-DPI
K. Hirschberg, R. Sijbesma and
B. Meijer, TUE

Structural properties of helical self-assembled polymers with hydrogen-bonding

Figure 1
Columnar arrangement of the monofunctional and bifunctional compounds.

The term 'polymer' is usually reserved for long chains or networks of monomers connected by covalent bonds. When non-covalent interactions, such as hydrogen bonds, are used to link the monomers, the polymerization process is reversible, and materials with novel properties emerge. Because they are specific and directional, hydrogen bonds are particularly useful interactions for the formation of reversible polymers [1,2]. Small-angle neutron scattering (SANS) have been used to investigate the structural properties and the conformation of these aggregates. The effects of concentration and temperature on the self-assembled polymers have been studied in different solvents. It was found that the length of the columns increases with the concentration and becomes less sensitive above a certain value, while the radius of the cylinders remains almost constant.

In this paper we are presenting a highly organised self-assembled polymer, which consists of bifunctional ureidotriazine units (compound 1) connected via a hexamethylene spacer. The molecules associate via quadruple hydrogen bonds of the ureidotriazine functional groups to form polymeric architectures. In order to introduce a second level of organisation in these structures, we have investigated the possibility of obtaining columnar order by π–π-stacking of trialkyloxyphenyl substituted s-triazine- bifunctional molecules with extended π–π -surfaces. In bulk and in alkane solvents, the polymers form highly organised superstructures with a columnar architecture, which persists in isotropic solution.

Both monofunctinal (2) and bifunctional (1) compounds 1 and 2 are thermotropic (between -26 °C and 178 °C and -30 °C and 180 °C respectively) as well as lyotropic in alkanes. Optical microscopy and X-ray diffraction have shown that both bifunctional compounds have a discotic hexagonal ordered (D_{ho}) structure. X-ray data are only compatible with a structure in which the molecules are folded, with the two functionalities of each molecule residing in adjacent discs of the same column (Figure 1).

Small angle neutron scattering experiments prove the presence of the columnar architectures in deuterated dodecane solutions for both 2 and 1a. In deuterated chloroform no large particle scattering is observed for 2, since the monofunctional molecules only exists
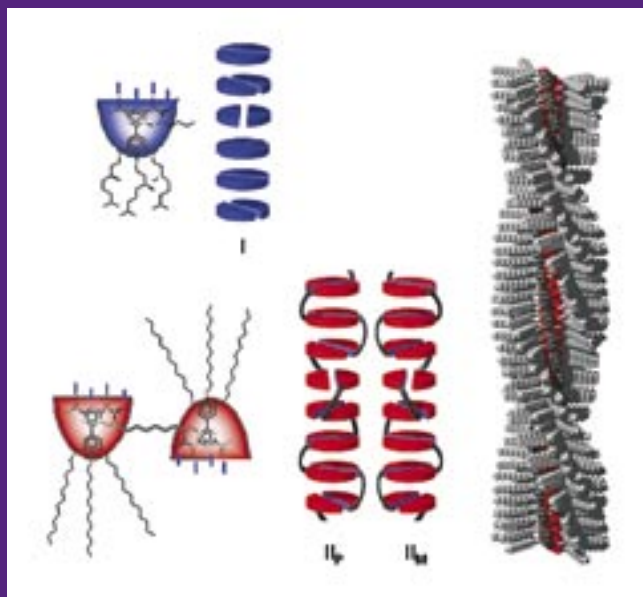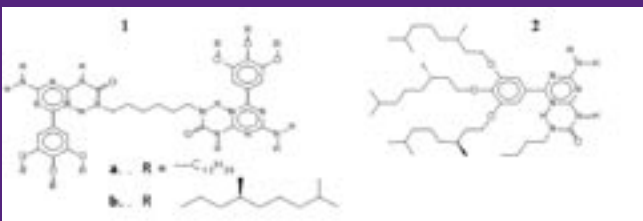
as dimers[3]. The scattering patterns obtained for compound 2 in deuterated dodecane solutions, however, indicate the presence of assembled particles and these patterns have been fitted by the cylindrical-like form factor. The radius of the columns is 15 (± 1) Å and independent on concentration, matching nicely with a column built up of stacked dimerised monofunctional molecules. The length of the colums is concentration dependent and increases from 100Å for a 0.2 wt.% solution to 190 Å for a 1.0 wt.% solution (˜60 molecules). The scattering patterns of 1a in dodecane have also been fitted with the cylindrical form factor, although the interpretation of the data at higher concentrations is hampered by inter-columnar interactions (i.e. gelation). The constant radius of the cylinders is 17 (±1) Å, somewhat larger than for monofunctional molecules which is in agreement with the difference in side-chain lenght of (a) and (b). In Figure 2 the results are given for a chain-stopper experiment; monofunctional molecules 2 has been mixed with bifunctional 1a in deuterated dodecane, while maintaining a constant 0.5 wt. % concentration. The radius of the columns slowly changes from 17 to 15 Å as expected, but the length decreases rapidly after additon of small amounts of monofunctional molecules, showing the formation of shorter and less stable columns than pure bifunctional 1a. The length of the columns is shorter for 2 due to the absence of the supramolecular polymeric backbone.

At elevated temperatures (~ 100 °C) the scattered intensity from the monofunctional compound in 0.96% (v/v) solution in dodecane decreases strongly, indicating the dissociation of the aggregates and the molecules only exist as dimers similar as in chloroform at room temperature, because the π–π-stacking is overcome (Figure 3).

References:

[1] J.-M. Lehn, Makromol. Chem. Makromol. Symp. **69**, 1 (1993).
[2] R.P. Sijbesma, Beijer, F.H., Brunsveld, L, Folmer, B.J.B., Hirschberg, J.H.K.K., Lange, R.F.M., Lowe, J.K.L., Meijer, E.W., Science **278**, 1601 (1997).
[3] J.H.K.K. Hirschberg, Brunsveld, L, Ramzi, A., Vekemans, J.A.J.M., Sijbesma, R.P., Meijer, E.W., Nature **407**, 167 (2000).

6.1 SOFT-CONDENSED MATTER
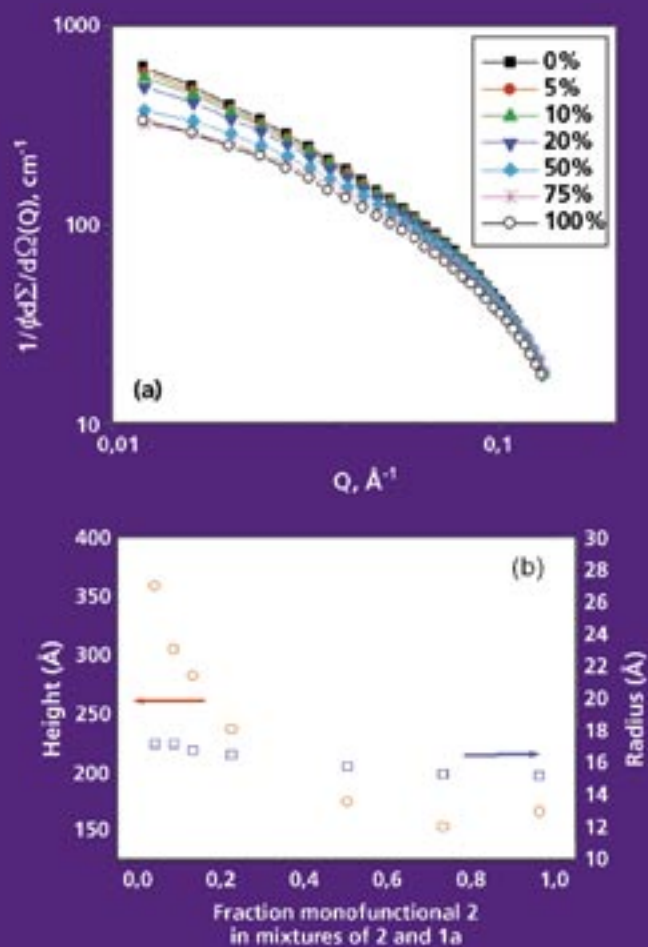
Figure 2
(a) Scatteirng patterns in log-log plot from mixtures of monofunctional (2) and bifunctional (1a) molecules as a function of the added monofunctional fraction at a constant total weight percentage of 0.5 %. (b) Dependence of the height (circle) and the radius (square) of the self-assembled columns.
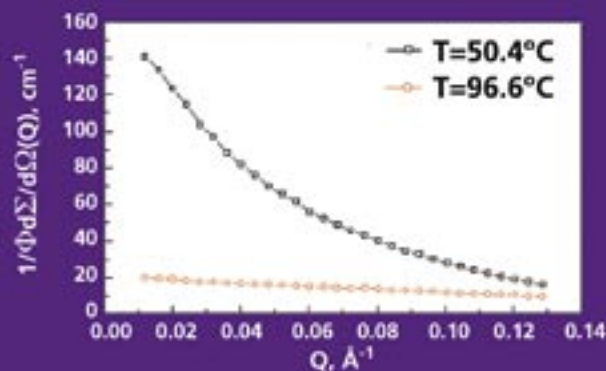
Figure 3
Temperature effect on the scattered intensity from monofunctional (1b) solution in dodecane at 0.96% (v/v) concentration.

**T.V. Krouglov, W.G. Bouwman,
J. Plomp, M.Th. Rekveldt, IRI-TUD
G.J. Vroege, A.V. Petukhov,
D.M.E. Thies-Weesie, UU-Debye**

Hard-sphere colloids studied by Spin-Echo Small-Angle Neutron Scattering
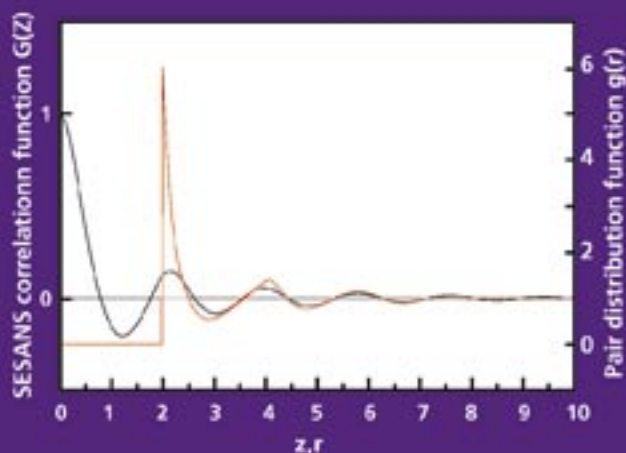
Figure 1
Comparison of SESANS correlation function with pair distribution function in real space.
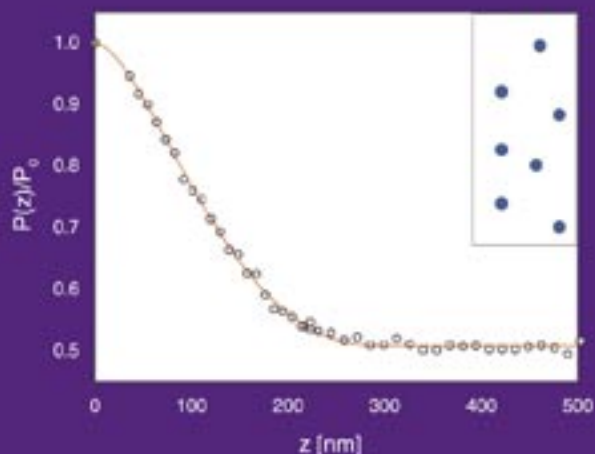
Figure 2
Dilute hard sphere colloid. Open circles - experiment. Solid line - fit. No correlations beyond the diameter of the spheres (300 nm).

The structure of hard sphere colloidal suspensions is measured at different concentrations using recently developed Spin-Echo Small-Angle Neutron Scattering (SESANS). SESANS measures correlations directly in real space.

The study of structure on the length scale of a hundred nanometers and bigger using neutron scattering is an extremely challenging task. For conventional scattering access to higher length scales requires beam collimation and leads thus to a loss of neutrons. Spin-echo small-angle neutron scattering (SESANS) (see the contribution of Bouwman et al. and references therein) circumvents this problem [1]. A significant difference of SESANS compared to conventional scattering techniques is that the former measures a real-space function. Numerical calculations showed that the SESANS correlation function is highly sensitive to the shape and size of particles [2,3]. An explicit connection with the particle correlation function allows to calculate SESANS correlation function for dilute spherical particles analytically [4].

The SESANS correlation function is a 2D projection of conventional correlation function. The behavior of the SESANS correlation function has a lot of similarities with that of conventional correlation function, so the analysis of SESANS signal basically reduces to the analysis of the corresponding conventional correlation function. Figure 1 shows an example how the pair distribution function and SESANS correlation function can be compared in real space.

A suspension of silica particles dissolved in deuterated cyclohexane was used as a model hard sphere system. Three concentration regimes were studied: dilute, semidilute and concentrated. The dilute suspension is the system of noninteracting particles. There is no correlation beyond the maximum size of a particle. As can be seen from Figure 2, there is a saturation level reached at the diameter of spheres (300nm). This constitutes the fact that there is no correlation between particles and they can be considered noninteracting. The fit determines two parameters independently: the radius of the particles and the total scattering probability, which is equal to the saturation level of the SESANS correlation function.

In order to observe the appearance of pair correlations between particles the semidilute solution was used as shown in Figure 3. In that case we have to take into account pair correlations, described by the pair distribution function. The first minimum arises from the excluded volume effect. For a semidilute solution three parameters can be determined simultaneously: the radius of the particles, their concentration and their scattering cross section.

The concentrated solution was used to observe the crystallisation process as a result of sedimentation induced by gravity. The top and the bottom curves in Figure 4 correspond to the top and the bottom part of the sediment. The saturation levels being proportional to the volume fraction are the same for the top part and the bottom part of the sample, which implies that the volume fraction of the colloid does not change with height. This suggests that the sample reached its maximum packing fraction. The calculated curves for random hexagonal close packed lattice, which is expected in case of hard spheres, and for a glass are superimposed in experimental data in both graphs. These graphs show that the top part of the sample develops much more pronounced crystalline ordering than the bottom part even being at the same concentration.

SESANS measurements on a hard sphere colloid demonstrate very good agreement with the theoretical curves for noninteracting spheres, a hard sphere liquid and a random hexagonal close-packed lattice. SESANS is demonstrated to be a powerful tool to study colloids [5].

References:

[1] M.Th. Rekveldt, W.G. Bouwman, W.H. Kraan, O. Uca, S. Grigoriev, S.Habicht, T.Keller, Neutron Spin Echno vol. **601** of Lecture Notes in Physics 87 (2003)
[2] W.G. Bouwman, M.Th. Rekveldt, Physica B **126**, 276 (2000)
[3] O. Uca, W.G. Bouwman, M.Th. Rekveldt, J.Appl.Cryst. **36** 109 (2003)
[4] T.V, Krouglov, I.M. de Schepper, W.G. Bouwman,M.Th. Rekveldt, J.Appl.Cryst. **36** 117 (2003)
[5] T.V. Krouglov, W.G. Bouwman, J. Plomp, M.Th. Rekveldt, G. J. Vroege, A.V. Petukhov, D.M.E. Thies-Weesie, J.Appl.Cryst., **36** 1417 (2003).

6.2 SOFT-CONDENSED MATTER
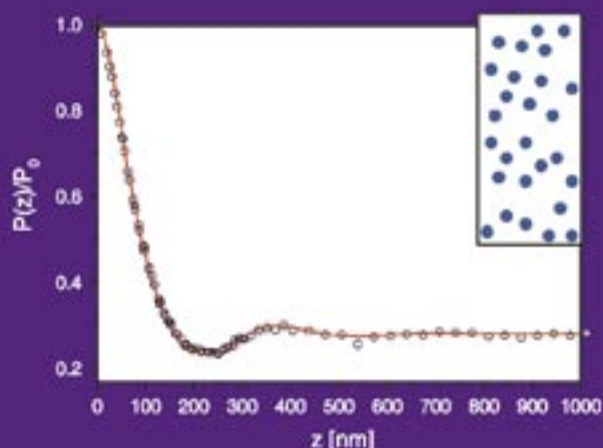
Figue 3
Semidilute hard sphere colloid. Open circles – experiment. Solid line – calculated curve for hard sphere liquid using Percus-Yevick equation.
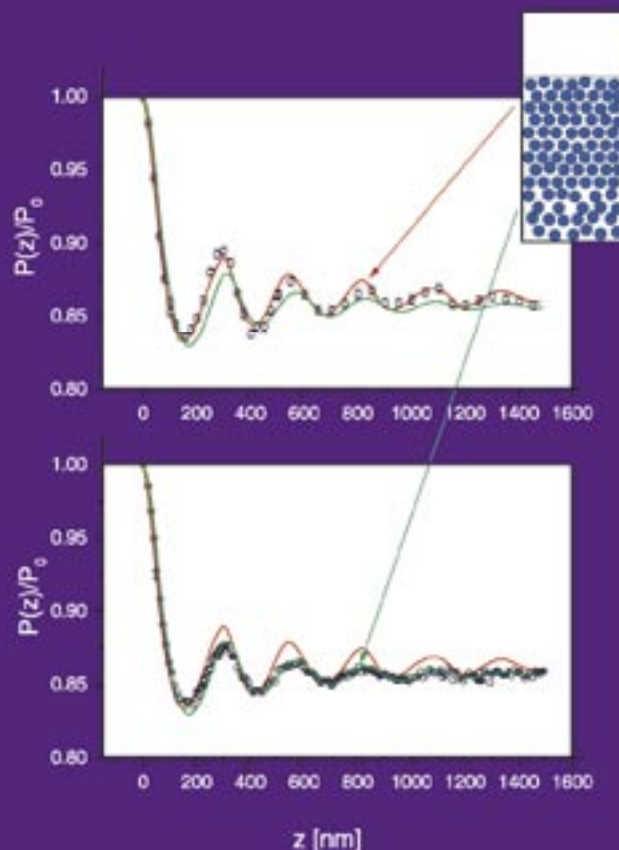
Figure 4
Top, circles: concentrated hard sphere colloid, top of the sediment. Bottom, circles: concentrated hard sphere colloid, bottom of the sediment. Green line - theoretical curve calculated using the Percus-Yevick equation correction. Red line - theoretical curve calculated for a random hexagonal close packed structure.

M.A. de Graaf, E.L.F. Nies,
C. Bastiaansen, TUE
A. Ramzi, TUE-DPI

Rayleigh scattering in amorphous polymeric glasses as seen by SANS
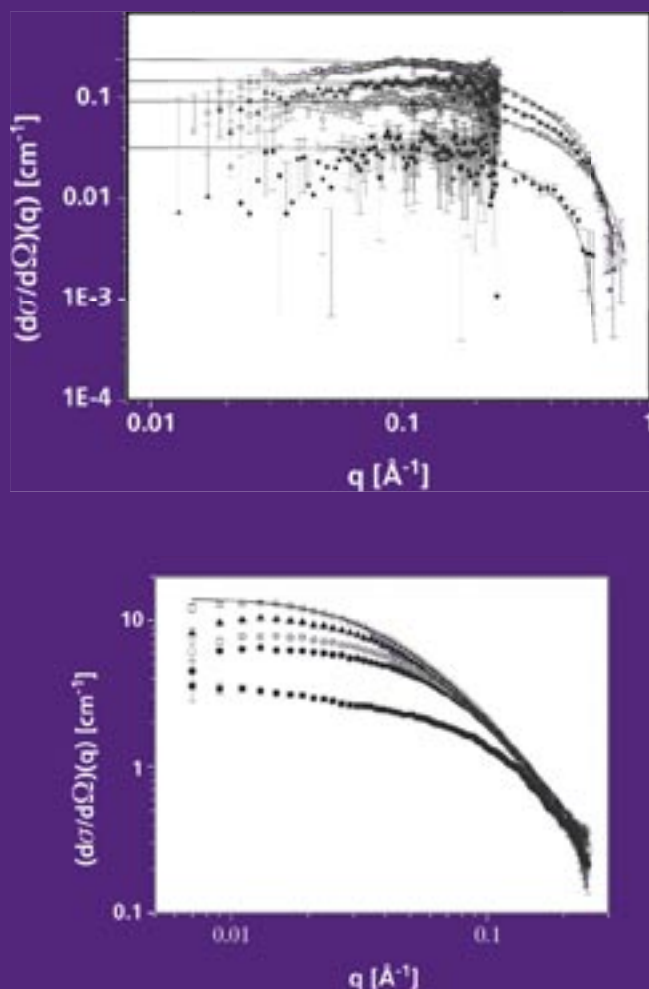
Figure 1
Coherent small-angle neutron scattering curves plotted on a double logarithmic scale for the PMMA-d_8/DPSO system for compositions comprising a volume fraction DPSO 0.05 (■), 0.10 (●), 0.14 (▲) and 0.21 (■) (top); Coherent scattering cross section of PMMA-d_8/ PTFPMA 73/27 v/v blend at various temperatures; 30°C (■), 160°C (●), 170°C (●), 180°C (▲) and 190 °(■) (bottom). Solid lines are fits by the Ornstein-Zernike model.

Small angle neutron scattering was applied to measure the intrinsic additional Rayleigh scattering originating from composition fluctuations of polymer-dopant systems, copolymers and polymer blends. The experimental results show that in accordance with theoretical expectations, for specific polymer-dopant and copolymer systems the additional Rayleigh scattering loss is very small. Therefore, these materials are suitable to be used in low-loss polymer optical devices.

Polymeric optical waveguides such as fibres, backlights and beam splitters are increasingly used to guide light in a wide variety of applications. Apart from homopolymers, ever more copolymers, polymer blends and doped polymers are used in order to tune the properties of the polymeric waveguides. A striking example is the preparation of graded index polymer optical fibres (GI-POFs) with a high bandwidth. Several techniques to obtain a parabolic-like refractive index profile in a POF, based on for example polymer-dopant systems [1], copolymers [2] or miscible polymer blends [3] have been suggested.

The use of copolymers, polymer blends or doped polymer systems often results in a high attenuation due to additional Rayleigh scattering originating from composition fluctuations. Dettenmaier [4] derived theoretically that the excess Rayleigh scattering due to concentration fluctuations in polymer blends and copolymer systems can be kept small once the proper conditions are met, i.e. a small refractive index mismatch and a large negative Flory-Huggins interaction parameter (χ_{FH}) between both components. Unfortunately, experimental data to verify the theoretical predictions were not available. The excess Rayleigh scattering in blends, copolymers and doped systems was therefore investigated, with an emphasis on the combination of theory and experimental verification using specific model systems.

As model systems, specific copolymers, miscible polymer blends and polymer-dopant systems were used. Several small-angle scattering techniques can be applied to determine the Rayleigh scattering in polymer systems, e.g. small-angle static light-, X-ray- and neutron scattering [3]. Because of the long wavelengths applied in light scattering experiments, this technique is especially sensitive to extrinsic causes of scattering, such as dust and orientation in the samples. The prime motivation for choosing small-angle neutron scattering to study the scattering behaviour of the model systems was the possibility to perform absolute intensity measurements routinely and because of the relatively straightforward sample preparation [6].

Small Angle Neutron Scattering (SANS) experiments were performed at the LOQ instrument at ISIS. Typical examples of SANS-curves of some of the model systems measured in this study

are shown in the figures below. On the top in Figure 1 scattering curves of a polymer-dopant system based on PMMA and diphenyl sulfoxide (DPSO) are shown for various compositions. On thebottom in Figure 1 scattering curves are shown of a blend of poly(methyl methacrylate) (PMMA) and poly(2,2,3,3-tetrafluoropropyl meth-acrylate) (PTFPMA) of specific composition measured at different temperatures. Figure 2 shows that there is a large difference in scattering behaviour for copolymers of different chemical composition. The random copolymer of methyl methacrylate (MMA) with benzylmethacrylate (BzMA) shows a very weak scattering signal, while a copolymer showing composition drift MMA with benzyl acrylte (BzA) shows a much stronger signal.

Theoretical predictions show that the excess Rayleigh scattering of miscible polymer blends and polymer-dopant systems depends strongly on their Flory-Huggins interaction parameter. The theoretical predictions also indicate that systems with a low additional Rayleigh scattering can be produced. Model systems based on polymer blends, copolymers and polymer-dopant systems were evaluated with respect to excess Rayleigh scattering to verify this. It is shown that Rayleigh scattering in blends, copolymers and doped systems is indeed highly dependent on their thermodynamic properties in a quantitative way.

In accordance with previous studies, it was found that doped systems based on poly(methyl methacrylate) (PMMA) and diphenyl sulfoxide exhibit a low Rayleigh scattering loss. Two model systems of miscible polymer blends, namely deuterated PMMA with PTFPMA and deuterated poly(2,2,2-trifluoroethyl methacrylate) (PTFEMA) with PTFPMA, were investigated using SANS. It was shown that the compositional fluctuations in a miscible polymer blend can be minimised by suitable combinations of thermodynamic properties (a large negative χ_{FH}) and the refractive indices of the constituents (a small refractive index mismatch). However, large-scale heterogeneities with a typical length scale of several hundreds of Angstroms were found, which were not expected based on thermodynamic considerations. These large-scale structures result in high additional scattering losses in miscible blends (several hundreds dB·km^{-1}), which reduces their practical usefulness in graded-index optics.

The scattering losses in copolymer systems with broad and narrow composition distributions were also investigated via SANS. It was observed experimentally that a high amount of composition drift in a copolymerising system results in high scattering losses. In random copolymers, extremely low scattering losses were obtained by proper selection of the monomeric units. The total intrinsic loss limit of random copolymers is even lower than that of the polymer-dopant systems. Consequently, random copolymers are extremely suitable candidates for the production of low-loss polymer optical waveguides.

References:

[1]   Y. Koike, *et al.*, J. Lightwave Technol. **13**, 1475 (1995)

[2]. Y. Koike, *et al.*, Appl. Opt., **29**, 2686 (1990)

[3]   F.G.H. van Duijnhoven, Bastiaansen, C.W.M., Adv. Mat., **11**, 567 (1999)

[4]   M. Dettenmaier, Chimia **47**, 397 (1993)

[5]   S.M. King, in Modern Techniques for Polymer Characterisation, Pethrick, R.A, Dawkins, J.V. (Eds.), John Wiley & Sons Ltd., (1999)

[6]   M.A. de Graaf, Ph.D. thesis, TUE, 2002.
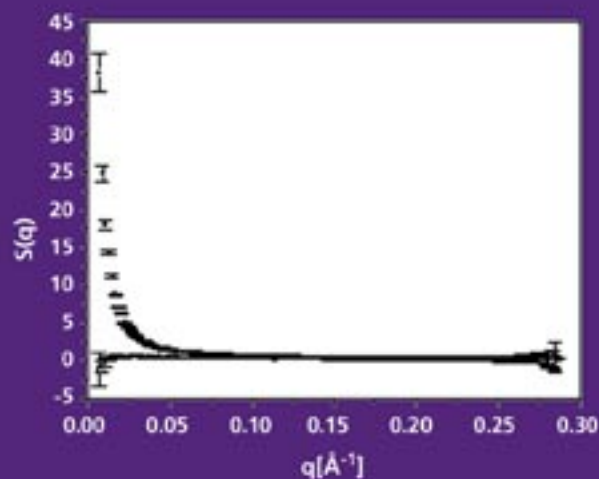
Figure 2:
Structure factors for copolymers of MMA-d$_8$-co-BzA (■) and MMA-d8-co-BzMA (●) comprising 80 vol% MMA-d$_8$.

E.L.F. Nies, KU Leuven, TUE
E. Loozen, H. Berghmans, KU Leuven
A. Ramzi, TUE-DPI

Adjacent miscibility gaps in poly(vinyl methyl ether)/water
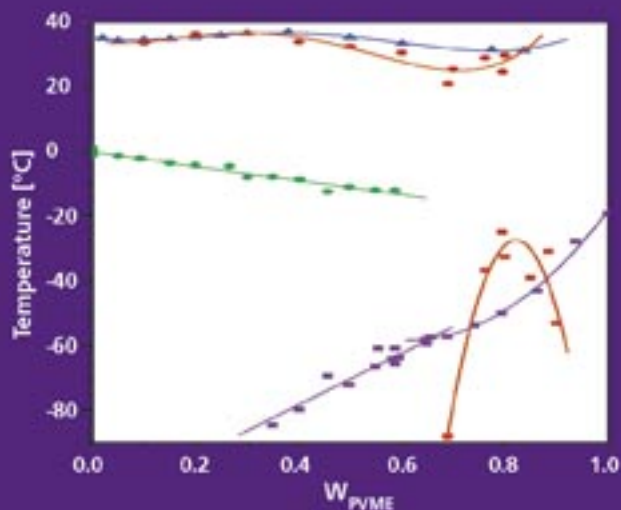
Figure 1
SANS determined spinodal temperatures versus the PVME composition (red solid circles and squares) compared to the theoretically predicted values. The red lines are shown to guide the eye.

Aqueous polymer solutions have already received considerable research interest from academic and practical points of view. Water-soluble polymers find numerous uses in e.g. food and or pharmaceutical applications. The academic interest is at least in part triggered by the often peculiar and complicated behavior shown by aqueous polymer solutions. In hindsight, the peculiar behavior often turns out to be essential for the practical applications. For instance the large changes in volume encountered when aqueous "intelligent" polymer gels change from a swollen to a collapsed state or *vice versa* with small changes in external parameters such as temperature or pH is well documented. For these polymer gels it has been demonstrated that the volume transition can be traced back to the unusual "high" temperature phase behaviour of the linear polymers in water. Apart from the high temperature phase behaviour, aqueous polymer solutions often also show peculiar behaviour at temperatures below the normal freezing point of water, i.e. water fails to crystallize at sufficiently high polymer concentrations. This peculiar behaviour can be interpreted to give prove to the existence of a molecular complex between water and polymer in which water molecules are bound by hydrogen bonding to a polymer repeat unit.

In any event, it is safe to say that hydrogen-bonding interactions in polymer solutions can lead to properties quite different from the usual solution behaviour. Both the experimental and theoretical understanding of these systems is still far from complete and neutron scattering experiments are extremely suited to give detailed information about these systems. Solutions of poly(vinyl methyl ether) (PVME) in H_2O and D_2O are an example at hand [1,2,3] the system possesses a bimodal lower critical solution temperature (LCST) miscibility gap at ca. 35°C spanning the full composition range. Below the LCST the system remains in the one phase region until the crystallisation of water occurs. However, crystallisation is only possible in mixtures with compositions smaller than $w_{PVME} < 0.6$. So far these experimental results have been interpreted in view of the existence of a hydrogen bonded polymer/water complex [1,4].

To get insight in the experimental observations theoretical calculations based on the thermodynamic perturbation theory of Wertheim

incorporating dispersive interactions as well as saturation interactions, such as hydrogen bonds have been performed. The theory provides a detailed picture of the Gibbs energy and its derivatives as a function of composition, temperature, polymer molar mass etc. The theory predicts that the interplay of these two types of interactions could yield *i*) the formation of polymer/solvent complex, *ii*) the occurrence of bimodal LCST miscibility at high temperature and, unexpectedly and surprisingly, *iii*) the presence of two adjacent narrow UCST miscibility gaps at low temperature.

Inspired by these predictions detailed small angle neutron scattering SANS experiments have been performed to investigate the concentration fluctuations in the system PVME/D$_2$O. The forward scattered intensity in a SANS experiment directly probes the concentration fluctuations in the mixture, $\partial^2 \Delta G/kT/\partial \phi_2^2$, becoming zero at the spinodal. The spinodal temperatures determined from these SANS experiments are depicted in Figure 1 as a function of composition (red solid circles and squares, the red lines are shown to guide the eye). In agreement with theoretical predictions an LCST at high T spanning the whole composition range and a UCST at high concentration and low T are found.

The SANS experiments also provide a quantification of the concentration fluctuations in PVME/D$_2$O spanning the whole composition and temperature range in the homogenous part of the phase diagram. In Figure 2a the experimentally determined values of $\partial^2 \Delta G/kT/\partial \phi_2^2$ are depicted as function of mixture composition. At the high concentrations we can already observe the upswing in related to the pure component effect. Also at smaller concentrations smaller than w$_{PVME}$ < 0.1 an upswing must occur but is not seen in figure as only concentrations w$_{PVME}$≥ 0.1 were investigated. However for the lower temperatures *T*=283 and *T*=273 K an unexpected upswing in $\partial^2 \Delta G/kT/\partial \phi_2^2$ is observed at intermediate concentrations notifying that molecular association sets in. In Figure 2b the predicted values of $\partial^2 \Delta G/kT/\partial \phi_2^2$ are shown also as a function of composition at the indicated temperatures and a qualitative agreement with experiment is found.

References:
[1]   F. Meeussen, Bauwens, Y., Moerkerke, R., Nies, E., Berghmans, H. Polymer, **41**, 3737 (2000).
[2]   H. Schafer-Soenen, Moerkerke, R., Berghmans, H., Koningsveld, R., Dusek, K., Solc, K. Macromolecules , **30**, 410 (1997).
[3]   R. Moerkerke, Koningsveld, R., Nies, E., Berghmans, H., Dusek, K., Solc, K. The Wiley Polymer Networks Group review Series, **1**, 463 (1998).
[4]   J. Zhang, Bergé, B., Meeussen, F., Nies, E.L.F., Berghmans, H., Shen, D. Macromolecules, **36**, In press (2003).
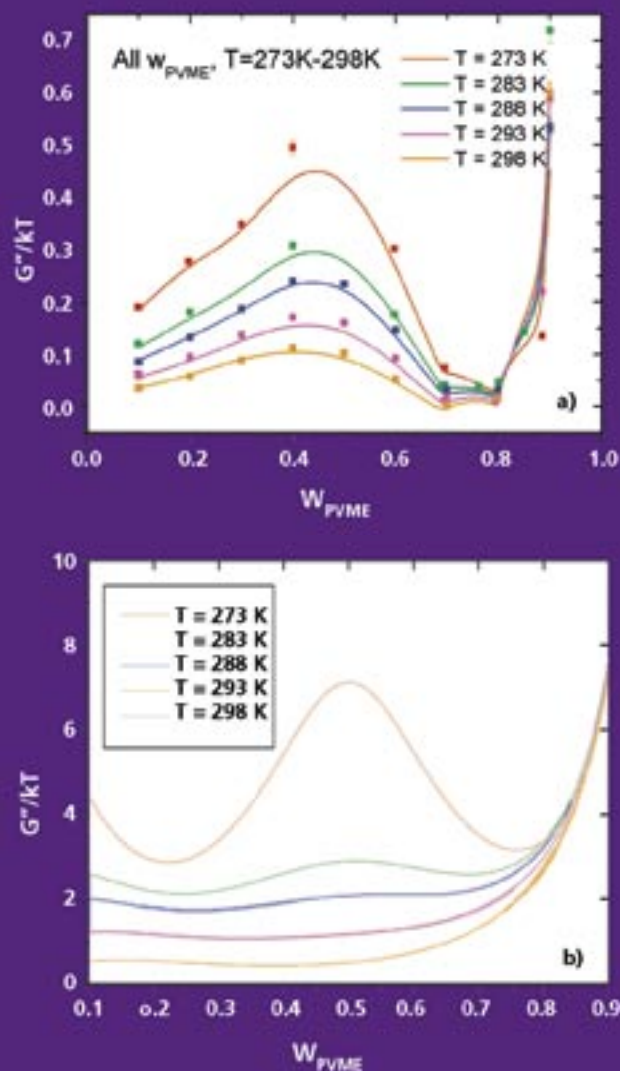
Figure 2
Concentration fluctuations determined experimentally (a) and theoretically (b) versus the PVME composition at different temperatures.

6.5 SOFT-CONDENSED MATTER

E.P.K. Currie, DSM
M. Wagemaker, A.A. van Well, IRI-TUD
M.A. Cohen Stuart, WUR-PCCS

Examining polymeric structures at sub-micron level using neutron reflectometry

Figure 1
Polymers in a) a hydrogel, and b) grafted to a substrate in a brushlike conformation.

A consequence of the drive to control matter on length scales between 1 and 100 nanometre is that interfaces become increasingly important. Accordingly, the ability to examine and characterise interfaces is essential to support these developments. As an example of such a study we present some results of characterisation of the structure of polymers grafted onto surfaces, and compare these with theoretical models.

In the current state of technology, control of matter on ever-decreasing length scales is becoming increasingly important. The developments in material science, electronics and chemistry are resulting in the emergence of nanotechnology, i.e. control of matter on length scales between one nanometre and 100 nanometres. Evidently, research in this field has not started with the coinage 'nanotechnology' but has been ongoing for decades. Previous research into (polymeric) micelles, aggregation, colloidal preparation and stabilisation could all now fall under the definition of nanotechnology.

One consequence of this drive towards smaller length scales is that interfaces are increasingly important. Whether the interest is e.g. into increasing the resolution of photoresists down to 150 nm or to control the delivery of drugs via nanometer-sized capsules, interface science is critical for successful developments. Accordingly, the ability to examine and characterise interfaces is essential to support the above developments. As an example of such a study we present some results of characterisation of the structure of polymers grafted onto surfaces.

Most current applications of polymers consist of polymers in the bulk state, i.e. randomly dispersed. In for instance hydrogels the hydrophilic gels are swollen to the point where the stretching of the polymer chains in less favourable than an increasing water uptake (see Figure 1a). Yet, in this swollen state there is no preferential orientation of the polymer chains. This situation changes when the polymers are end-grafted to the surface. In this case the chains may stretch as well due to water uptake, yet they are all oriented normal to the surface (see Figure 1b). When the chains are grafted at high densities there is a strong degree of orientation and the resulting layers can be quite thick, of the order of 50 nm (see Figure 3).

A lot of theoretical modeling on end-grafted polymers has been performed by, amongst others, Pierre-Gilles de Gennes [1]. Such models predict the thickness of the brush, the overall density and the segment distribution as function of the density of grafted chains, the chain length and their distribution and the solvent. One of the challenges in this field is linking the experimental properties of such

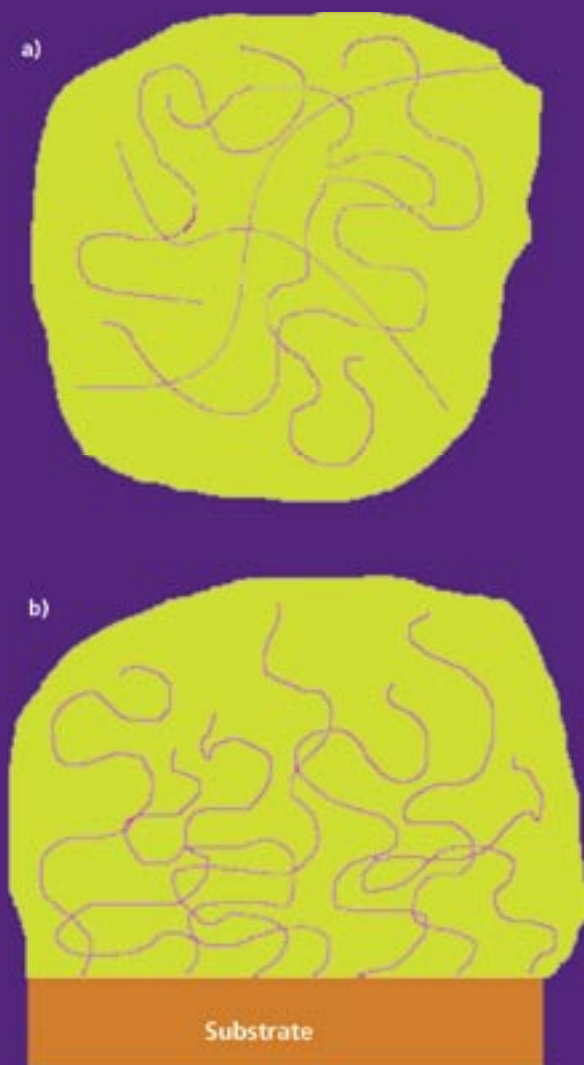surfaces with grafted polymers to the various theoretical models. For instance, how does the structure of a polymer brush change with increasing grafting density? This is not a trivial issue, as several studies are performed into the relationship between the brush structure and the ability of polymer brushes to prevent adsorption of e.g. bacteria for non-fouling applications [2]. To answer such questions one must be able to determine the structure of the brush in detail, and in our case this was done with neutron reflectivitometry at the IRI institute in Delft and on SURF at ISIS in the U.K.

In a nutshell [3], poly(ethyleneoxide) (PEO) brushes were formed at an air/D_2O interface via compression of a monolayer. Hydrophobic polystyrene (PS) groups bound to the PEO chains anchored the PEO to the interface, whereas the hydrophilic PEO chains stretched into the water phase, as depicted in Figure 1b. As the scattering length density of the PEO is considerably less than that of D_2O, the PEO brush translated into a gradient in scattering density at the interface. This is shown in Figure 2, where for the longest PEO chains (700 segments) the relative reflectivity is plotted vs. the normal wave vector q at three densities. It is clear that as the brush density increases, i.e. the area per PEO molecule decreases, the relative reflectivity decreases.

Using numerical methods developed at IRI we fitted several density profiles for polymer brushes to the reflectivity data. The most simple case was a block profile, i.e. all chains stretch to an equal distance, and the density within the brush is constant. This was found to be inconsistent with the data. In the literature analytical models suggested a parabolic density decrease in the brush, whereas numerical models suggested a more gradual, exponential decay [1,2]. Matching the reflectivity data to such models lead to the conclusion that at low densities the density profile has an exponential decay, whereas at high densities the decay is parabolic. Comparison of the fitted profiles with numerically calculated profiles showed good agreement. These profiles are shown in Figure 3.

One may ask what the long-term outcome is of such studies. Evidently, neutron reflectometry allows detailed examination of sub-micron structures, as shown above. Beyond this, detailed understanding of the structure of grafted polymers for e.g. biomedical applications is essential. For instance, in order to understand the adsorption of nanocolloids and blood proteins on our PEO brushes insight into the brush stuctures proved to be essential [4]. Neutron reflectometry can therefore provide valuable information in the area of interface science, which is expected to be of increasing importance in the predicted era of nanotechnology.

References:

[1] For an overview see e.g. G.J. Fleer *et al*, *Polymers at Interfaces*, Chapman & Hall, London (1993).

[2] The literature of biofouling of polymer surfaces is vast and scattered. An overview of adsorption on surfaces with grafted polymers is given in E.P.K. Currie *et al*, Adv. in Coll. & Int. Sci., **205**, 100 (2003)

[3] For details we refer to E.P.K. Currie, M. Wagemaker, M.A. Cohen Stuart, A.A. van Well, Macromolecules, **32**, 9041 (1999)

[4] R.A. Gage *et al*, Macromolecules 34, 5078 (2001) ; E.P.K. Currie *et al*, Pure & Appl. Chem. **71**, 1227 (1999).

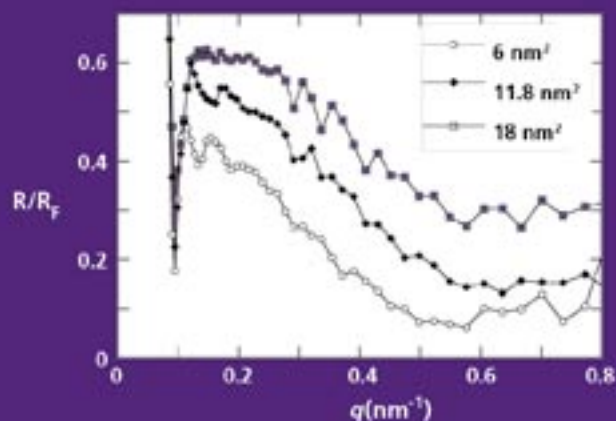## 6.5 SOFT-CONDENSED MATTER

Figure 2
The relative reflectivity's for PEO brushes consisting of 700 segments for three areas per molecule. R_F is the Fresnel reflectivity as measured for the pure D_2O-air interface.
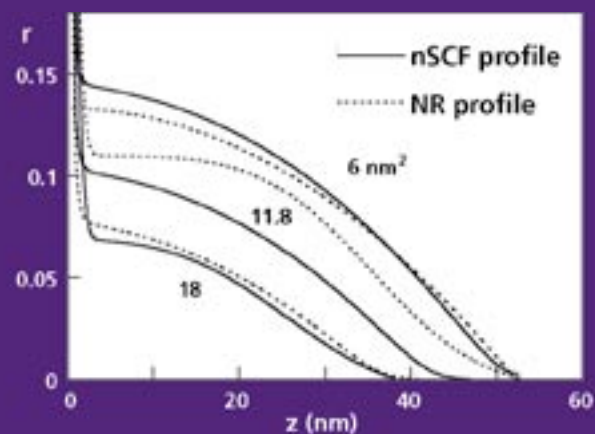

Figure 3
Volume density profiles gained from neutron reflectivity (dashed curves) and from numerical calculations (solid curves) for the samples shown in Figure 2.

**S.E. Offerman, L.J.G.W. van Wilderen,
N.H. van Dijk and M.Th. Rekveldt,
IRI-TUD
J. Sietsma and S. van der Zwaag,
TUD-TNW**

Evolving microstructure in pearlitic steel studied by neutron depolarisation

= Magnetic domain

**Figure 1
Schematic drawing of the 3DND technique. The
polarized neutrons interact with the magnetic
domains in side the material (cross-sectional view).**

**Three-dimensional neutron depolarisation methods are used to
study the technologically important austenite to perlite transfor-
mation in a nearly eutectoid steel. This approach provides unique
information on the perlite fraction, the average size of the perlite
colonies, and the spatial distribution of these colonies – all in the
bulk of the specimen under "isothermal" conditions. It transpires
that the growth-rate is determined by carbon diffusion through
the bulk of the grains, and not via the grain boundaries. It was also
found that a commonly accepted theory is not valid because the
perlite colonies have a non-random distribution throughout the
sample.**

A long-standing problem in the field of materials science is the
understanding of the evolution of the microstructure during the
formation of polycrystalline materials like metals and ceramics. The
most important reasons for this are the limitations of the currently
used experimental and modeling techniques that prevent a detailed
study of the grain (crystal) nucleation and growth mechanisms. The
neutron depolarization technique has the advantage that nucle-
ation and growth rates can be measured in-situ and in the bulk of
steel. These measurements are of vital importance for technological
applications, because a better understanding of the evolution of
the microstructure opens the opportunity for the industrial develop-
ment of materials with superior strength and formability.

Due to a combination of fundamental scientific interest and
technological importance steel has been investigated extensively.
Pearlitic steel consists of iron and carbon (approximately 0.77 wt.%)
with small quantities of alloying elements, and exists in three
stable crystalline phases: austenite (FCC iron), ferrite (BCC iron),
and cementite (orthorhombic Fe_3C). The production process of
steel involves several phase transformations that take place during
cooling of the liquid metal to room temperature. An important
phase transformation in pearlitic steel is from the high-temperature
austenite phase to the low-temperature pearlite structure. This is
the most well-known eutectoid transformation.

Pearlite is a common constituent of a wide variety of steels and
provides a substantial contribution to the strength. A pearlite
colony consists of two interpenetrating single crystals of ferrite
and cementite, which are primarily ordered as alternating plates.
Pearlite that consists of fine plates is harder and stronger than
pearlite that consists of coarse plates. This morphology of pearlite
is largely determined by the evolution of the austenite/pearlite
phase transformation during the production process. Control of the
pearlite phase transformation kinetics is thus of vital importance for
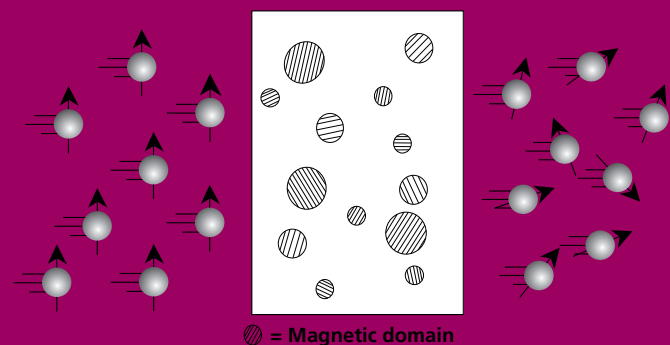the production of tailor-made steels.

Three-dimensional neutron depolarisation (3DND) is one of the few techniques that provide in-situ information about the evolution of the microstructure in the bulk of steel. 3DND involves the use of a monochromatic beam of polarized neutrons. The polarized neutrons interact with the ferromagnetic phase (in this case ferrite) that is embedded in the paramagnetic matrix (in this case austenite) [1,2], as shown in Figure 1. The technique simultaneously gives information about the fraction of ferromagnetic phase, the average magnetic domain size, and the spatial distribution of the magnetic domains. By relating the magnetic domain structure to the microstructure, we obtain information about the fraction pearlite, the average pearlite colony size and the spatial distribution of the pearlite colonies during the austenite decomposition, as shown in Figure 2. From these measurements nucleation and growth rates, as well as the overall transformation rate are determined, which can be compared to theoretical models.

The pearlitic steel was heated at 900°C for 30 min and subsequently quenched to the isothermal transformation temperature of 943 K, where the measurement started. From the neutron depolarization measurements pearlite nucleation and growth rates were deter- mined that give information on the evolution of the microstructure during the transformation [3]. A better insight was obtained on the underlying mechanism of pearlite nucleation. For the studied steel the ferrite nucleates first and thereafter the cementite. It was found that the activation energy for the cementite nucleation is much higher than for the ferrite, probably because under the given condi- tions ferrite nucleates at grain boundaries with a high energy and the cementite at grain boundaries with a low-energy. Furthermore, a distinction could be made between two competing theories on the rate controlling mechanism for pearlite growth. It was found that under the given conditions pearlite growth is dominated by the volume diffusion of carbon atoms, and not via the grain boundary diffusion of carbon atoms as was predicted by the other theory. Finally, it was found that the most widely used phase transforma- tion theory developed by Kolmogorov, Johnson, Mehl, and Avrami, can not be used to describe the austenite/pearlite transformation in the studied pearlitic steel, because the pearlite colonies were not randomly distributed over the sample during the transformation (Figure 2c).

These insights into the evolution of the microstructure in pearlitic steel also apply to other materials with an eutectoid phase trans- formation and contribute to the development of materials with optimal properties.

References:
[1]   M.Th. Rekveldt, Z. Phys., **259**, 391 (1973)
[2]   R. Rosman, M.Th. Rekveldt, J. Magn. Magn. Mater., **95**, 319 (1991)
[3]   S.E. Offerman, L.J.G.W. van Wilderen, N.H. van Dijk, J. Sietsma, M.Th. Rekveldt, S. van der Zwaag, Acta Materialia, **51**, 3927 (2003)

7.1 METALS
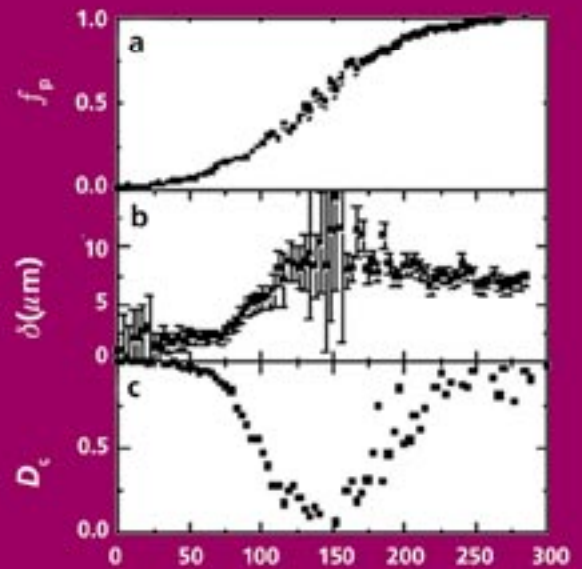
Figure 2
Parameters that can be measured with neutron depolarization are the fraction ferromagnetic phase (in this case pearlite) f_p (a), the average magnetic domain radius δ (b), and the cluster factor Dc (c) as a function of the transformation time t. For D_c=1 the magnetic domains are randomly distributed.

**N.H. van Dijk, S.E. Offerman,
W.G. Bouwman, M.Th. Rekveldt,
IRI-TUD
J. Sietsma, S. van der Zwaag, TUD-TNW
A. Bodin, CORUS
R.K. Heenan, ISIS**

High temperature SANS experiments on Nb(C,N) and MnS precipitates in HSLA steel

Small concentrations of niobium play an important role in the production process of modern high-strength low-alloy (HSLA) steels. The addition of niobium leads to the formation of Nb(C,N) precipitates which prevents recrystallisation of deformed grains during hot rolling. As a consequence, both the grain boundaries and the deformation bands can act as nucleation sites for the phase transformation from the high-temperature austenite phase to the low-temperature ferrite phase. This leads to a significant refinement of the ferrite grain size in comparison with steels without niobium and hence improves the strength and toughness of the steel. Small-angle neutron scattering (SANS) measurements on LOQ at ISIS have characterised the particle volume distribution of the Nb(C,N) and MnS precipitates in HSLA steel as a function of temperature in the high-temperature austenite phase.

In order to study the Nb(C,N) precipitates in HSLA steel three steels with a different niobium concentration were produced at CORUS RD&T in IJmuiden. The composition of the steels Nb0, Nb5, and Nb10 is listed in the table below. As all the steels contain significant amounts of manganese and sulphur, the presence of both Nb(C,N) and MnS precipitates is expected. The samples were mounted in a vacuum furnace and heated to the single-phase austenite region (T > 900 °C) and subsequently heated in steps of 25 °C to a maximum temperature of 1200 °C. The measurement time at each temperature was 30 min. In Figure 1 the scattered intensity $(d\Sigma/d\Omega)(Q)$ as a function of wave vector transfer Q is shown. The wave vector transfer $Q = 4\pi\sin(\theta)/\lambda$ is directly related to the scattering angle 2θ and the neutron wave length λ. For increasing temperature the scattered intensity is strongly reduced for all three samples. At the maximum temperature of 1200 °C, however, a finite scattered intensity remains at low Q.
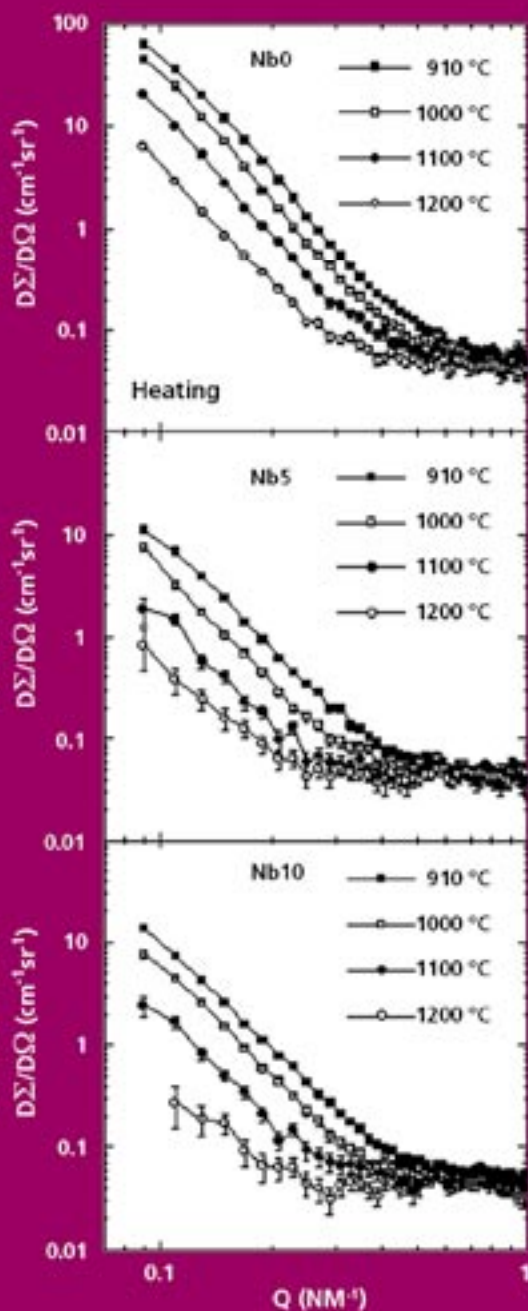
Figure 1

Scattered intensity (d∑/dΩ)(*Q*) of sample Nb0, Nb5, and Nb10 as a function of the wave vector transfer *Q* for increasing temperatures at *T* = 910, 1000, 1100, and 1200 °C.

In Figure 2 the particle volume distribution $D_V(R)$ as a function of particle radius R is shown, which was deduced from the scattered intensity as a function of Q in Figure 1. The Nb0 sample without niobium shows a single peak around 20 nm, while the niobium containing samples Nb5 and Nb10 reveal an additional peak around 5 nm. A comparison of the peak heights indicates that the first peak around 5 nm roughly scales with the niobium concentration, while the second peak around 20 nm scales with the sulphur concentration. This suggests that the smaller particles mainly correspond to Nb(C,N) precipitates and the larger ones to MnS precipitates. Transmission electron microscopy studies indeed confirm that Nb(C,N) precipitates are predominantly found in the size range up to 10 nm, while MnS precipitates are observed in sizes up to several μm. Thermodynamical calculations on the stability of NbC and MnS have been performed for the compositions of the studied steels and indicate that NbC gradually dissolves for increasing temperatures, while MnS is stable up to the maximum temperature of 1200 °C. This strongly suggests that the decreasing particle volume distribution for increasing temperatures (Figure 2), reflects a simultaneous dissolution of Nb(C,N) precipitates and coarsening of MnS precipitates.

Table

Chemical composition of the steels in wt.%					
	C	Si	Mn	Nb	S
Nb0	0.082	0.484	0.067	–	0.029
Nb5	0.082	0.519	0.090	0.049	0.004
Nb10	0.076	0.526	0.086	0.097	0.004
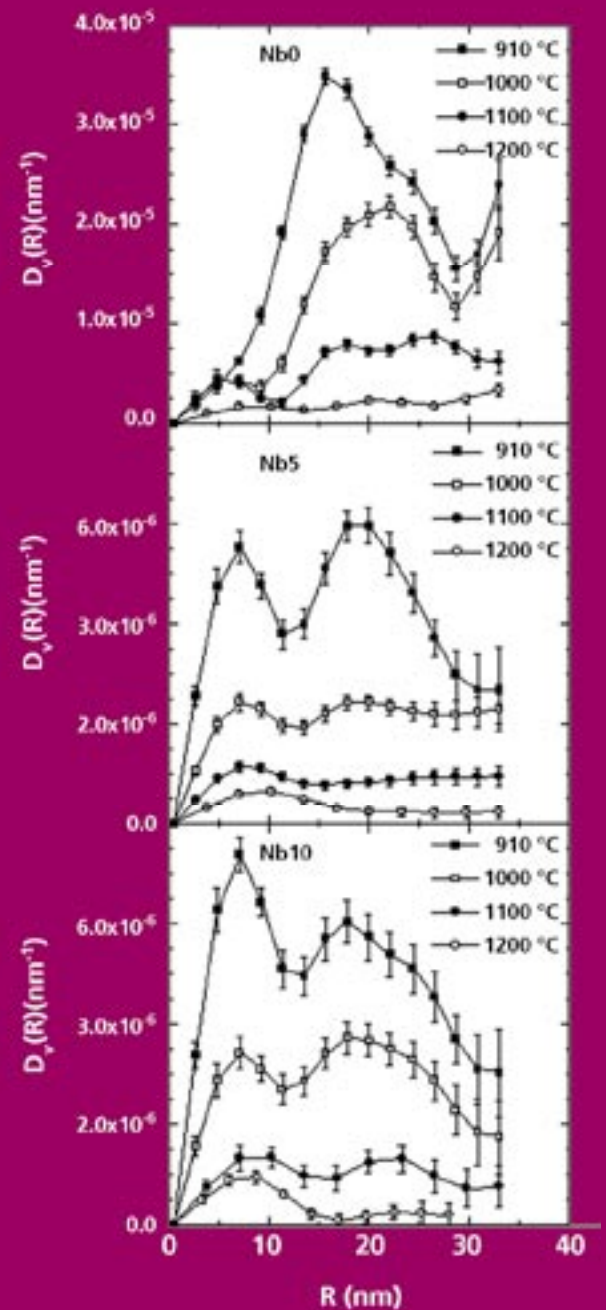
Figure 2
Particle volume distribution $D_V(R)$ of MnS and Nb(C,N) precipitates as a function of the particle radius R for increasing temperatures at T = 910, 1000, 1100, and 1200 °C in sample Nb0, Nb5, and Nb10. Note the differences in the vertical scale.

**M. Álvarez, F.J. Bermejo,
CSIC Madrid
P. Verkerk, IRI-TUD
B. Roessli, ETH**

High-frequency dynamics in a molten binary alloy

Figure 1
The experimental data are shown by symbols, the fitted model by blue lines, and the quasielastic and inelastic components by red and green lines, respectively.

The nature of the finite wavelength collective excitations in liquid binary mixtures composed of atoms of very different masses has been of interest for more than a decade. The most prominent fact is the high frequencies at which they appear, well above those expected for a continuation to large wave vector of hydrodynamic sound. To better understand the microscopic dynamics of such systems, an inelastic neutron scattering experiment was performed on the molten alloy Li_4Pb. We present the high-frequency excitations of molten Li_4Pb which indeed show features substantially deviating from those expected for the propagation of an acoustic mode.

The presence of overdamped high-frequency collective excitations within the microscopic regime in liquid binary mixtures composed of atoms of disparate masses has been observed by scattering experiments and computer simulations, in different systems, such as molten salts, simple liquid mixtures, molecular liquids and metallic alloys. Kinetic-theory predictions portray such excitations as being supported by the light component only so that they apparently travel with phase velocities close to those characteristic of the lighter pure component, which are well above those given by the elastic constants of the mixture. From the exploration of the phase velocity trend within the low-Q region of such systems, the presence of a mode of acoustic nature (where the atoms execute in-phase displacements) propagating with a velocity well above that corresponding to hydrodynamic sound has been inferred. However, some aspects are still the subject of controversy in regard to, on the one hand, the adequacy of describing the nature of excitations appearing at relatively large-Q in terms of constructs which only retain full sense within the realm of hydrodynamics (i.e. a sound mode), and on the other hand, the assignment of the observed frequencies to a definite underlying microscopic mechanism in the absence of further information.

In order to get a coherent understanding of the high-frequency dynamics in these mixtures, we chose to study a system which has been a flagship for tests of the above mentioned phenomena, namely molten Li_4Pb (at 1075 K). The measurements were carried out on the three-axis spectrometer IN1, at ILL.

The full accessible dynamical range at each wavenumber of the experimental dynamic structure-factors, S(Q,), is shown in Figure 1. These data reveal heavily damped excitations, i.e. a broad but relatively intense inelastic signal. The total S(Q,) was fitted using two main components, the central quasielastic part plus the inelastic contribution. The model used for the latter was the damped harmonic oscillator which is defined in terms of three parameters, IQ, excitation strength, Q, the frequency and $Q (Q-1 Q2)$, the linewidth.
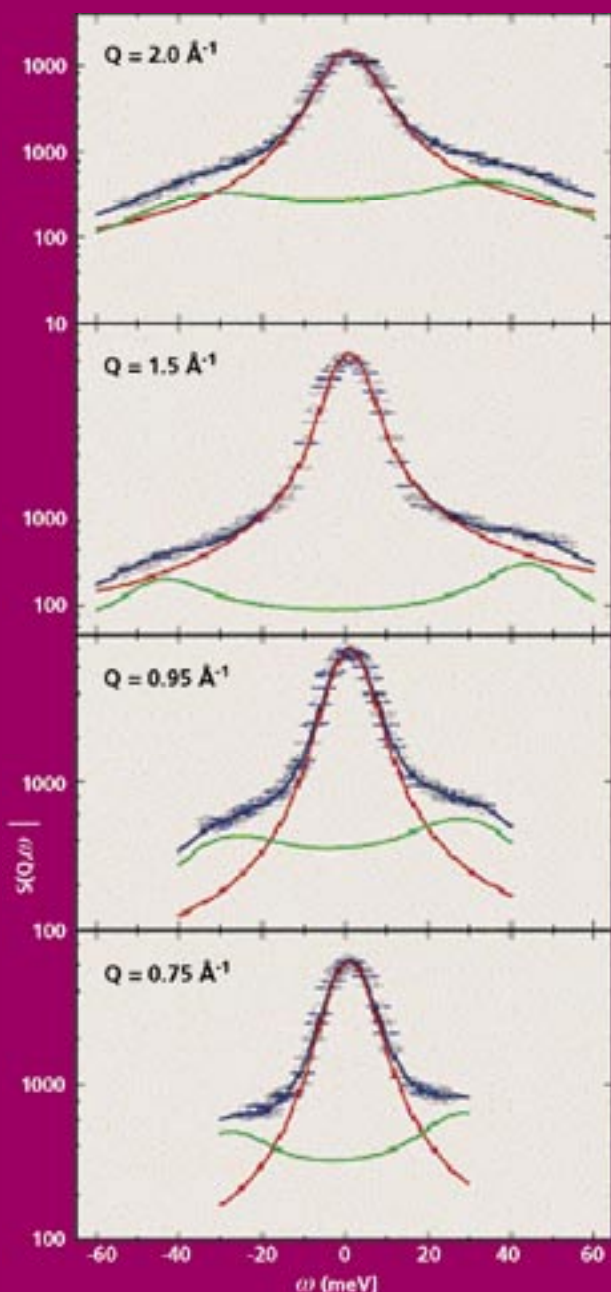
The experiment covered a kinematic range (0.6<Q< 2.4 Å^{-1}, 60 meV) which enabled an unambiguous characterisation of such excitations by studying the wavevector dependence of their frequencies, lifetimes and signal amplitudes. The fitted parameters vs. Q are all plotted in Figure 2. The Q dependence of the inelastic integrated intensity, IQ (Figure 2a), does not follow the form of the static structure factor of the mixture (S(Q), blue circles), as the quasielastic integrated intensity does. This fact indicates that the collective mode does not propagate through the whole network of atoms, or in other words, it is a signature of a non-acoustic behaviour.

On the other hand, the dispersion relation, ω_Q vs Q, is displayed in Figure 2b. It shows a maximum at about Qm/2, where Qm is the position of the first peak of S(Q) for pure Li, which confirms that these excitations are supported by the lighter component of the alloy. Moreover, the phase velocity, approaches the sound propagation velocity in pure Li (blue line). The Q-dependence of T$_Q$ is also plotted in Figure 2c. This provides an estimate of the lifetime of the collective excitations being sampled, 0.02 ps, which implies that these excitations are of a localised nature. In summary, the Q-dependence of the inelastic intensity is considered here on the same footing as that shown by the excitation frequencies and linewidths, since it provides a direct access to the relative phases of the motion of atoms taking place at frequencies well above hydrodynamic sound. The results confirm the presence of overdamped excitations in a molten alloy composed of particles with a disparate mass ratio. In agreement with predictions from kinetic theories, such motions are shown to be supported by the light component only. However, the experiment provides for the first time clear indications that these motions are mostly out-of-phase and very much like the 'optic' modes in binary crystals.

The situation is highly reminiscent of liquid water and ice polycrystals, where a similar effect ('fast sound') has repeatedly been reported. Thus, our measurements provide new evidence pointing towards a microscopic origin of the steep dispersion. This gives an alternative view to that based on the interpretation of the deceptively simple 'dispersion' in terms of a unique acoustic excitation which travels at speeds several times higher than hydro-dynamic sound. The results also show the unique capabilities of IN1, the three-axis spectrometer for liquids and amorphous materials research at ILL, when dealing with liquid mixtures composed of atoms of very different masses and when steep dispersions come into play.

7.3 METALS
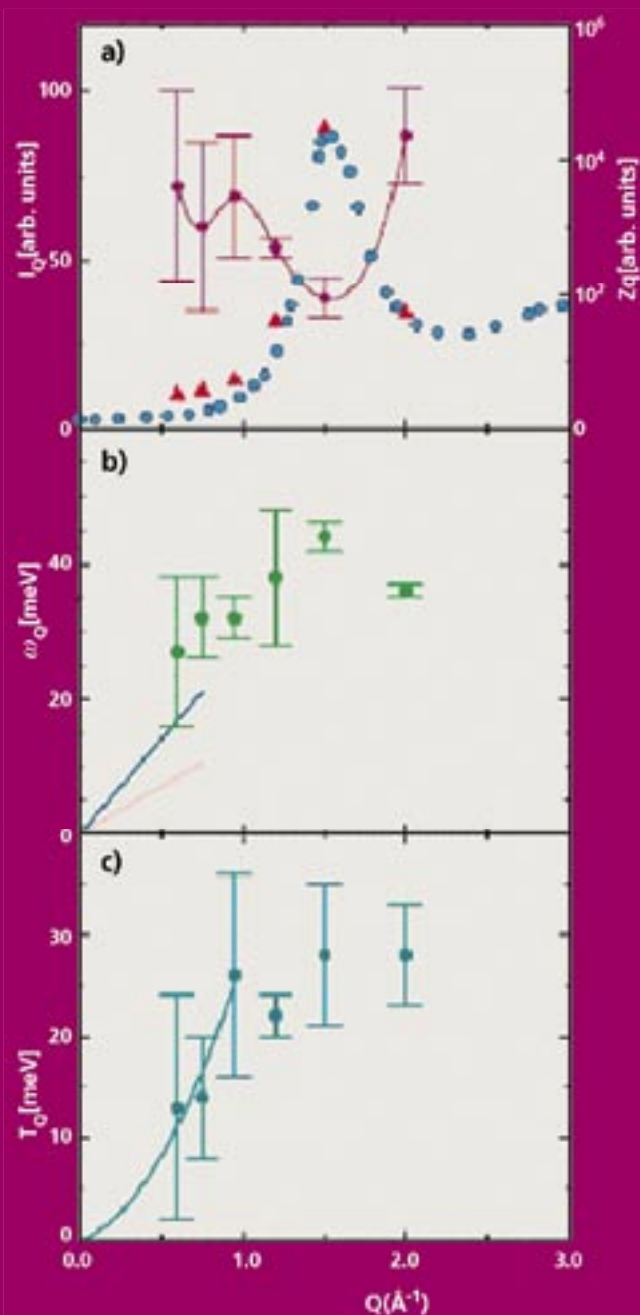
Figure 2
Wave-vector dependence of the damped harmonic oscillator parameters. The Q dependence of both the integrated intensities of the quasi-elastic component (Zq,) and the inelastic part (IQ,), together with the static structure factor of the mixture (S(Q),), is shown in frame a). The dispersion relation is displayed in frame b), together with the expected positions at high Q of the hydrodynamic sound modes corresponding to pure liquid Li (blue line) and to liquid Li$_4$Pb (pink line). The wavevector dependence of the inelastic linewidth Q is also plotted in frame c); the line merely shows the Q$_2$dependence at low Q values, from which the lifetime, Q, can be estimated (see text).
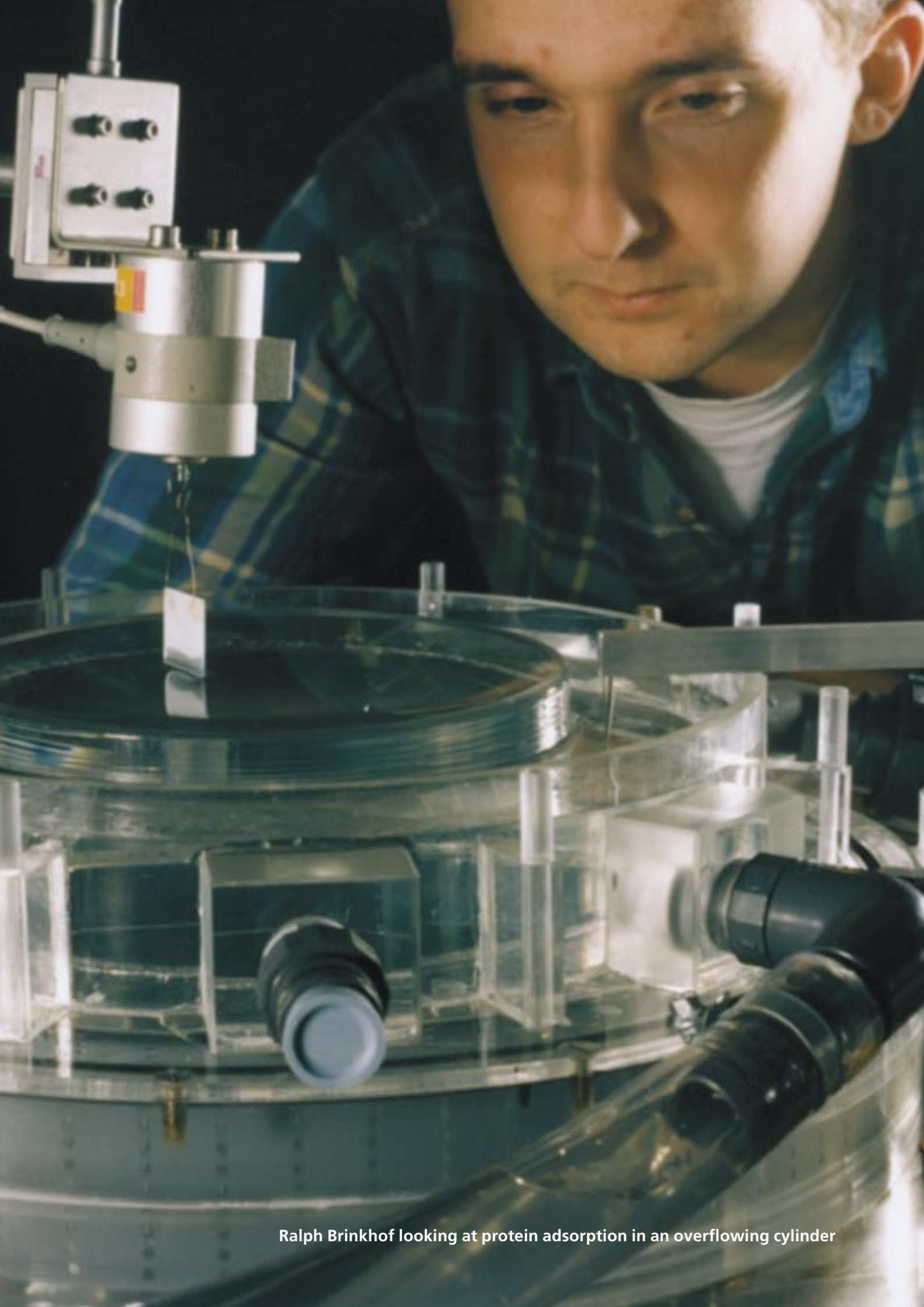
Ralph Brinkhof looking at protein adsorption in an overflowing cylinder

Glossary of abbreviations

Affiliations

CEA: Commissariat de l' Energy Atomique, Departement de Recherche Fondamentale sur la Matière Condesée, 380549 Grenoble Cedex 9, France (http://www.cea.fr/)

CSIC: Consejo Superior de Investigaciones Ceintíficas, Administración Central: c/o Serrano, 117, 28006 Madrid, Spain (http://www.csic.es/english/)

CUT: Chalmers University of Technology, Department of Chemistry and Biosciences, P.O. Box 462, SE-405 30 Göteborg, Sweden (http://www.chalmers.se/Home-E.html)

CORUS: Wenckebachstr 1, 1951 JZ Velsen Noord, The Netherlands (http://www.corusgroup.com/)

DSM: Research, Materials Science Center, P.O. Box 18, 6160 MD Geleen, The Netherlands (http://www.dsm.com/en_US/html/campus/home.htm)

ETH: Eidgenössische Technische Hochschule Zürich, ETH Zentrum, HG Rämistrasse 101, CH-8092 Zürich, Switzerland (http://www.ethz.ch/)

FOM: Stichting voor Fundamenteel Onderzoek der Materie (Foundation for Fundamental Research on Matter) P.O. Box 3021, 3502 GA Utrecht, The Netherlands (http://www.fom.nl)

FZ Jülich: Forschungszentrum Jülich, Institut für Festkörperforschung, Weiche Materie, 52425 Jülich, Germany (http://www.fz-juelich.de/iff/)

HMI: Hahn-Meitner Institut, Abteilung SF2, Glienicker Straße 100, 14109 Berlin, Germany (http://www.hmi.de/index_en.html)

ILL: Institut Laue-Langevin, 6, rue Jules Horowitz, BP 156 - 38042 Grenoble Cedex 9 - France (http://www.ill.fr/)

IRI-TUD: Interfacultair Reactor Instituut (Interfaculty Reactor Institute), Delft University of Technology, Mekelweg 15, 2629 JB Delft, The Netherlands (http://www.iri.tudelft.nl/)

JRC: Joint Research Centre, European Commission, Institut for Advanced Materials, P.O. Box 1, 1755 ZG Petten (http://www.jrc.cec.eu.int/)

ISIS: UK Spallation Source, Rutherford Appleton Laboratory, Chilton Didcot OX11 0QX, United Kingdom (http://www.isis.rl.ac.uk/)

KU Leuven: Katholieke Universiteit Leuven, Laboratory for Polymer Research, Oude Markt 13, 3000 Leuven, Belgium (http://www.kuleuven.ac.be/)

LLB: Laboratoire Léon Brillouin, CEA/CNRS, 91191 Gif-sur-Yvette Cedex, France (http://www-llb.cea.fr/index_e.htm)

MPI: Max Planck Institut Stuttgart, Heisenbergstraße 1-3, 70569 Stuttgart, Germany (http://www.mpi-stuttgart.mpg.de/)

NIZO: NIZO food research, 2 Kernhemseweg, P.O. Box 20, 6710 BA Ede, The Netherlands (http://www.nizo.com/)

NVNV: Nederlandse Vereniging voor Neutronen Verstrooiing (The Dutch Neutron Scattering Society), Mekelweg 15, 2629 JB Delft, The Netherlands (http://www.nvnv.nl)

NWO: Nederlandse Organisatie voor Wetenschappelijk Onderzoek (The Netherlands Organisation for Scientific Research) P.O. Box 93128, 2509 AC, The Hague, The Netherlands (http://www.nwo.nl)

PNPI: Petersburg Nuclear Physics Institute (PNPI), Gatchina, Leningrad district, 188350 Russia (http://www.pnpi.spb.ru/)

PSI: Paul Scherrer Institut, Laboratory for Muon-Spin Spectroscopy, CH-5292 Villigen PSI, Switzerland (http://www.psi.ch/)

RUG-BIOSON: Rijksuniversiteit Groningen (University of Groningen), BIOSON research institute, Nijenborgh 4, 9747 AG Groningen, The Netherlands (http://md.chem.rug.nl/bioson.html)

RUG-MSC: Rijksuniversiteit Groningen (University of Groningen), Materials Science Center, Nijenborgh 4, 9747 AG Groningen, The Netherlands (http://rugth30.phys.rug.nl/msc_newweb/)

TUD-TNW: Technische Universiteit Delft (Delft University of Technology), Faculty of Applied Sciences, Microstructural Control in Metals, Rotterdamseweg 137, 2628 AL Delft, The Netherlands (http://www.tnw.tudelft.nl/)

TUD-DCT: Technische Universiteit Delft (Delft University of Technology), Faculty of Applied Sciences, DelftChemTech, Julianalaan 136, 2628 BL Delft, The Netherlands (http://www.dct.tudelft.nl/)

TUE: Technische Universiteit Eindhoven (Eindhoven University of Technology), P.O. Box 513, 5600 MB, Eindhoven, The Netherlands (http://www.chem.tue.nl/)

TUE-DPI: Technische Universiteit Eindhoven (Eindhoven University of Technology), The Dutch Polymer Institute, P.O. Box 902, 5600 AX, Eindhoven, The Netherlands (http://www.polymers.nl/)

UE: University of Edinburgh, Department of Physics and Astronomy, Edinburgh EH9 3JZ, United Kingdom (http://www.ed.ac.uk/)

UK: Universität Karlsruhe (TH), Physik. Inst., Wolfgang-Gaede-Str. 1, 76131 Karlsruhe, Postfach 6980, D-76128 Karlsruhe (http://www.physik.uni-karlsruhe.de/)

UL-KO: Universiteit Leiden (Leiden Univerisity), Kamerlingh Onnes Institute, Niels Bohrweg 2, 2333 CA Leiden/P.O. Box 9504, 2300 RA Leiden, The Netherlands (http://www.physics.leidenuniv.nl/sections/cm/welcome.htm)

UL-LIC: Universiteit Leiden (Leiden University), Leiden Institute of Chemistry, Gorlaeus Laboratories, P.O. Box 9502, 2300 RA Leiden, The Netherlands (http://wwwchem.leidenuniv.nl/)

UU-Debye: Universiteit Utrecht (University of Utrecht), Anorganic Chemistry, Debye Research Institute, University of Utrecht, Padualaan 8, 3584 CH Utrecht, The Netherlands (http://www1.phys.uu.nl/debye/)

UU-FCC: Universiteit Utrecht (University of Utrecht), Sectie Fysische- en Colloidale Chemie, Padualaan 8, 3584 CH Utrecht, The Netherlands (http://www.chem.uu.nl/fcc/www/fcc.html)

UvA: Universiteit van Amsterdam, Postbus 19268, 1000 GG Amsterdam, The Netherlands (http://www.uva.nl/)

UW: University of Warwick, Coventry CV4 7AL, United Kingdom (http://www.warwick.ac.uk/)

WUR-PCCS: Wageningen University and Research Center, Department of Physical Chemistry and Colloid Science, Dreijenplein 6, 6703 HB Wageningen, The Netherlands (http://www.fenk.wau.nl/)

Abbreviations

ESS: European Spallation Source

SNS: Spallation Neutron Source, Oakridge USA

JSNS: Japanese Spallation Neutron Source

INS: Inelastic Neutron Scattering

SANS: Small-Angle Neutron Scattering

SESANS: Spin-Echo Small-Angle Neutron Scattering

QENS: Quasielastic Neutron Scattering

3DND: Three-dimensional Neutron Depolarisation

HRPD: High-resolution Powder Neutron Diffractometer at ISIS

Acknowledgements

Part of the Delft neutron reflectometer ROG

Useful web-pages

There is now a vast number of web-sites dealing with all aspects of neutron scattering: access, instrumentation, techniques, teaching primers and data bases. Rather than list all of these we direct the reader to the European portal for neutrons and muons from which virtually all other relevant pages can be found.

European portal for neutron/muons

(http://www.neutron-eu.net)
via this site a.o. information about:
ENSA: European Neutron Scattering Association
NMI3: neutrons/muons in EU, 6th Framework Programme (FP6)
ESS: European Spallation Source

Neutron Scattering home page

(http://www.neutron.anl.gov)

Anja van der Graaf is powdering chopper disks

Publications 2000-2003

involving neutron/muon research

PhD theses 2000 - 2003

Theses 2003

Y. Janssen
Interplay between magnetic anisotropy and exchange interactions in rare-earth transition-metal ferrimagnets
University of Amsterdam

E.V.D. van Loef
Halide scintillators
Delft University of Technology

S.E. Offerman
Evolving microstructures in carbon steel. A neutron and synchrotron radiation study
Delft University of Technology

P.D. Thang
Permanent magnets based on iron-platinum alloys
University of Amsterdam

O. Uca
Spin-echo small-angle neutron scattering development
Delft University of Technology

M. Wagemaker
Structure and dynamics of lithium in anatase TiO_2
Delft University of Technology

Theses 2002

F. Galli
Coexistence of charge density waves and magnetism in intermetallic compounds
Leiden University

M.A. de Graaf
Transmissive and emissive polymer waveguides for communication and illumination
Eindhoven University of Technology

R.W.E. van de Kruijs
Specular and off-specular reflection of polarized neutrons from magnetic thin films and multilayers
Delft University of Technology

O.S. Roubeau
Solid state properties of triazole-based Fe(II) materials
Leiden University

S.S. Zakharova
Ordering in dense DNA phases
Leiden University

Theses 2001

C.P. Allier
Micromachined Si-well scintillator pixel detectors
Delft University of Technology

B. de Boer
Design, synthesis, morphology and properties of semiconducting block-copolymers for photonic applications
University of Groningen

J.H.K. Ky Hirschberg
Supramolecular polymers
Eindhoven University of Technology

C.T. Kaiser
Diffusion, reorientation and small magnetic fields, studied by μSR
Delft University of Technology

E. Kemner
Organometallics in confined geometries: Ferrocene in zeolite Y
Delft University of Technology

M. Marsman
Ab-initio calculations in scintillator research:
On the structure and optical properties of $LiBaF_3$:Ce^{3+} and the lattice dynamics of ionic compounds
Delft University of Technology

V.W.J. Verhoeven
A fundamental study on materials for Li-ion batteries
Delft University of Technology

Theses 2000

F.D. van den Berg
Gas-filled micro-patterned radiation detectors
Delft University of Technology

E.P.K. Currie
Brushes and soap, gafted polymers and their interaction with nanocolloids
Wageningen University

P. Estrela
Non-Fermi liquid behaviour in uranium-based heavy-fermion compounds
University of Amsterdam

B. Mos
Dynamics in classical and complex fluids studied by neutron scattering
Delft University of Technology

Publications 2003, to September 1

M. Blaauw, *Hydrogen precipitation in titanium observed with neutron incoherent scattering and prompt gamma neutron activation analysis.* Nuclear Instruments & Methods in Physics Research Section A- Accelerators Spectrometers Detectors and Associated Equipment 505, 20-24 (2003).

H. Degenaar and M. Blaauw, *The neutron energy distribution to use in Monte Carlo modeling of neutron capture in thermal neutron beams.* Nuclear Instruments & Methods in Physics Research Section B- Beam Interactions with Materials and Atoms 207, 131-135 (2003).

N.E. Benes, H. Jobic, V. Reat, H.J M. Bouwmeester and H. Verweij, *Mobility of hydrogen in microporous silica studied with quasi- elastic neutron scattering.* Separation and Purification Technology 32, 9-15 (2003).

H. Gotz, B. Ewen, U. Maschke, M. Monkenbusch and G. Meier, *Chain expansion and chain localisation in the homogenous regime of blends of liquid low molar mass polysiloxanes as revealed by neutron scattering investigations.* E-Polymers art-011 (2003).

T.S. van Erp and E.J. Meijer, *Ab initio molecular dynamics study of aqueous solvation of ethanol and ethylene.* Journal of Chemical Physics 118, 8831-8840 (2003).

J.R.C. van der Maarel, S.S. Zakharova, W. Jesse, C. Backendorf, S.U. Egelhaaf and A. Lapp, *Supercoiled DNA; plectonemic structure and liquid crystal formation.* Journal of Physics-Condensed Matter 15, S183-S189 (2003).

T. Krouglov, W.H. Kraan, J. Plomp, M.Th. Rekveldt and W.G. Bouwman, *Spin-echo small-angle neutron scattering to study particle aggregates.* Journal of Applied Crystallography 36, 816-819 (2003).

P. Schobinger-Papamantellos, C. Ritter and K.H.J. Buschow, *On the magnetic ordering of Nd6Fe13-xAl1+x (x=1-3) and La6Fe11Al3 compounds.* Journal of Magnetism and Magnetic Materials 260, 156-172 (2003).

C. Nöldeke, B. Asmussen, W. Press, H. Büttner and G. Kearley, *Small rotational barriers for H2O flips in phase III of [Me(H2O)(6)](ClO4)(2) with Me = Mg, Ni, and Zn.* Chemical Physics 289, 275-280 (2003).

F. M. Mulder, J. Stride, S.J. Picken, P.H.J. Kouwer, M. P. de Haas, L.D.A. Siebbeles and G.J. Kearley, *Dynamics of a triphenylene discotic molecule, HAT6, in the columnar and isotropic liquid phases.* Journal of the American Chemical Society 125, 3860-3866 (2003).

H.J. Snijder, P.A. Timmins, K.H. Kalk and B.W. Dijkstra, *Detergent organisation in crystals of monomeric outer membrane phospholipase A.* Journal of Structural Biology 141, 122-131 (2003).

I. Maksimov, F.J. Litterst, S. Sullow, R. Feyerherm and J.A. Mydosh, *Structural and magnetic ordering in UPd1.85Sn.* Acta Physica Polonica B 34, 967-970 (2003).

H. Nakotte, S. Chang, A.M. Alsmadi, M.H. Jung, A.H. Lacerda, K. Prokes, E. Brück and M. Mihalik, *Hard-axis magnetoresistance and metamagnetic transition in UPdSn.* Acta Physica Polonica B 34, 987-990 (2003).

M. Yokoyama, J. Nozaki, H. Amitsuka, K. Watanabe, S. Kawarazaki, H. Yoshizawa and J.A. Mydosh, *Nonequilibrium antiferromagnetic state in the heavy electron compound URu2Si2.* Acta Physica Polonica B 34, 1067-1070 (2003).

M.J. Bull, B. Fåk, K.A. Mcewen and J.A. Mydosh, *Search for novel order in URu2Si2 by neutron scattering.* Acta Physica Polonica B 34, 1265-1268 (2003).

AJ.E. O'Connell, V.Y. Grinberg and C.G. de Kruif, *Association behavior of beta-casein. Journal of Colloid and Interface.* Science 258, 33-39 (2003).

J.M. Bradley, S.G. Carling, D. Visser, P. Day, D. Hautot and G.J. Long, *Structural and physical properties of the ferromagnetic tris- dithiooxalato compounds, A[(MCrIII)-Cr-II(C2S2O2)(3)], with A(+) = N(n-CnH2n+1)(4)(+) (n=3-5) and P(C6H5)(4)(+) and M-II = Mn, Fe, Co, and Ni.* Inorganic Chemistry 42, 986-996 (2003).

A. Vrij, *Neutron scattering of colloidal particle dispersions; contrast variation with homogeneous and granular solvents. Colloids and Surfaces.* A-Physicochemical and Engineering Aspects 213, 117-129 (2003).

C. Holt, C.G. de Kruif, R. Tuinier and P.A. Timmins, *Substructure of bovine casein micelles by small-angle X-ray and neutron scattering.* Colloids and Surfaces A-Physicochemical and Engineering Aspects 213, 275-284 (2003).

H. Amitsuka, K. Tenya, M. Yokoyama, A. Schenck, D. Andreica, F.N. Gygax, A. Amato, Y. Miyako, Y.K. Huang and J. A. Mydosh, *Inhomogeneous magnetism in URu2Si2 studied by muon spin relaxation under high pressure.* Physica B-Condensed Matter 326, 418-421 (2003).

R.H. Heffner, J.E. Sonier, D. E. MacLaughlin, G.J. Nieuwenhuys, F. Mezei, G. Ehlers, J.F. Mitchel and S.W. Cheong, *Inhomogeneity in the spin channel of ferromagnetic CMR manganites.* Physica B-Condensed Matter 326, 494-499 (2003).

O. Uca, W.G. Bouwman and M.Th. Rekveldt, *Magnetic design of a spin-echo small-angle neutron-scattering instrument.* Nuclear Instruments & Methods in Physics Research Section A- Accelerators Spectrometers Detectors and Associated Equipment 496, 437-445 (2003).

M. Wagemaker, G J. Kearley, A.A. van Well, H. Mutka and F.M. Mulder, *Multiple li positions inside oxygen octahedra in lithiated TiO2 anatase.* Journal of the American Chemical Society 125, 840-848 (2003).

O. Uca, W.G. Bouwman and M.Th. Rekveldt, *Model calculations for the spin-echo small-angle neutron- scattering correlation function.* Journal of Applied Crystallography 36, 109-116 (2003).

T. Krouglov, I.M. de Schepper, W.G. Bouwman and M.Th. Rekveldt, *Real-space interpretation of spin-echo small-angle neutron scattering.* Journal of Applied Crystallography 36, 117-124 (2003).

R. Tuinier and A. Brulet, *On the long-range attraction between proteins due to nonadsorbing polysaccharide.* Biomacromolecules 4, 28-31 (2003).

C. M. Fang, G.A. de Wijs, E. Orhan, G. de With, R.A. de Groot, H.T. Hintzen and R. Marchand, *Local structure and electronic properties of BaTaO2N with perovskite-type structure.* Journal of Physics and Chemistry of Solids 64, 281-286 (2003).

H. Amitsuka, K. Tenya, M. Yokoyama, A. Schenck, D. Andreica, F.N. Gygax, A. Amato, Y. Miyako, Y.K. Huang and J. A. Mydosh, *Inhomogeneous magnetism in URu2Si2 studied by muon spin relaxation under high pressure.* Physica B-Condensed Matter 326, 418-421 (2003).

P. Chandra, P. Coleman, J.A. Mydosh and V. Tripathi, *The case for phase separation in URu2Si2.* Journal of Physics-Condensed Matter 15, S1965-S1971 (2003).

K. Ishida, D.E. MacLaughlin, O.O. Bernal, R.H. Heffner, G. . Nieuwenhuys, O. Trovarelli, C. Geibel and F. Steglich, *Spin dynamics in a structurally ordered non-Fermi-liquid compound: YbRh2Si2.* Physica B-Condensed Matter 326, 403-405 (2003).

K. Ishida, D.E. MacLaughlin, K. Okamoto, Y. Kawasaki, Y. Kitaoka, G.J. Nieuwenhuys, O.O. Bernal, A. Koda, W. Higemoto, R. Kadono, C. Geibel and F. Steglich, *mu SR and low-temperature antiferromagnetism in the ordered non-Fermi-liquid compound YbRh2Si2.* Physica B-Condensed Matter 329, 589-590 (2003).

R.H. Heffner, J.E. Sonier, D.E. MacLaughlin, G.J. Nieuwenhuys, F. Mezei, G. Ehlers, J.F. Mitchel and S.W. Cheong, *Inhomogeneity in the spin channel of ferromagnetic CMR manganites.* Physica B-Condensed Matter 326, 494-499 (2003).

D.E. MacLaughlin, M.S. Rose, B.L. Young, O O. Bernal, R. . Heffner, G.D. Morris, K. Ishida, G.J. Nieuwenhuys and J.E. Sonier, *mu SR and NMR in f-electron non-Fermi liquid materials.* Physica B-Condensed Matter 326, 381-386 (2003).

E. Morenzoni, R. Khasanov, H. Luetkens, T. Prokscha, A. Suter, N. Garifianov, H. Gluckler, M. Birke, E. Forgan, H. Keller, J. Litterst, C. Niedermayer and G. Nieuwenhuys, *Low energy muons as probes of thin films and near surface regions.* Physica B-Condensed Matter 326, 196-204 (2003).

G.D. Morris, R.H. Heffner, J.E. Sonier, D.E. MacLaughlin, O.O. Bernal, G.J. Nieuwenhuys, A.T. Savici, P.G. Pagliuso and J.L. Sarrao, *Magnetism and superconductivity in CeRh1-xIrxIn5 heavy fermion materials.* Physica B-Condensed Matter 326, 390-393 (2003).

A.M. Mulders, C.T. Kaiser, S.J. Harker, P.C.M. Gubbens, A. Amato, F.N. Gygax, A. Schenck, P. Dalmas de Réotier, A. Yaouanc, K.H.J. Buschow and A. A. Menovsky, *Muon location and muon dynamics in DyNi5.* Physical Review B 67, art-014303 (2003).

A.Yaounc, P. Dalmas de Réotier, P. Bonville, J.A. Hodges, P.C.M. Gubbens, C.T. Kaise, and S. Sakatya, *Spin dynamics in geometrically frustrated compounds,* Physica B 326, 456-459 (2003).

C.T. Kaiser, P.C.M. Gubbens, F.M. Mulder, P.D. de Réotier, A. Yaounc, L.J. de Jongh, G. Schmid, P.J.C. King and A. Amato. *μSR investigation of a cluster of mondisperse Pd nanoparticles,* Physica B 326, 484-488 (2003).

W.H. Kraan, S.V. Grigoriev, M.Th. Rekveldt,H.Fredrikze, C.F. de Vroege and J. Plomp, *Test of adiabatic spin flippers for application at pulsed neutron sources.* Nuclear Instruments & Methods in Physics Research Section A- Accelerators Spectrometers Detectors and Associated Equipment 510, 334-345 (2003).

W. Montfrooij, M.C. Aronson, B.D. Rainford, J.A. Mydosh, A.P. Murani, P. Haen and T. Fukuhara, *Extended versus local fluctuations in quantum critical Ce(Ru1- xFex)(2)Ge-2 (x = x(c)=0.76) .* Physical Review Letters 91, art-087202 (2003).

J.K. Wolterink, J. van Male, M. Daoud and O.V. Borisov, *Starburst polyelectrolytes: Scaling and self-consistent-field theory.* Macromolecules 36, 6624-6631 (2003).

R. Jacimovic, M. Maucec and A. Trkov, *Verification of Monte Carlo calculations of the neutron flux in typical irradiation channels of the TRIGA reactor,* Ljubljana. Journal of Radioanalytical and Nuclear Chemistry 257, 513-517 (2003).

N. Iqbal, N.H. van Dijk, V.W.J. Verhoeven, W. Montfrooij, T. Hansen, L. Katgerman and G.J. Kearley, *Experimental study of ordering kinetics in aluminum alloys during solidification.* Acta Materialia 51, 4497-4504 (2003).

P. Schobinger-Papamantellos, K.H J. Buschow, C. Ritter and L. Keller, *The magnetic phase diagram of the HoCo2X2 (X = Ge, Si) and DyCo2Ge2 compounds by neutron diffraction.* Journal of Magnetism and Magnetic Materials 264, 130-141 (2003).

G.R. Burns, F. Favier, D.J. Jones, J. Roziere and G.J. Kearley, *Potential model for tetrathiafulvalene based on inelastic neutron scattering and Raman spectra.* Journal of Chemical Physics 119, 4929-4933 (2003).

V.A. Yartys, F.R. de Boer, K.H.J. Buschow, B. Ouladdiaf, H.W. Brinks and B.C. Hauback, *Crystallographic and magnetic structure of Pr6Fe13AuD13.* Journal of Alloys and Compounds 356, 142-146 (2003).

K. Prokes, H. Nakotte, V. Sechovsky and E. Brück, *Neutron scattering studies on uranium compounds in high magnetic fields. Journal of Physics-Condensed Matter 15,* S1985-S1989 (2003).

G.J. Kearley, F.M. Mulder, S.J. Picken, P.H.J. Kouwer and J. Stride, *Dynamics of discotic methoxy triphenylene molecules from quasielastic neutron scattering and molecular dynamics simulations.* Chemical Physics 292, 185-190 (2003).

A.V. Sidorenko, P.A. Rodnyi and C.W.E. van Eijk, *New storage phosphors for thermal neutron detection.* Technical Physics Letters 29, 586-588 (2003).

S.E. Offerman, L.J.G.W. van Wilderen, N.H. van Dijk, J. Sietsma, M.Th. Rekveldt and S. van der Zwaag, *In-situ study of pearlite nucleation and growth during isothermal austenite decomposition in nearly eutectoid steel.* Acta Materialia 51, 3927-3938 (2003).

R.L.C. Vink and G.T. Barkema, *Large well-relaxed models of vitreous silica, coordination numbers, and entropy.* Physical Review B 67, art-245201 (2003).

E. Mendes, S. Viale, O. Santin, M. Heinrich and S J. Picken, *A small-angle neutron scattering investigation of rigid polyelectrolytes under shear.* Journal of Applied Crystallography 36, 1000-1005 (2003).

R. Pynn, M.R. Fitzsimmons, H. Fritzsche, J. Major and M.Th. Rekveldt, *Does beam divergence matter for neutron reflectometry?* Physica B-Condensed Matter 336, 1-7 (2003).

M. Wagemaker, R. van de Krol and A.A. van Well, *Nanomorphology of lithiated thin film TiO2 anatase probed with in situ neutron reflectometry.* Physica B-Condensed Matter 336, 124-129 (2003).

S.V. Grigoriev, S.V. Maleyev, A.I. Okorokov, H. Eckerlebe, N.H. van Dijk and E. Brück, *Polarized SANS: critical scattering in invars.* Physica B-Condensed Matter 335, 30-33 (2003).

S.E. Offerman, L.J.G.W. van Wilderen, N.H. van Dijk, M.Th. Rekveldt, J. Sietsma and S. van der Zwaag, *Cluster formation of pearlite colonies during the austenite/ pearlite phase transformation in eutectoid steel.* Physica B-Condensed Matter 335, 99-103 (2003).

E.A. Kelberg, S.V. Grigoriev, A.I. Okorokov, H. Eckerlebe, N. . Grigorieva, W H. Kraan, A.A. Eliseev, A.V. Lukashin, A.A. Vertegel and K.S. Napolskii, *SANS study of new magnetic nanocomposites embedded into the mesoporous silica.* Physica B-Condensed Matter 335, 123-126 (2003).

L. Koszegi, Z. Somogyvari, N. H. van Dijk and M.Th. Rekveldt, *Neutron depolarisation study of nanocrystalline Fe73.5Nb3Cu1Si13.5B9 alloy.* Physica B-Condensed Matter 335, 140-142 (2003).

Th. Brückel, R. Eccleston, H. Lauter, S. Maleyev, Th. Rekveldt, A. Schreyer, J. Schweizer and B. Toperverg, *Polarized neutron methods and instrumentation for pulsed sources.* Physica B-Condensed Matter 335, 143-146 (2003).

Th. Rekveldt, W.G. Bouwman, W.H. Kraan, T.V. Krouglov and J. Plomp, *Larmor precession applications: magnetised foils as spin flippers in spin-echo SANS with varying wavelength.* Physica B-Condensed Matter 335, 164-168 (2003).

A.F. Schebetov, S.V. Metelev, B.G. Peskov, N.K. Pleshanov, V.M. Pusenkov, V.G. Syromyatnikov, V.A. Ul'yanov, W.H. Kraan, C.F. de Vroege and M.Th. Rekveldt, *Improved multichannel neutron polarizers on basis of CoFeV/TiZr supermirrors with TiZrGd underlayer.* Physica B-Condensed Matter 335, 223-225 (2003).

S.V. Grigoriev, Y.O. Chetverikov, W.H. Kraan and M.Th. Rekveldt, *Neutron multiwave interference experiments with many resonance coils.* Physica B-Condensed Matter 335, 243-246 (2003).

R. Zangi and A.E. Mark, *Bilayer ice and alternate liquid phases of confined water.* Journal of Chemical Physics 119, 1694-1700 (2003).

G.A. Stewart, I.M. McPherson, P.C.M. Gubbens, C.T. Kaiser, P. Dalmas de Réotier, A. Yaounc, S.P. Cottrell, *Search for magnetic Cu – Cu ordering in Ga2BaCuO5.* J. Alloys and Comp. 358, 7-11 (2003).

S.V. Grigoriev, Yu. O. Chetverikov, A.V. Syromyatnikov, W.H. Kraan, M.Th. Rekveldt. *Neutron-multiwave-interference experiments with many resonance coils.* Phys. Rev. A 68, art 033603/1-033603/9 (2003)

S.E. Offerman. L.J.G.W. van Wilderen, N.H. van Dijk, J. Sietsma, M.Th. Rekveldt, S. van der Zwaag. *In-situ study of perlite nucleation and growth during isothermal austenite decomposition in nearly eutectoid steel.* Acta Materialia 51, 3927-3938 (2003)

Publications 2002

S.G. Carling, D. Visser, D. Hautot, I.D. Watts, P. Day, J. Ensling, P. Gutlich, G.J. Long and F. Grandjean, *Polarized neutron diffraction and Mossbauer spectral study of short-range magnetic correlations in the ferrimagnetic layered compounds (PPh4) [(FeFeIII)-Fe-II(ox)(3)] and (NBu4) [(FeFeIII)-Fe-II(ox)(3)].* Physical Review B 66, art-104407 (2002).

A. Yaouanc, P. Dalmas de Réotier, P.C.M. Gubbens, C.T. Kaiser, A.A. Menovsky, M. Mihalik and S.P. Cottrell, *Evidence for weak itinerant long-range magnetic correlations in UGe2.* Physical Review Letters 89, art-147001 (2002).

P. Svoboda, P. Javorsky, V. Sechovsky, A.A. Menovsky, M. Hofmann and N. Stusser, *Magnetic phase diagram and critical scattering of UNi2Si2.* Physica B 322, 248-251 (2002).

H.B. Eitouni, N.P. Balsara, H. Hahn, J.A. Pople and M A. Hempenius, *Thermodynamic interactions in organometallic block copolymers: Poly(styrene-block-ferrocenyldimethylsilane).* Macromolecules 35, 7765-7772 (2002).

K. Mortensen, E. Theunissen, R. Kleppinger, K. Almdal and H. Reynaers, *Shear-induced morphologies of cubic ordered block copolymer micellar networks studied by in situ small-angle neutron scattering and rheology.* Macromolecules 35, 7773-7781 (2002).

P. Khalifah, R. Osborn, Q. Huang, H. W. Zandbergen, R. Jin, Y. Liu, D. Mandrus and R.J. Cava, *Orbital ordering transition in La4Ru2O10.* Science 297, 2237-2240 (2002).

V.O. de Haan, H.P.M. Gibcus, R.M. Gommers, F. Labohm, A.A. van Well, P.F.A. de Leege, A. Schebetov and V. Pusenkov, *A new method to determine in situ the transmission of a neutron-guide system at a reactor source.* Nuclear Instruments & Methods in Physics Research Section A- Accelerators Spectrometers Detectors and Associated Equipment 484, 451-458 (2002).

N.H. Van Dijk, S.E. Offerman, W.G. Bouwman, M.Th. Rekveldt, J. Sietsma, S. Van der Zwaag, A. Bodin and R. K. Heenan, *High temperature SANS experiments on Nb(C,N) and MnS precipitates in HSLA steel.* Metallurgical and Materials Transactions A-Physical Metallurgy and Materials Science 33, 1883-1891 (2002).

J.T. Padding and W.J. Briels, *Time and length scales of polymer melts studied by coarse- grained molecular dynamics simulations.* Journal of Chemical Physics 117, 925-943 (2002).

P. Chandra, P. Coleman, J.A. Mydosh and V. Tripathi, *Hidden orbital order in the heavy fermion metal URu2Si2.* Nature 417, 831-834 (2002).

S.F. Parker, N.A. Marsh, L.M. Camus, M.K. Whittlesey, U. A. Jayasooriya and G.J. Kearley, Ethylidyne tricobalt nonacarbonyl: Infrared, FT-Raman, and inelastic neutron scattering spectra. Journal of Physical Chemistry A 106, 5797-5802 (2002).

E. Kemner, A. R. Overweg, L. van Eijck, A.N. Fitch, E. Suard, I.M. de Schepper and G.J. Kearley, *Localization of ferrocene in NaY zeolite by powder x-ray and neutron diffraction.* Journal of Chemical Physics 116, 10838-10845 (2002).

C.G. de Kruif, R. Tuinier, C. Holt, P.A. Timmins and H.S. Rollema, *Physicochemical study of kappa- and beta-casein dispersions and the effect of cross-linking by transglutaminase.* Langmuir 18, 4885-4891 (2002).

P. Chandra, P. Coleman and J.A. Mydosh, *Pressure-induced magnetism and hidden order in URu2Si2.* Physica B 312, 397-400 (2002).

K. Prokes, P. Javorsky, A. Gukasov, E. Brück and V. Sechovsky, *Field-induced change of the antiferromagnetic structure of UNiAl.* Physica B 312, 872-874 (2002).

H. Nakotte, R.A. Robinson, T.M. Kelley, S. Chang, T. Swan-Wood and E. Brück, *Inelastic neutron scattering studies on UNiGe.* Physica B-Condensed Matter 312, 875-876 (2002).

W.T. Fu, D. Visser and D.J.W. Ijdo, *On the crystal structure of BaTbO3.* Journal of Solid State Chemistry 165, 393-396 (2002)

D.W. Boukhvalov, A.I. Lichtenstein, V.V. Dobrovitski, M.I. Katsnelson, B.N. Harmon, V.V. Mazurenko and V.I. Anisimov, *Effect of local Coulomb interactions on the electronic structure and exchange interactions in Mn-12 magnetic molecules.* Physical Review B 65, art-184435 (2002).

G.R. Blake, T.T.M. Palstra, Y. Ren, A.A. Nugroho and A.A. Menovsky, *Neutron diffraction, x-ray diffraction, and specific heat studies of orbital ordering in YVO3.* Physical Review B 65, art-174112 (2002).

R.W.E. van de Kruijs and J. de Blois, *Fast two-dimensional position-sensitive detection of neutrons in a time-of-flight reflectometer.* Nuclear Instruments & Methods in Physics Research Section A- Accelerators Spectrometers Detectors and Associated Equipment 482, 347-354 (2002).

G.J. Kearley, P. Johansson, R.G. Delaplane and J. Lindgren, *Structure, vibrational-dynamics and first-principles study of diglyme as a model system for poly(ethyleneoxide).* Solid State Ionics 147, 237-242 (2002).

K. Prokes, T. Tahara, Y. Echizen, T. Takabatake, T. Fujita, I.H. Hagmusa, J. C. P. Klaasse, E. Brück, F.R. de Boer, M. Divis and V. Sechovsky, *Electronic properties of a URhGe single crystal.* Physica B 311, 220-232 (2002).

K. Prokes, P.F. de Chatel, E. Brück, F.R. de Boer, K. Ayuel, H. Nakotte and V. Sechovsky, *Canted ferromagnetic structure of UNiGe in high magnetic fields.* Physical Review B 65, art-144429 (2002).

M. Kenzelmann, R. Coldea, D.A. Tennant, D. Visser, M. Hofmann, P. Smeibidl and Z. Tylczynski, *Order-to-disorder transition in the XY-like quantum magnet Cs2CoCl4 induced by noncommuting applied fields.* Physical Review B 65, art-144432 (2002).

J. Perez-Ramirez, G. Mul, F. Kapteijn, J.A. Moulijn, A.R. Overweg, A. Domenech, A. Ribera and I.W.C.E. Arends, *Physicochemical characterization of isomorphously substituted FeZSM-5 during activation.* Journal of Catalysis 207, 113-126 (2002).

M. Alvarez, E. Lomba, P. Verkerk, S.A. van der Aart, M. Bionducci, I. Mirebeau and W. van der Lugt, *Neutron diffraction investigation of liquid alkali metal- gallium alloys. Giant cluster formation?* Zeitschrift fur Anorganische und Allgemeine Chemie 628, 553-558 (2002).

S.E. Offerman, N.H. Van Dijk, M.Th. Rekveldt, J. Sietsma and S. Van der Zwaag, *Ferrite/pearlite band formation in hot rolled medium carbon steel.* Materials Science and Technology 18, 297-303 (2002).

M. Jung, B.H. Robinson, D.C. Steytler, A.L. German and R.K. Heenan, *Polymerization of styrene in DODAB vesicles: A small-angle neutron scattering study.* Langmuir 18, 2873-2879 (2002).

S.J. Harker, B.D. van Dijk, A.M. Mulders, P.C.M. Gubbens, G.A. Stewart, C.F. de Vroege and K.H.J. Buschow, *Crystal fields and magnetic interactions in TmT2Si2 (T = Co, Ni, Cu).* Journal of Physics-Condensed Matter 14, 2705-2714 (2002).

G.A. de Wijs, C.M. Fang, G. Kresse and G. de With, *First-principles calculation of the phonon spectrum of MgAl2O4 spinel.* Physical Review B 65, art-094305 (2002).

K. Prokes, O. Tegus, E. Brück, J.C.P. Klaasse, F.R. de Boer and K.H.J. Buschow, *Magnetic properties and magnetic structure of HoTiGe and ErTiGe.* Journal of Alloys and Compounds 335, 62-69 (2002).

F.A.F. Fraga, L.M.S. Margato, S.T.G. Fetal, M.M.F.R. Fraga, R.F. Marques, A.J.P.L. Policarpo, B. Guerard, A. Oed, G. Manzini and T. van Vuure, *CCD readout of GEM-based neutron detectors.* Nuclear Instruments & Methods in Physics Research Section A- Accelerators Spectrometers Detectors and Associated Equipment 478, 357-361 (2002).

J.J.M. Franse, *Anomalous superconductivity and antiferro-magnetism in the U(Pt,Pd)(3) system.* Acta Physica Polonica A 100, 153-176 (2001).

J.A. Hodges, P. Bonville, A. Forget, A. Yaouanc, P. Dalmas de Réotier, G. Andre, M. Rams, K. Krolas, C. Ritter, P.C.M. Gubbens, C.T. Kaiser, P.J.C. King and C. Baines, *First-order transition in the spin dynamics of geometrically frustrated Yb2Ti2O7.* Physical Review Letters 88, art-077204 (2002).

R.W.E. van de Kruijs, M.Th. Rekveldt, H. Fredrikze, J.T. Kohlhepp, J.K. Ha and W J.M. de Jonge, *Magnetic interlayer exchange coupling in epitaxial Fe/Si/Fe(001) studied by polarized neutron reflectometry.* Physical Review B 65, art-064440 (2002).

C.W.E. van Eijk, *Neutron PSDs for the next generation of spallation neutron sources.* Nuclear Instruments & Methods in Physics Research Section A- Accelerators Spectrometers Detectors and Associated Equipment 477, 383-390 (2002).

H. Grull, A.R. Esker, S.K. Satija and C.C. Han, *Polymer transport across isotope-selective interdiffusion barriers.* Europhysics Letters 57, 533-539 (2002).

B.I. Ostrovskii, S.N. Sulyanov, N.I. Boiko, V.P. Shibaev and W.H. de Jeu, *Structure and frustration in liquid crystalline polyacrylates I.* Bulk behaviour. European Physical Journal e 6, 277-285 (2001).

A. Ramzi, R. Scherrenberg, J. Joosten, P. Lemstra and K. Mortensen, *Structure-property relations in dendritic polyelectrolyte solutions at different ionic strength.* Macromolecules 35, 827-833 (2002).

H. Retsos, A.F. Terzis, S.H. Anastasiadis, D.L. Anastassopoulos, C. Toprakcioglu, D.N. Theodorou, G.S. Smith, A. Menelle, R.E. Gill, G. Hadziioannou and Y. Gallot, *Mushrooms and brushes in thin films of diblock copolymer/homopolymer mixtures.* Macromolecules 35, 1116-1132 (2002).

K.D.F. Wensink and B. Jerome, *Dewetting induced by density fluctuations.* Langmuir 18, 413-416 (2002).

M.Th. Rekveldt, W. Kraan and T. Keller, *High-resolution diffraction using Larmor precession of polarized neutrons.* Journal of Applied Crystallography 35, 28-33 (2002).

A. Remhof, G. Song, D. Labergerie, J. Isidorsson, A. Schreyer, F. Guthoff, J. Hartwig and H. Zabel, *On the structure of epitaxial YHx films.* Journal of Alloys and Compounds 330, 276-279 (2002).

J.A. Hodges, P. Bonville, A. Forget, A. Yaouanc, P. Dalmas de Réotier, G. Andre, M. Rams, K. Krolas, C. Ritter, P.C.M. Gubbens, C.T. Kaiser, P.J.C. King and C. Baines, *First-order transition in the spin dynamics of geometrically frustrated Yb2Ti2O7.* Physical Review Letters 88, art-077204 (2002).

R.H. Heffner, D.E. MacLaughlin, G.J. Nieuwenhuys, J.L. Sarrao and J.E. Sonier, *Magnetic phase diagram for Li-doped La2CuO4.* Physica B 312, 65-67 (2002).

A.M. Mulders, P.C.M. Gubbens, C T. Kaiser, A. Amato, F. N. Gygax, A. Schenck, P. Dalmas de Réotier, A. Yaouanc, K. H.J. Buschow, F. Kayzel and A.A. Menovsky, *Muon localization along a six-fold ring-shaped site and muon quantum hopping in GdNi5.* Journal of Alloys and Compounds 330, 454-457 (2002).

W. Kockelmann, M. Hofmann, O. Moze, S J. Kennedy and K.H.J. Buschow, *Crystal structure and magnetic ordering of RNi10Si2 compounds.* European Physical Journal B 30, 25-32 (2002).

V.Y. Pomjakushin, A.M. Balagurov, T.V. Elzhov, D.V. Sheptyakov, P. Fischer, D.I. Khomskii, V.Y. Yushankhai, A.M. Abakumov, M.G. Rozova, E.V. Antipov, M.V. Lobanov and S.J.L. Billinge, *Atomic and magnetic structures, disorder effects, and unconventional superexchange interactions in A(2)MnGaO(5+delta) (A = Sr, Ca) oxides of layered brownmillerite-type structure.* Physical Review B 66, art-184412 (2002).

G. Riou, S. Jandl, M. Poirier, V. Nekvasil, M. Marysko, J. Fabry, K. Jurek, M. Divis, J. Holsa, I.M. Sutjahja, A.A. Menovsky, S.N. Barilo, S.V. Shiryaev and L.N. Kurnevich, *Infrared transmission study of crystal-field excitations in La2-x-yNdxSryCuO4.* Physical Review B 66, art-224508 (2002).

O. Isnard, G.J. Long, D. Hautot, K.H.J. Buschow and F. Grandjean, *A neutron diffraction and Mossbauer spectral study of the magnetic spin reorientation in Nd6Fe13Si.* Journal of Physics-Condensed Matter 14, 12391-12409 (2002).

W.T. Fu, D. Visser and D.J.W. Ijdo, *High-resolution neutron powder diffraction study on the structure of Sr2SnO4.* Journal of Solid State Chemistry 169, 208-213 (2002).

B.B. Van Aken, A. Meetsma, Y. Tomioka, Y. Tokura and T. T.M. Palstra, *Structural response to O*-O ' and magnetic transitions in orthorhombic perovskites.* Physical Review B 66, art-224414 (2002).

S.V. Grigoriev, W.H. Kraan and M.Th. Rekveldt, *Precession phase of the neutron spin after adiabatic passage through a resonant spin flipper.* Applied Physics A-Materials Science & Processing 74, S76-S78 (2002).

W.H. Kraan, S.V. Grigoriev, M.Th. Rekveldt, W.G. Bouwman and O. Uca, S*pin-echo SANS based on adiabatic HF flippers in dipole magnets with skew poles.* Applied Physics A-Materials Science & Processing 74, S79-S81 (2002).

M.Th. Rekveldt, W.G. Bouwman, W.H. Kraan, S. Grigoriev, J. Plomp and O. Uca, *Magnetised foils as pi-flippers in spin-echo spectrometry.* Applied Physics A-Materials Science & Processing 74, S94-S96 (2002).

W.G. Bouwman, O. Uca, S.V. Grigoriev, W.H. Kraan, J. Plomp and M.Th. Rekveldt, *First quantitative test of spin-echo small-angle neutron scattering.* Applied Physics A-Materials Science & Processing 74, S115-S117 (2002).

T. Keller, M.Th. Rekveldt and K. Habicht, *Neutron Larmor diffraction measurement of the lattice-spacing spread of pyrolytic graphite.* Applied Physics A-Materials Science & Processing 74, S127-S129 (2002).

O. Uca, W.G. Bouwman, J. Plomp, W.H. Kraan and M.Th. Rekveldt, *Line-integral corrections in Larmor-precession devices.* Applied Physics A-Materials Science & Processing 74, S174-S176 (2002).

M. T. Rekveldt, W.G. Bouwman, W.H. Kraan, S. Grigoriev, O. Uca and T. Keller, *Overview of new Larmor precession techniques.* Applied Physics A-Materials Science & Processing 74, S323-S325 (2002).

V.W.J. Verhoeven, I.M. de Schepper and E.M. Mulder, *Magnetic signature of charge ordering in Li[Mn1.96Li0.04]O-4 and Li-0.2[Mn1.96Li0.04]O-4.* Applied Physics A-Materials Science & Processing 74, S574-S576 (2002).

N.H. van Dijk, P. Rodière, B. Fåk, A. Huxley, J. Flouquet, M. T. Fernandez-Diaz and F. Yakhou, *Uniaxial pressure dependence of the antiferromagnetic order in UPt3.* Applied Physics A-Materials Science & Processing 74, S586-S588 (2002).

S. Neov, L. Dabrowski, M. Hofmann and H.J.M. Bouwmeester, *Neutron-diffraction and Mossbauer-spectroscopy study of La0.6Sr0.4Fe1-xCoxO3-y (x=0, 0.5) perovskites.* Applied Physics A-Materials Science & Processing 74, S664-S666 (2002).

V.N. Zabenkin, L.A. Axelrod, G.P. Gordeev, W.H. Kraan, I.M. Lazebnik, D.N. Orlova and A.A. Vorobiev, *Neutron depolarisation in ferrofluids during magnetising/demagnetising cycles.* Applied Physics A-Materials Science & Processing 74, S710-S712 (2002).

S.V. Grigoriev, S.V. Maleyev, V.V. Deriglazov, A.I. Okorokov, N.H. van Dijk, E. Brück, J.C.P. Klaasse, H. Eckerlebe and G. Kozik, *Spin-wave dynamics in Invar Fe65Ni35 alloy studied by small- angle polarized neutron scattering.* Applied Physics A-Materials Science & Processing 74, S719-S721 (2002).

N.H. van Dijk, S.E. Offerman, W.G. Bouwman, M.Th. Rekveldt, J. Sietsma, S. van der Zwaag, A. Bodin and R.K. Heenan, *SANS experiments on Nb(C, N) and MnS precipitates in HSLA steel.* Applied Physics A-Materials Science & Processing 74, S978-S980 (2002).

L.J.G.W. van Wilderen, S.E. Offerman, N.H. van Dijk, M.Th. Rekveldt, J. Sietsma and S. van der Zwaag, *Neutron depolarization study of the austenite/pearlite phase transformation in steel.* Applied Physics A-Materials Science & Processing 74, S1052-S1054 (2002).

F.G.B. Ooms, M. Wagemaker, A.A. van Well, F.M. Mulder, E.M. Kelder and J. Schoonman, *Structure determination of high-voltage LiMg delta Ni0.5-delta Mn1.5O4 spinels for Li-ion batteries.* Applied Physics A-Materials Science & Processing 74, S1089-S1091 (2002).

E. Kemner, C. F. de Vroege, M. Telling, I.M. de Schepper and G.J. Kearley, *Low-frequency modes of ferrocene in zeolite Y.* Applied Physics A-Materials Science & Processing 74, S1348-S1350 (2002).

E. Kemner, A.R. Overweg, U.A. Jayasooriya, S.F. Parker, I.M. de Schepper and G.J. Kearley, *Ferrocene-zeolite interactions measured by inelastic neutron scattering.* Applied Physics A-Materials Science & Processing 74, S1368-S1370 (2002).

C. Ohms, A.G. Youtsos and P. van den Idsert, *Structural integrity assessment based on the HFR Petten neutron beam facilities.* Applied Physics A-Materials Science & Processing 74, S1443-S1445 (2002).

R.W.E. van de Kruijs, V.A. Ul'yanov, M.Th. Rekveldt, H. Fredrikze, S. Langridge, N.K. Pleshanov, V.M. Pusenkov, A.F. Schebetov and V.G. Syromyatnikov, *Polarization analysis of off-specular neutron scattering from domains and rough interfaces in a FeCoV/TiZr multilayer.* Applied Physics A-Materials Science & Processing 74, S1550-S1553 (2002).

A.G. Youtsos and C. Ohms, *European standardization activities on residual stress analysis by neutron diffraction.* Applied Physics A-Materials Science & Processing 74, S1716-S1718 (2002).

B. Fåk, N.H. van Dijk and A.S. Wills, *Comment on Magnetic field effects on neutron diffraction in the antiferromagnetic phase of UPt3.* Physical Review B 66, art-216401 (2002).

F. Galli, G.J. Nieuwenhuys, D.E. MacLaughlin, R. H. Heffner, A. Amato, O.O. Bernal and J.A. Mydosh, *mu SR studies on the charge density waves in RE5Ir4Si10.* Physica B 319, 282-285 (2002).

D.E. MacLaughlin, R.H. Heffner, O.O. Bernal, J.E. Sonier, M.S. Rose, R. Chauf, M.B. Maple and B. Andraka, *Slow spin dynamics in non-fermi-liquid UCu5-xPdx, x = 1.0 and 1.5.* Physica B 312, 453-455 (2002).

P. Javosrky, P.C.M. Gubbens, A.M. Mulders, K.Prokes, N. Stüsser, T.J. Gortermulder and R.W.A. Hendrikx, *Incommensurate magnetic structure in TmCuAl at low temperatures,* J. Magn. Magn. Mat. 251, 123-126 (2002)

M. Kenzelmann, R. Coldea, D.A. Tennant, D.Visser, M. Hoffmann, P. Smeibidl, Z. Tylczynski. *Field dependence of magnetic ordering in the frustrated X_-magnet Cs2CoCl4.* Applied Physics A-Materials Science & Processing 74, S904-S906 (2002).

M. Alvarez, P. Verkerk, W. van der Lugt. *Extended superstructures inelectron-deficient Zintl-type alloys. J of non-crystalline solids.* 312-314, 15-21 (2002).

D. Champoin, J. Tomkinson, G. J. Kearley. *a-Climax: a new INS analytical tool.* Applied Physics A- Material Science & Processing 74 , S1302-1304 (2002).

C. Cabrillo, F.J. Bermejo, P. Verkerk, A. Maira-Vidal, S.M. Bennington, D. Martin. *How well do we know atomic motions of simple liquids?* Phys. Rev. Lett. 87, 075508 1-4 (2002)

W. van der Lugt and P. Verkerk. *Molten Zintl alloys. In Meyer, Gerd, Naumann, Dieter & Wesemann.* Inorganic chemistry Highlights. 1-19. Weinheim, Germany: Wiley-VCH Verlag.

F.G.B. Ooms, E.M. Kelder, J. Schoonman, M. Wagemaker, F.M. Mulder. *High-voltage LiMgNi0.5-Mn1.5O4 spinels for Li-ion batteries.* Solid State Ionics 152-153, 143-153. (2002).

R. Pynn, M.R. Fitzsimmons, M.Th. Rekveldt, J. Major, H. Fritzsche, D. Weller, E.C. Johns. *Optimizating the resolution and intensity of neutron scattering experiments using Neutron Spin Echo: Application to the discrimination of diffuse scattering in neutron reflectivity experiments.* Review of scientific instruments 73, 2948-2957 (2002).

A. Navarro, J. Vazquez, M. Montejo, J.J. Lopez Gonzalez, G.J. Kearley. *A re-investigation of the v7 and v10 modes of pyridazine on the basis of the inelastic neutron scattering spectrum analysis.* Chem. Phys. Lett. 381, 483-491.

G.J. Kearley, P. Schiebel, M. Johnson, E. Brück. *The isomorphous transition between Co(NH3)6(PF6)2 and Ni(NH3)6(PF6)2.* Applied Physics A- Material Science & Processing 74 , S76 - S78 (2002).

B. Fåk, N.H. van Dijk , A.S. Wills. *Comment on 'Magnetic field effects on neutron diffraction in the antiferromagnetic phase of UPT3.'* Phys. Rev. B 66 216401-3 (2002).

L. van Eijck, L.D.A. Siebbeles, F.C. Grozema, I.M. de. Schepper, G.J. Kearley. *INS as a probe of inter-monomer angles in polymers.* Applied Physics A- Material Science & Processing 74 , S496 – S498 (2002).

N.H. van Dijk, P. Rodière, B. Fåk, A. Huxley, J. Flouquet. *Weak antiferromagnetic order and superconductivity in UPt3 studied by neutron scattering.* Physica B 319, 220-232 (2002).

Publications 2001

E.P. van Klaveren, J.P.J. Michels, J A. Schouten, D.D. Klug and J.S. Tse, *Molecular dynamics simulation study of the properties of doubly occupied N-2 clathrate hydrates.* Journal of Chemical Physics 115, 10500-10508 (2001).

P. Vassilev, C. Hartnig, M.T.M. Koper, F. Frechard and R.A. van Santen, *Ab initio molecular dynamics simulation of liquid water and water-vapor interface.* Journal of Chemical Physics 115, 9815-9820 (2001).

W.H. Kraan, M.Th. Rekveldt, V.A. Ul'yanov, V.N. Zabenkin, L.A. Akselrod, G.P. Gordeev, V.M. Pusenkov and R. Sellmann, *Study of domain structures in FeCo/TiZr multilayers by means of 3D neutron depolarisation.* Journal of Magnetism and Magnetic Materials 236, 302-311 (2001).

P. Schobinger-Papamantellos, J. Rodriguez-Carvajal, G. Andre, N.P. Duong, K.H J. Buschow and P. Toledano, *Simultaneous structural and magnetic transitions in YFe4Ge2 studied by neutron diffraction and magnetic measurements.* Journal of Magnetism and Magnetic Materials 236, 14-27 (2001).

K. Prokes, O. Tegus, E. Brück, T.J. Gortenmulder, F.R. de Boer and K.H.J. Buschow, *Magnetic properties of TbTiGe.* Journal of Magnetism and Magnetic Materials 236, 28-36 (2001).

T.L. van Vuure, C.W.E. van Eijk, F. Fraga, R.W. Hollander and L. Margato, *High-pressure GEM operation aiming at thermal neutron detection.* Ieee Transactions on Nuclear Science 48, 1092-1094 (2001).

C.P. Allier, R.W. Hollander, C.W.E. van Eijk, P.M. Sarro, M. de Boer, J.B. Czirr, J.P. Chaminade and C. Fouassier, *Thin photodiodes for a neutron scintillator silicon-well detector.* Ieee Transactions on Nuclear Science 48, 1154-1157 (2001).

O. Moze, J.M. Cadogan, Y. Janssen, F.R. de Boer, K.H.J. Buschow and S J. Kennedy, *Magnetic structure and anisotropy of YFe6Ga6 and HoFe6Ga6.* European Physical Journal B 23, 29-36 (2001).

P.F. de Chatel, *Heavy fermions: recent developments and open questions.* Philosophical Magazine B-Physics of Condensed Matter Statistical Mechanics Electronic Optical and Magnetic Properties 81, 1389-1395 (2001).

H. Kepa, J. Kutner-Pielaszek, J. Blinowski, A. Twardowski, C.F. Majkrzak, T. Story, P. Kacman, R.R. Galazka, K. Ha, H.J.M. Swagten, W J.M. De Jonge, A.Y. Sipatov, V. Volobuev and T.M. Giebultowicz, *Antiferromagnetic interlayer coupling in ferromagnetic semiconductor EuS/PbS(001) superlattices.* Europhysics Letters 56, 54-60 (2001).

V. Lisy, B. Brutovsky, A.V. Zatovsky and A.V. Zvelindovsky, *On the theory of light and neutron scattering from droplet microemulsions.* Journal of Molecular Liquids 93, 113-118 (2001).

K. Prokes, V. Sechovsky, F. Bourdarot, P. Burlet, J. Kulda and A. Menovsky, *Magnetic structure of a UNiAl single crystal under pressure.* Journal of Magnetism and Magnetic Materials 226, 1186-1187 (2001).

K. Mortensen, K. Almdal, E. Theunissen, R. Kleppinger and H. Reynaers, *Texture of ordered SEBS block copolymer micellar networks studied by small-angle neutron scattering.* Abstracts of Papers of the American Chemical Society 222, 71-PMSE (2001).

P. Verkerk, *Dynamics in liquids.* Journal of Physics-Condensed Matter 13, 7775-7799 (2001).

J.C. Toledano, R.S. Berry, P.J. Brown, A.M. Glazer, R. Metselaar, D. Pandey, J.M. Perez-Mato, R.S. Roth and S.C. Abrahams, *Nomenclature of magnetic, incommensurate, composition-changed morphotropic, polytype, transient-structural and quasicrystalline phases undergoing phase transitions. II. Report of an IUCr Working Group on Phase Transition Nomenclature.* Acta Crystallographica Section A 57, 614-626 (2001).

S.V. Grigoriev, S.A. Klimko, W.H. Kraan, S.V. Maleyev, A.I. Okorokov, M.Th. Rekveldt and V.V. Runov, *Magnetic phase transition in disordered Fe-Ni alloys studied by means of small-angle neutron scattering and three-dimensional analysis of the neutron depolarization.* Physical Review B 6409, art-094426 (2001).

A.S. Wills, G.S. Oakley, D. Visser, J. Frunzke, A. Harrison and K H. Andersen, *Short-range order in the topological spin glass (D3O)Fe- 3(SO4)(2)(OD)(6) using xyz polarized neutron diffraction.* Physical Review B 6409, art-094436 (2001).

H. Nakotte, S. Chang, Z. Tun, K. Prokes, P. Svoboda, V. Sechovsky and E. Brück, *Field dependence of the incommensurate magnetic order in UNiGe.* Journal of Magnetism and Magnetic Materials 226, 70-71 (2001).

F. Honda, G. Oomi, P. Svoboda, A. Syshchenko, V. Sechovsky, S. Khmelevski, M. Divis, A.V. Andreev, N. Takeshita, N. Mori and A.A. Menovsky, *Magnetic phase diagram of UNi2Si2 under magnetic field and high-pressure.* Journal of Magnetism and Magnetic Materials 226, 585-587 (2001).

B.L. Mojet, J. Eckert, R.A. van Santen, A. Albinati and R.E. Lechner, *Evidence for chemisorbed molecular hydrogen in Fe-ZSM5 from inelastic neutron scattering.* Journal of the American Chemical Society 123, 8147-8148 (2001).

M.B.J. Meinders, G.G M. van den Bosch and H.H.J. de Jongh, *Adsorption properties of proteins at and near the air/water interface from IRRAS spectra of protein solutions.* European Biophysics Journal with Biophysics Letters 30, 256-267 (2001).

D.E. MacLaughlin, O.O. Bernal, R. H. Heffner, G.J. Nieuwenhuys, M.S. Rose, J.E. Sonier, B. Andraka, R. Chau and M.B. Maple, *Glassy spin dynamics in non-fermi-liquid UCu5-xPdx, x=1.0 and 1.5.* Physical Review Letters 8706, art-066402 (2001).

B. de Boer, U. Stalmach, P.F. van Hutten, C. Melzer, V.V. Krasnikov and G. Hadziioannou, *Supramolecular self-assembly and opto-electronic properties of semiconducting block copolymers.* Polymer 42, 9097-9109 (2001).

G.J. Kearley, M.R. Johnson, M. Plazanet and E. Suard, *Structure and vibrational dynamics of the strongly hydrogen- bonded model peptide: N-methyl acetamide.* Journal of Chemical Physics 115, 2614-2620 (2001).

J.A. Stride, U.A. Jayasooriya, N. Mbogo, R.P. White, A. Nicolai and G.J. Kearley, *Hydrogen-bonding in the self-organising system 3,5- dimethylpyrazole.* New Journal of Chemistry 25, 1069-1072 (2001).

P. Schobinger-Papamantellos, G. Andre, J. Rodriguez-Carvajal, K.H.J. Buschow and L. Durivault, *Magnetic ordering of CeNi0.78Sn2 and Ce3Ni2Sn7 compounds by neutron diffraction.* Journal of Alloys and Compounds 325, 29-36 (2001).

S.V. Grigoriev, R. Kreuger, W.H. Kraan, F.M. Mulder and M.Th. Rekveldt, *Neutron wave-interference experiments with adiabatic passage of neutron spin through resonant coils.* Physical Review A 6401, art-013614 (2001).

M. Van Bruijnsvoort, R. Tijssen and W.T. Kok, *Assessment of the diffusional behavior of polystyrene sulfonates in the dilute regime by hollow-fiber flow field flow fractionation.* Journal of Polymer Science Part B-Polymer Physics 39, 1756-1765 (2001).

C. Dekker, B. Agianian, M. Weik, G. Zaccai, J. Kroon, P. Gros and B. de Kruijff, *Biophysical characterization of the influence of salt on tetrameric SecB.* Biophysical Journal 81, 455-462 (2001).

K. Miyazaki and I.M. de Schepper, *Dynamic structure factor of a dilute Lennard-Jones gas.* Physical Review e 6306, art-060201 (2001).

H.G. Schimmel, W. Montfrooij, G.J. Kearley, V.W J. Verhoeven and I.M. de Schepper, *Neutron scattering investigation of the spin dynamics in Li[Mn1.94Li0.04]O-3.94.* Physical Review B 6321, art-214409 (2001).

P. Schobinger-Papamantellos, G. Andre, J. Rodriguez-Carvajal, N.P. Duong and K.H.J. Buschow, *Multiple competing interactions and reentrant ferrimagnetism in Tb0.8Nd0.2Mn6Ge6.* Journal of Magnetism and Magnetic Materials 231, 121-134 (2001).

P. Schobinger-Papamantellos, G. Andre, J. Rodriguez-Carvajal, O. Moze, W. Kockelmann, L.D. Tung and K. H.J. Buschow, *Magnetic ordering of PrCoAl4 a neutron diffraction study.* Journal of Magnetism and Magnetic Materials 231, 162-171 (2001).

E.T.F. Gelade, B. Goderis, C.G. de Koster, N. Meijerink, R.A. T.M. van Benthem, R. Fokkens, N.M.M. Nibbering and K. Mortensen, *Molecular structure characterization of hyperbranched polyesteramides.* Macromolecules 34, 3552-3558 (2001).

W.T. Fu and D.J W. IJdo, *Crystal structure of superconducting BaPb0.7Bi0.15Sb0.15O3.* Solid State Communications 118, 291-294 (2001).

V.W J. Verhoeven, I.M. de Schepper, G. Nachtegaal, A.P. M. Kentgens, E.M. Kelder, J. Schoonman and F.M. Mulder, *Lithium dynamics in LiMn2O4 probed directly by two-dimensional Li-7 NMR.* Physical Review Letters 86, 4314-4317 (2001).

L.A.M.M. Barbosa, R.A. van Santen and J. Hafner, *Stability of Zn(II) cations in chabazite studied by periodical density functional theory.* Journal of the American Chemical Society 123, 4530-4540 (2001).

C. Martin, A. Maignan, M. Hervieu, C. Autret, B. Raveau and D.I. Khomskii, *Magnetic phase diagram of Ru-doped Sm1-xCaxMnO3 manganites: Expansion of ferromagnetism and metallicity.* Physical Review B 6317, art-174402 (2001).

M.Th. Rekveldt, T. Keller and R. Golub, *Larmor precession, a technique for high-sensitivity neutron diffraction.* Europhysics Letters 54, 342-346 (2001).

M.P. Fernandez-Liencres, A. Navarro, J.J. Lopez-Gonzalez, M. Fernandez-Gomez, J. Tomkinson and G.J. Kearley, *Measurement and ab initio modeling of the inelastic neutron scattering of solid melamine - Evidence of the anisotropy in the external modes spectrum.* Chemical Physics 266, 1-17 (2001).

M.Th. Rekveldt, T. Keller and W.H. Kraan, *New instrumentation using Larmor precession of polarised neutrons.* Physica B-Condensed Matter 297, 18-22 (2001).

W.H. Kraan, S.V. Grigoriev, R. Kreuger, F M. Mulder and M.Th. Rekveldt, *Zero-field precession induced by adiabatic RF spin flippers.* Physica B 297, 23-27 (2001).

O. Uca, W.H. Kraan, W.G. Bouwman and M.Th. Rekveldt, *Line integral corrections in spin-echo small angle neutron scattering instrument.* Physica B 297, 28-31 (2001).

V.P. Plakhty, S.V. Maleyev, J. Kulda, E.D. Visser, J. Wosnitza, E.V. Moskvin, T. Bruckel and R.K. Kremer, *Spin chirality and polarised neutron scattering.* Physica B 297, 60-66 (2001).

H. Fredrikze and R.W.E. van de Kruijs, *Calibration of a polarized neutron reflectometer.* Physica B-Condensed Matter 297, 143-147 (2001).

R.W.E. van de Kruijs, V.A. Ul'yanov, M.Th. Rekveldt, H. Fredrikze, N.K. Pleshanov, V.M. Pusenkov, V.G. Syromyatnikov, A F. Schebetov and S. Langridge, *Probing magnetic structures by neutron reflectometry: Off- specular scattering from interfaces and domains in FeCoV/TiZr multilayers.* Physica B 297, 180-184 (2001).

S.V. Grigoriev, N.H. van Dijk, W.H. Kraan, S.V. Maleyev, M.Th. Rekveldt, V.V. Runov and A.I. Okorokov, *Three-dimensional neutron depolarization study of the ferromagnetic-phase transition in a disordered system.* Physica B 297, 250-252 (2001).

K.H.J. Buschow, S.J. Hu, O. Tegus, L. Zhang, E. Brück and F.R. de Boer, *Anisotropy and spin-reorientations in Co-rich rare earth compounds.* Journal of Alloys and Compounds 317, 2-7 (2001).

Z.F. Gu, Z. Y. Liu, D.C. Zeng, S.Z. Liang, J.C.P. Klaasse, E. Brück, F.R. de Boer and K.H.J. Buschow, *On the occurrence of spin-reorientation transitions in R2Co17- xGax and R2Co17-xAlx compounds.* Journal of Alloys and Compounds 319, 37-42 (2001).

S.W. de Leeuw, A. Van Zon and G.J. Bel, *Structural relaxation in poly(ethyleneoxide) and poly(ethyleneoxide)-sodium iodide systems: a molecular dynamics study.* Electrochimica Acta 46, 1419-1426 (2001).

A. Van Zon and S.W. de Leeuw, *A Rouse model for polymer electrolytes.* Electrochimica Acta 46, 1539-1544 (2001).

A. Van Zon, B. Mos, P. Verkerk and S.W. de Leeuw, *On the dynamics of PEO-NaI polymer electrolytes.* Electrochimica Acta 46, 1717-1721 (2001).

N.E. Benes, H. Jobic and H. Verweij, *Quasi-elastic neutron scattering study of the mobility of methane in microporous silica.* Microporous and Mesoporous Materials 43, 147-152 (2001).

Y. Janssen, R.T. Gramsma, J.C.P. Klaasse, E. Brück, K.H.J. Buschow and F.R. de Boer, *Magnetic properties of RFe6Ga6 compounds (R = Gd, Dy, Ho, Er, Tm).* Physica B 294, 208-211 (2001).

N.P. Duong, E. Brück, F.R. de Boer and K.H.J. Buschow, *Magnetic properties of GdFe4Al8 and related compounds.* Physica B-Condensed Matter 294, 212-216 (2001).

C.W.E. van Eijk, *Inorganic-scintillator development.* Nuclear Instruments & Methods in Physics Research Section A- Accelerators Spectrometers Detectors and Associated Equipment 460, 1-14 (2001).

G. Auffermann, A. Simon, T. Gulden, G.J. Kearley and A. Ivanov, *Location and vibrations of hydrogen in La2C3H1.5.* Zeitschrift fur Anorganische und Allgemeine Chemie 627, 307-311 (2001).

P. van Gelderen, P.J. Kelly and G. Brocks, *Phonon spectrum of YH3: Evidence for a broken symmetry structure.* Physical Review B 6310, art-100301 (2001).

N.H. van Dijk, P. Rodière, F. Yakhou, M.T. Fernandez-Diaz, B. Fåk, A. Huxley and J. Flouquet, *Magnetic order of UPt3 under uniaxial pressure.* Physical Review B 6310, art-104426 (2001).

N.H. Luong, J.J. M. Franse and N.H. Hai, *Effect of the crystalline electric field on the Neel temperatures of RCu2 compounds.* Journal of Magnetism and Magnetic Materials 224, 30-32 (2001).

N.P. Duong, J.C.P. Klaasse, E. Brück, F.R. de Boer and K.H.J. Buschow, *Magnetic properties of GdT4Al8 and GdT6Al6 compounds (T=Cr, Mn, Cu).* Journal of Alloys and Compounds 315, 28-35 (2001).

U. Bafile, P. Verkerk, E. Guarini and F. Barocchi, *Neutron Brillouin scattering study of collective dynamics in a dense He-Ne gaseous mixture.* Physical Review Letters 86, 1019-1022 (2001).

P. Schobinger-Papamantellos, K.H.J. Buschow, N.P. Duong and C. Ritter, *Magnetic phase diagram of ErCuSi studied by neutron diffraction and magnetic measurements.* Journal of Magnetism and Magnetic Materials 223, 203-214 (2001).

M. Blaauw and H.H. Chen-Mayer, *Neutron incoherent scattering as a tool to determine hydrogen concentrations and chemical state in titanium.* Abstracts of Papers of the American Chemical Society 220, 115-NUCL (2000).

B. Nicolai, G.J. Kearley, A. Cousson, W. Paulus, F. Fillaux, F. Gentner, L. Schroder and D. Watkin, *Structure of manganese diacetate tetrahydrate and low- temperature methyl-group dynamics.* Acta Crystallographica Section B-Structural Science 57, 36-44 (2001).

N.P. Duong, I.H. Hagmusa, E. Brück, F.R. de Boer and K.H. J. Buschow, *Magnetic properties of TbFe4Al8.* Journal of Alloys and Compounds 313, 21-25 (2000).

J. Frunzke, T. Hansen, A. Harrison, J.S. Lord, G.S. Oakley, D. Visser and A.S. Wills, *Magnetic ordering in diluted kagome antiferromagnets.* Journal of Materials Chemistry 11, 179-185 (2001).

S.G.E. te Velthuis, N.H. van Dijk, M.Th. Rekveldt, J. Sietsma and S. van der Zwaag, *Domain size determination of granular ferromagnetic systems with neutron depolarization.* Journal of Applied Physics 89, 1275-1280 (2001).

B. Rietveld, D. Bedeaux and J.A.M. Smit, *Osmotic compressibility of poly(propylene imine) dendrimers in deuterated methanol.* Journal of Colloid and Interface Science 232, 317-325 (2000).

R.H. Heffner, J.E. Sonier, D.E. MacLaughlin, G J. Nieuwenhuys, G.M. Luke, Y.J. Uemura, W. Ratcliff, S.W. Cheong and G. Balakrishnan, *Muon spin relaxation study of La1-xCaxMnO3.* Physical Review B 6309, art-094408 (2001).

K.G. Pettigrew, D. Visser, A. Harrison, D.H. Nicholson, S.H. Kilcoyne, P. Manuel and A.P. Murani, *Magnetic properties of pure deuteronium and diamagnetically- doped hydronium iron jarosite.* Canadian Journal of Physics 79, 1517-1523 (2001).

K. Prokes, O. Tegus, E. Brück, J.C.P. Klaasse, F.R. de Boer and K.H.J. Buschow, *Magnetic properties and magnetic structure of DyTiGe.* Physica B 307, 169-174 (2001).

A.M. Mulders, P.C.M. Gubbens, C T. Kaiser, A. Amato, F.N. Gygax, A. Schenck, P. Dalmas de Réotier, A. Yaouanc, K.. J. Buschow, F. Kayzel and A.A. Menovsky, *Muon spin dynamics and sites in GdNi5.* Hyperfine Interactions 133, 197-201 (2001).

I.D. Watts, S.G. Carling, P. Day, D. Visser. *Muon spin relaxation studies of magnetic ordering in the molecular-based ferrimagnets P(Ph)4Mn(II)Fe(III)(C2O4)3 and (n-C4H9)4NFe(II)Fe(III)(C2O4)3.* J. Cond. Matter 13, 2225-2227 (2001).

V.P. Plahkty, W. Schweika, Th. Brückel, J. Kulda, S.V. Gavrilov, L-P. Regnault, D. Visser. *Chiral criticality in helimagnet Ho studied by polarization neutron scattering.* Phys. Rev. B 64, R110402 (2001)

S.V. Grigoriev, W.H. Kraan, S.V. Maleyev, M.Th. Rekveldt, A.I. Okorokov, V.,V. Runov. *On the intrinsic anosotropy in neutron depolarisation in precence of a magnetic field.* Journal of Neutron Research 8, 155-174 (2001).

M.R. Johnson, G.J. Kearley. *L'effect tunnel et les protéines.* Pour la Science 281, 177-180 (2001).

L. Zhao, N.H. van Dijk, E. Brück, J. Sietsma, S. van der Zwaag. *Magnetic and X-ray diffraction measurements for the determionation of retained austenite in TRIP steels.* Material Science and Engeneering A 313, 145-152 (2001).

I.B. Rietveld, W.G. Bouwman, W.P.L. Baars, R.K. Heenan. *Location of the outer shell and influence of pH on carboxylic acid-fuctionalized Poly(propyleneimine) dendrimers.* Macromolecules 34 , 8380-8383 (2001).

Publication 2000

F. Galli, R. Feyerherm, R.W.A. Hendrikx, S. Ramakrishnan, G.J. Nieuwenhuys and J.A. Mydosh, *Magnetic structure of the Er3+ moments in the charge-density- wave compound Er5Ir4Si10.* Physical Review B 62, 13840-13843 (2000).

S.V. Grigoriev, W.H. Kraan, F.M. Mulder and M.Th. Rekveldt, *Neutron-wave-interference experiments with two resonance coils.* Physical Review A 6206, art-063601 (2000).

M.R. Johnson and G.J. Kearley, *Quantitative atom-atom potentials from rotational tunneling: Their extraction and their use.* Annual Review of Physical Chemistry 51, 297-321 (2000).

M. Dusek, G. Chapuis, P. Schobinger-Papamantellos, C. Wilkinson, V. Petricek, L.D. Tung and K.H.J. Buschow, *Modulated structure of La2Co1.7 from neutron and X-ray diffraction data.* Acta Crystallographica Section B-Structural Science 56, 959-971 (2000).

W T. Fu, M.J. Polderman and F.M. Mulder, *Structural and transport properties of the BaBi1-xInxO3 system.* Materials Research Bulletin 35, 1205-1211 (2000).

P. Khalifah, Q. Huang, D. M. Ho, H.W. Zandbergen and R.J. Cava, *La7Ru3O18 and La4.87Ru2O12: Geometric frustration in two closely related structures with isolated RuO6 octahedra.* Journal of Solid State Chemistry 155, 189-197 (2000).

C. Massobrio, F.H.M. van Roon, A. Pasquarello and S.W. De Leeuw, *Breakdown of intermediate-range order in liquid GeSe2 at high temperatures.* Journal of Physics-Condensed Matter 12, L697-L704 (2000).

V.P. Plakhty, J. Kulda, D. Visser, E.V. Moskvin and J. Wosnitza, *Chiral critical exponents of the triangular-lattice antiferromagnet CsMnBr3 as determined by polarized neutron scattering.* Physical Review Letters 85, 3942-3945 (2000).

F. Haarmann, H. Jacobs, B. Asmussen, C. Nöldeke, G.J. Kearley and J. Combet, *Reorientational motion of the HS-ions in hydrogensulfides of alkali metals (NaHS, KHS, RbHS): A quasielastic neutron scattering study.* Journal of Chemical Physics 113, 8161-8167 (2000).

I.B. Rietveld and D. Bedeaux, *Self-diffusion of poly(propylene imine) dendrimers in methanol.* Macromolecules 33, 7912-7917 (2000).

P. Schiebel, K. Burger, H.G. Büttner, G.J. Kearley, M. Lehmann and W. Prandl, *ND3-density distribution in orientationally disordered Ni(ND3)(6)Cl-2 observed by means of neutron Laue diffraction.* Journal of Physics-Condensed Matter 12, 8567-8576 (2000).

P. Vorderwisch, S. Hautecler, G J. Kearley and F. Kubanek, *Influence of the guest molecule on the rotational potential for NH3 groups in Hofmann clathrates.* Chemical Physics 261, 157-164 (2000).

M. Plazanet, M.R. Johnson, J.D. Gale, T. Yildirim, G.J. Kearley, M.T. Fernandez-Diaz, D. Sanchez-Portal, E. Artacho, J.M. Soler, P. Ordejon, A. Garcia and H.P. Trommsdorff, *The structure and dynamics of crystalline durene by neutron scattering and numerical modelling using density functional methods.* Chemical Physics 261, 189-203 (2000).

F. Partal, M. Fernandez-Gomez, J.J.Lopez-Gonzalez, A. Navarro and G.J. Kearley, *Vibrational analysis of the inelastic neutron scattering spectrum of pyridine.* Chemical Physics 261, 239-247 (2000).

W.T. Fu, *A neutron powder diffraction study on BaBi0.5Sb0.5O3.* Solid State Communications 116, 461-464 (2000).

R.H. Heffner, J.E. Sonier, D.E. MacLaughlin, G.J. Nieuwenhuys, G. Ehlers, F. Mezei, S.W. Cheong, J.S. Gardner and H. Roder, *Observation of two time scales in the ferromagnetic manganite La1-xCaxMnO3, x approximate to 0.3.* Physical Review Letters 85, 3285-3288 (2000).

A.A. van Well and R. Brinkhof, *Protein adsorption at a static and expanding air-water interface: a neutron reflection study.* Colloids and Surfaces A-Physicochemical and Engineering Aspects 175, 17-21 (2000).

J.R C. van der Maarel, W. Groenewegen, S U. Egelhaaf and A. Laap, *Salt-induced contraction of polyelectrolyte diblock copolymer micelles.* Langmuir 16, 7510-7519 (2000).

F.H.M. van Roon, C. Massobrio, E. de Wolff and S W. De Leeuw, *Structure of liquid GeSe: A first principle study.* Journal of Chemical Physics 113, 5425-5431 (2000).

O. Moze, M. Hofmann and K.H.J. Buschow, *Chromium sublattice magnetic ordering in a compound of the ThCr2Si2 type structure: HoCr2Si2.* Journal of Alloys and Compounds 308, 60-63 (2000).

H. Amitsuka, M. Yokoyama, K. Tenya, T. Sakakibara, K. Kuwahara, M. Sato, N. Metoki, T. Honma, Y. Onuki, S. Kawarazaki, Y. Miyako, S. Ramakrishnan and J.A. Mydosh, *Pressure-induced magnetic phase transition of the 5f electron system URu2Si2.* Journal of the Physical Society of Japan 69, 5-12 (2000).

P. Schobinger-Papamantellos, G. Andre, J. Rodriguez-Carvajal, H.G.M. Duijn and K.H.J. Buschow, *Magnetic ordering in DyMn6-xCrxSn6 (x=1,2) compounds studied by neutron diffraction and magnetic measurements.* Journal of Magnetism and Magnetic Materials 219, 22-32 (2000).

C. Nöldeke, B. Asmussen, W. Press, H. Büttner, G. Kearley, R.E. Lechner and B. Ruffle, *Hydrogen dynamics in [Me(H2O)(6)](ClO4)(2) with Me=Mg, Mn, Fe, Ni, and Zn investigated with quasielastic neutron scattering.* Journal of Chemical Physics 113, 3219-3225 (2000).

M.Th. Rekveldt, *High-resolution diffraction using Larmor precession of polarised neutrons.* European Powder Diffraction, Pts 1 and 2 321-3, 258-263 (2000).

K. Prokes, R.T. Gramsma, Y. Janssen, E. Brück, K.H.J. Buschow and F.R. de Boer, *Magnetic properties of ErFe6Ga6 studied by magnetization and neutron diffraction.* European Physical Journal B 16, 429-434 (2000).

M.J. Knitel, V.R. Bom, P. Dorenbos, C.W.E. van Eijk, I. Berezovskaya and V. Dotsenko, *The feasibility of boron containing phosphors in thermal neutron image plates, in particular the systems M2B5O9X: Eu2+ (M = Ca, Sr, Ba; X = Cl, Br). Part I: simulation of the energy deposition process.* Nuclear Instruments & Methods in Physics Research Section A- Accelerators Spectrometers Detectors and Associated Equipment 449, 578-594 (2000).

M.J. Knitel, B. Hommels, P. Dorenbos, C.W.E. van Eijk, I. Berezovskaya and V. Dotsenko, *The feasibility of boron containing phosphors in thermal neutron image plates, in particular the systems M2B5O9X: Eu2+ (M = Ca, Sr, Ba; X = Cl, Br) Part II: experimental results.* Nuclear Instruments & Methods in Physics Research Section A- Accelerators Spectrometers Detectors and Associated Equipment 449, 595-601 (2000).

A. van Zon, G.J. Bel, B. Mos, P. Verkerk and S.W. De Leeuw, *Structural relaxation in poly(ethylene oxide)-salt solutions.* Computational Materials Science 17, 265-268 (2000).

P. Schobinger-Papamantellos, K.H.J. Buschow, C.H. de Groot, F.R. de Boer and C. Ritter, *Magnetic ordering of the R6Fe13Sn (R = Nd, Pr) compounds studied by neutron diffraction.* Journal of Magnetism and Magnetic Materials 218, 31-41 (2000).

A. Huxley, P. Rodière, D.M. Paul, N.H. van Dijk, R. Cubitt and J. Flouquet, *Realignment of the flux-line lattice by a change in the symmetry of superconductivity in UPt3.* Nature 406, 160-164 (2000).

B. Jerome, E. Cecchetto, N.R. de Souza and A.L. Demirel, *Relaxation dynamics in confined glasses.* Journal de Physique Iv 10, 227-232 (2000).

F.M. Mulder, S.V. Grigoriev, W.H. Kraan and M.Th. Rekveldt, *Observation of polarized neutron interference in spin space.* Europhysics Letters 51, 13-19 (2000).

P.J. van der Zaag, Y. Ijiri, J.A. Borchers, L F. Feiner, R.M. Wolf, J.M. Gaines, R.W. Erwin and M. A. Verheijen, *Difference between blocking and Neel temperatures in the exchange biased Fe3O4/CoO system.* Physical Review Letters 84, 6102-6105 (2000).

A. Yaouanc, P. Dalmas de Réotier, P.C.M. Gubbens, A.M. Mulders and Y. Isikawa, *Zero- and longitudinal-field muon spin depolarization measurements of CeNiSn.* Physica B 289, 28-31 (2000).

P. Schobinger-Papamantellos, N.P. Duong, K.H.J. Buschow, D. Andreica, F.N. Gygax, M. Pinkpank and A. Schenck, *Comparative study of the magnetic properties of TbFe4Al8 and YFe4Al8 compounds.* Physica B 289, 277-281 (2000).

C. Wilkinson, P. Schobinger-Papamantellos, D. Myles, L.D. Tung and K.H.J. Buschow, *On the modulated structure of La2Co1.7: a neutron Laue diffraction study.* Journal of Magnetism and Magnetic Materials 217, 55-64 (2000).

P. Schobinger-Papamantellos, G. Andre, J. Rodriguez-Carvajal, H.G.M. Duijn and K.H.J. Buschow, *Magnetic ordering in TbMn6-xCrxSn6 (x=1, 2) compounds studied by neutron diffraction and magnetic measurements.* Journal of Alloys and Compounds 306, 47-55 (2000).

K. Ayuel and P.F. de Chatel, *Spin and orbital contributions to the magnetic scattering of neutrons.* Physical Review B 61, 15213-15220 (2000).

R.J. Bruls, H.T. Hintzen, R. Metselaar and C.K. Loong, *Anisotropic thermal expansion of MgSiN2 from 10 to 300 K as measured by neutron diffraction.* Journal of Physics and Chemistry of Solids 61, 1285-1293 (2000).

E. Kemner, I.M. de Schepper, G.J. Kearley and U.A. Jayasooriya, *The vibrational spectrum of solid ferrocene by inelastic neutron scattering.* Journal of Chemical Physics 112, 10926-10929 (2000).

B. Mos, P. Verkerk, S. Pouget, A. van Zon, G.J. Bel, S.W. De Leeuw and C.D. Eisenbach, *The dynamics in polyethyleneoxide-alkali iodide complexes investigated by neutron spin-echo spectroscopy and molecular dynamics simulations.* Journal of Chemical Physics 113, 4-7 (2000).

A. Sergi, M. Ferrario, F. Buda and I.R. McDonald, *Structure of phosphorus-selenium glasses: results from ab initio molecular dynamics simulations.* Molecular Physics 98, 701-707 (2000).

S.V. Grigoriev, W.H. Kraan, F.M. Mulder and M.Th. Rekveldt, *Neutron wave interference in experiments with two resonance spin flippers.* Physica B 283, 393-396 (2000).

W. Groenewegen, A. Lapp, S.U. Egelhaaf and J.R.C. van der Maarel, *Counterion distribution in the coronal layer of polyelectrolyte diblock copolymer micelles.* Macromolecules 33, 4080-4086 (2000).

R. Tuinier, C. Holt, P.A. Timmins and K. de Kruif, S*mall-angle neutron scattering of aggregated whey protein colloids with an exocellular polysaccharide.* Journal of Applied Crystallography 33, 540-543 (2000).

W.G. Bouwman, M. van Oossanen, O. Uca, W.H. Kraan and M.Th. Rekveldt, *Development of spin-echo small-angle neutron scattering.* Journal of Applied Crystallography 33, 767-770 (2000).

A. Vrij, *New equation for the light and neutron scattering intensity of fluid mixtures.* Journal of Chemical Physics 112, 9489-9497 (2000).

T. Mizokawa, D.I. Khomskii and G A. Sawatzky, *Spin and charge ordering in self-doped Mott insulators.* Physical Review B 61, 11263-11266 (2000).

W. Groenewegen, S.U. Egelhaaf, A. Lapp and J.R.C. van der Maarel, *Neutron scattering estimates of the effect of charge on the micelle structure in aqueous polyelectrolyte diblock copolymer solutions.* Macromolecules 33, 3283-3293 (2000).

O. Moze, W. Kockelmann, J.P. Liu, F.R. de Boer and K.H.J. Buschow, *Magnetic structure of LaFe10.8Al2.2 and LaFe10.8Al2.2N3 cluster compounds.* Journal of Applied Physics 87, 5284-5286 (2000).

O. Moze, S. Rosenkranz, R. Osborn and K.H J. Buschow, *Magnetic excitations in tetragonal HoCr2Si2.* Journal of Applied Physics 87, 6283-6285 (2000).

I.H. Hagmusa, J.C.P. Klaasse, E. Brück, F.R. de Boer and K.H.J. Buschow, *Magnetic and thermal properties of ErMn4Al8 and ErCr4Al8 in high magnetic fields.* Journal of Applied Physics 87, 6806-6808 (2000).

P.F. Willemse, F.M. Mulder, W. Wei, M.Th. Rekveldt and K.S. Knight, *Residual stress measurements in an SiC continuous fiber reinforced Ti matrix composite.* Scripta Materialia 42, 775-779 (2000).

S. Sullow, S.A.M. Mentink, T.E. Mason, R. Feyerherm, G.J. Nieuwenhuys, A.A. Menovsky and J A. Mydosh, *Disorder to order transition in the magnetic and electronic properties of URh2Ge2 .* Physical Review B 61, 8878-8887 (2000).

N.H. van Dijk, B. Fåk, T. Charvolin, P. Lejay and J.M. Mignot, *Magnetic excitations in heavy-fermion CePd2Si2.* Physical Review B 61, 8922-8931 (2000).

H. Amitsuka, K. Kuwahara, M. Yokoyama, K. Tenya, T. Sakakibara, M. Mihalik and A.A. Menovsky, *Non-Fermi-liquid behavior in R1-xUxRu2Si2 (R = Th, Y and La; x <= 0.07).* Physica B 281, 326-331 (2000).

E.P.K. Currie, M. Wagemaker, M.A. Cohen Stuart and A.A. van Well, *Structure of grafted polymers, investigated with neutron reflectometry.* Physica B 283, 17-21 (2000).

R.W.E. van de Kruijs, H. Fredrikze, M T. Rekveldt, A.A. van Well, Y.V. Nikitenko and V.G. Syromyatnikov, *Polarization analysis of neutron reflectometry on non-collinear magnetic media: polarized neutron reflectometry experiments on a thin cobalt film.* Physica B 283, 189-193 (2000).

B. Toperverg, A. Vorobyev, G. Gordeyev, B. Nickel, W. Donner, H. Dosch and T. Rekveldt, *Reflectivity and off-specular neutron scattering from ferrofluid.* Physica B 283, 203-207 (2000).

M. Wagemaker, F.J.G. Boerboom, H J. Bos and A.A. van Well, *Overflowing cylinder for neutron reflection research at expanding surfaces.* Physica B 283, 278-281 (2000).

A.A. van Well, V.O. de Haan, H. Fredrikze and D. Clemens, *On the use of a multilayer monochromator in neutron reflectometry.* Physica B 283, 282-284 (2000).

W. Sikora, P. Schobinger-Papamantellos and K.H.J. Buschow, *Symmetry analysis of the magnetic ordering in RFe4Al8 (R = La, Ce, Y, Lu and Tb) compounds (II).* Journal of Magnetism and Magnetic Materials 213, 143-156 (2000).

M.Th. Rekveldt, *Novel instrumentation concepts using polarised neutrons.* Physica B 276, 55-58 (2000).

W.G. Bouwman and M.Th. Rekveldt, *Spin-echo small-angle neutron scattering calculations.* Physica B 276, 126-127 (2000).

F.M. Mulder, R. Kreuger, S.V. Grigoriev, W. H. Kraan, M.Th. Rekveldt and A.A. van Well, *Spectrometer combining time-of-flight and Larmor modulation.* Physica B 276, 132-133 (2000).

M. van Oossanen, W.H. Kraan, W.G. Bouwman and M.Th. Rekveldt, *Test of magnetised foils as a polarisation rotator for a spin echo small-angle neutron scattering instrument.* Physica B 276, 134-135 (2000).

O. Uca, W.G. Bouwman, W.H. Kraan and M.Th. Rekveldt, *An analysis of magnetic field inhomogeneities in a spin-echo small-angle neutron scattering instrument.* Physica B 276, 136-137 (2000).

C. Ohms, A.G. Youtsos, A. Bontenbal and F M. Mulder, **Neutron diffraction facilities at the high flux reactor,** Petten. Physica B 276, 160-161 (2000).

D. Visser, R.G. Delaplane and W J.A. Maaskant, *Structural study of the high-temperature phases of the hexagonal perovskite KNiCl3.* Physica B 276, 300-301 (2000).

B. Mos, P. Verkerk, A. van Zon and S.W. De Leeuw, *The dynamics in polyethyleneoxide-alkali iodide complexes in short and intermediate time ranges.* Physica B 276, 351-352 (2000).

S.V. Grigoriev, S.A. Klimko, W.H. Kraan, M T. Rekveldt, A I. Okorokov and V.V. Runov, *Magnetic phase transition in a disordered FeNi alloy: percolative scenario.* Physica B 276, 556-557 (2000).

F. Galli, R. Feyerherm, K. Prokes and G.J. Nieuwenhuys, *Magnetic structure of U2Rh3Si5 in external fields up to 14.5 T.* Physica B 276, 632-633 (2000).

P.J. van der Zaag, L F. Feiner, R.M. Wolf, J.A. Borchers, Y.Y. Ijiri and R.W. Erwin, *The blocking and Neel temperature in exchange-biased Fe3O4/CoO multilayers.* Physica B 276, 638-639 (2000).

W.H. Kraan, M.Th. Rekveldt, V.A. Ul'yanov, L.A. Akselrod, G P. Gordeev, N.K. Pleshanov, V.M. Pusenkov and R. Sellmann, *Magnetic properties of FeCoV/TiZr multilayers studied by 3D neutron depolarisation and SQUID.* Physica B 276, 640-641 (2000).

R.W.E. van de Kruijs, H. Fredrikze and M.Th. Rekveldt, *Polarization analysis of neutron reflectometry on non-magnetic structures deposited on a magnetic layer.* Physica B 276, 642-643 (2000).

P. Svoboda, P. Javorsky, V. Sechovsky and A.A. Menovsky, *Magnetic phase diagram of UNi2Si2 in high fields.* Physica B 276, 686-687 (2000).

A. Vorobiev, B. Toperverg, L. Axelrod, G. Gordeev, V. Kraan, I. Lazebnik, D. Orlova and M.Th. Rekveldt, *Study of the ferrofluid structure in low magnetic field by polarized neutrons.* Physica B 276, 694-695 (2000).

S.E. Offerman, N.H. van Dijk, M.Th. Rekveldt, J. Sietsma and S. van der Zwaag, *3D neutron depolarization experiments on the gamma/alpha phase transformation in steel.* Physica B 276, 868-869 (2000).

V.W J. Verhoeven, F.M. Mulder and I.M. de Schepper, *Influence of Mn by Li substitution on the Jahn-Teller distortion in LiMn2O4.* Physica B 276, 950-951 (2000).

N.A. Babushkina, L.M. Belova, A.N. Taldenkov, V.L. Aksenov, A.M. Balagurov, V.Y. Pomjakushin, D.V. Sheptyakov, O.Y. Gorbenko, A.R. Kaul, K.I. Kugel and D.I. Khomskii, *Isotopically driven transitions in LaPrCaMnO system.* Physica B 280, 323-324 (2000).

M.J. Knitel, P. Dorenbos, C.W.E. van Eijk, B. Plasteig, D. Viana, A. Kahn-Harari and D. Vivien, *Photoluminescence, and scintillation/thermoluminescence yields of several Ce3+ and Eu2+ activated borates.* Nuclear Instruments & Methods in Physics Research Section A- Accelerators Spectrometers Detectors and Associated Equipment 443, 364-374 (2000).

E. Kemner, I.M. de Schepper, A.J.M. Schmets and H. Grimm, *Model independent determination of the elastic incoherent structure factor in neutron scattering experiments.* Nuclear Instruments & Methods in Physics Research Section B- Beam Interactions with Materials and Atoms 160, 544-549 (2000).

S.G.E.T. Velthuis, N.H. van Dijk, M T. Rekveldt, J. Sietsma and S. van der Zwaag, *Field-dependent neutron depolarization study of the ferrite formation in medium-carbon steels.* Acta Materialia 48, 1105-1114 (2000).

R.H.E. van Doorn and A.J. Burggraaf, *Structural aspects of the ionic conductivity of La1-xSrxCoO3- delta.* Solid State Ionics 128, 65-78 (2000).

E. Kemner, I.M. de Schepper, A.J.M. Schmets, H. Grimm, A.R. Overweg and R.A. van Santen, *Molecular motion of ferrocene in a faujasite-type zeolite: A quasielastic neutron scattering study.* Journal of Physical Chemistry B 104, 1560-1562 (2000).

A.M. Mulders, W.H.Kraan, P.C.M. Gubbens, K.H.J. Buschow, N. Stusser and M. Hofmann, *Observation of magnetic nanodomains in TmFeAl.* Journal of Alloys and Compounds 299, 88-93 (2000).

R. Tuinier, J.K.G. Dhont and C.G. De Kruif, *Depletion-induced phase separation of aggregated whey protein colloids by an exocellular polysaccharide.* Langmuir 16, 1497-1507 (2000).

P.A. Rodnyi, V.B. Mikhailik, G.B. Stryganyuk, A.S. Voloshinovskii, C.W.E. van Eijk and G.F. Zimmerer, *Luminescence properties of Ce-doped Cs2LiLaCl6 crystals.* Journal of Luminescence 86, 161-166 (2000).

P. Tils, M. Loewenhaupt, K.H.J. Buschow and R.S. Eccleston, *Exchange fields in Gd-Fe intermetallics studied by inelastic neutron scattering.* Journal of Magnetism and Magnetic Materials 210, 196-202 (2000).

S.J. Hu, O. Tegus, X.Z. Wei, L. Zhang, D.C. Zeng, Z.Y. Liu, F.R. de Boer and K.H.J. Buschow, *Structure and magneto-crystalline anisotropy of Ho-2(Co, Si)(17) compounds.* Acta Physica Sinica 49, 355-360 (2000).

G. Klose and Y.K. Levine, *Membranes of palmitoyloleoylphosphatidylcholine and C12E4 - A lattice model simulation.* Langmuir 16, 671-676 (2000).

F.J. Bermejo, B. Fåk, S.M. Bennington, R. Fernandez-Perea, C. Cabrillo, J. Dawidowski, M.T. Fernandez-Diaz and P. Verkerk, *Microscopic collective dynamics in liquid para-H-2.* Physical Review B 60, 15154-15162 (1999).

S.G.E. te Velthuis, N.H. van Dijk, M.Th. Rekveldt, J. Sietsma and S. van der Zwaag, *A three-dimensional model for the development of the microstructure in steel during slow cooling.* Materials Science and Engineering A-Structural Materials Properties Microstructure and Processing 277, 218-228 (2000).

A. Topp, B.J. Bauer, T.J. Prosa, R. Scherrenberg and E.J. Amis, *Size change of dendrimers in concentrated solution.* Macromolecules 32, 8923-8931 (1999).

E.P.K. Currie, M. Wagemaker, M.A.Cohen Stuart and A.A. van Well, *Structure of monodisperse and bimodal brushes.* Macromolecules 32, 9041-9050 (1999).

S.A. van der Aart, V.W.J. Verhoeven, P. Verkerk and W. van der Lugt, *Structure of liquid caesium-bismuth alloys studied by neutron diffraction.* Journal of Chemical Physics 112, 857-863 (2000).

P. Dalmas de Réotier, A. Yaouanc, P.C.M. Gubbens, C.T. Kaiser, A.M. Mulders, F.N. Gygax, A. Schenck, A. Amato, C. Baines, A. de Visser, R.J. Keizer, P. Bonville, P.J.C. King, *A. Huxley and A. A. Menovsky, Magnetism and superconductivity of UPt3 by muon spin techniques.* Physica B 289, 10-14 (2000).

P. Dalmas de Réotier, A. Yaouanc, R.H. Heffner, J.L. Smith, P.C.M. Gubbens and C.T. Kaiser, *Muon spin relaxation and rotation measurements on single crystals of the heavy-fermion superconductor UBe13.* Physical Review B 61, 6377-6380 (2000).

A. de Visser, M.J. Graf, P. Estrela, A. Amato, C. Baines, D. Andreica, F.N. Gygax and A. Schenck, *Magnetic quantum critical point and superconductivity in UPt3 doped with Pd.* Physical Review Letters 85, 3005-3008 (2000).

C.T. Kaiser, V.W.J. Verhoeven, P.C.M. Gubbens, F.M. Mulder, I. de Schepper, A. Yaouanc, P. Dalmas de Réotier, S.P. Cottrell, E.M. Kelder and J. Schoonman, *Li mobility in the battery cathode material Li- x[Mn1.96Li0.04]O-4 studied by muon-spin relaxation.* Physical Review B 62, R9236-R9239 (2000).

D. E. MacLaughlin, R.H. Heffner, J.E. Sonier, G.J. Nieuwenhuys, R. Chau, M.B. Maple, B. Andraka, G.M. Luke, Y. Fudamoto, Y.J. Uemura, A. Amato and C. Baines, *Muon spill rotation and non-Fermi liquid behavior in UCu4Pd.* Physica B 289, 15-18 (2000).

D.E. MacLaughlin, R.H. Heffner, G.J. Nieuwenhuys, P.C. Canfield, A. Amato, C. Baines, A. Schenck, G.M. Luke, Y. Fudamoto and Y.J. Uemura, *Moon spin relaxation and nonmagnetic Kondo state in PrInAg2.* Physical Review B 61, 555-563 (2000).

G J. Nieuwenhuys, N.G. Patil, H. Noijons, D.G. Tomuta, D.E. MacLaughlin, R.H. Heffner and A. Amato, *Determination of the muon site in URh2Ge2.* Physica B 289, 228-231 (2000).

A. Schenck, F N. Gygax, D. Andreica, M. Pinkpank, G.J. Nieuwenhuys, J. Aarts, S. Freisem, M. Hesselberth, J.A. Mydosh, E. Morenzoni, H. Gluckler, T. Prokscha and A. Amato, *Low-energy muon study of CMR and spin-glass films.* Physica B 289, 331-333 (2000).

C. Ohms, A.G. Youtsos, P. Van der Idsert and T. Timke, *Residual stress measurements in thick structural weldments by means of neutron diffraction.* Ecrs 5: Proceedings of the Fifth European Conference on Residual Stresses 347-3, 658-663 (2000).

G. Bruno, A. Carrado, B. Dunn, F. Fiori, E. Girardin, T. Pirling and F. Rustichelli, *Neutron diffraction measurements for the determination of residual stress in Ti6Al4V welded plates.* Ecrs 5: Proceedings of the Fifth European Conference on Residual Stresses 347-3, 684-689 (2000).

A.M. Mulders, C.T. Kaiser ,P.C.M. Gubbens, A. Amato, F.N. Gygax, M. Pinkpank, P.D. de Reotier, A. Yaouanc, K.H.J. Buschow, F. Kayzel *Positive muon diffusion and localisation sites in GdNi5.* Physica B 289, 451-454 (2000).

D. Visser, A.R. Monteith, H.R. Rønnow, W.J.A. Maaskant. *Acoustic Phonons in the hexagonal perovskite CsNiCl3 around the Γ-point.* Physica B 276-278, 302-305 (2000).

A. Harrison, K.M. Kojima, A.S. wills, Y. Fudamato, M.I. Larkin, G.M. Luke, B. Nachumi, Y.J. Uemera. D.Visser, J.S. Lord. *MUSR studies of the kagome antiferromag-net (H3O)Fe3(OH)6(SO4)2.* Physica B 289-290, 217-220 (2000)

F.J. Bermejo, K. Kinugawa, C. Cabrillo, S.M. Bennington, B. Fåk, M.T. Fernandez-Diaz, P.Verkerk, R Dawidowski, R. Fernandez-Perea. *Quantum effects on liquid dynamics as evidenced by the presence of well-defined collective excitations in liquid para-hydrogen* Phys. Rev. Lett. 84, 5359-5362 (2000).

H.R. Glyde. B. Fåk, N.H. van Dijk, H. Godfrin, K. Guckelsberger, R. Scherm. *Effective mass, spin fluctuations, and zer sound in liquid 3-He.* Phys. Rev. B 61, 1421-1432 (2000).

C.T. Kaiser, V.W.J. Verhoeven, P.C.M. Gubbens, F.M. Mulder, I.M.de Schepper, A. Yaounc, P. Dalmas de Réotier. S.P. Cottrell, E.M. Kelder, J. Schoonman. *Li-mobility in the battery cathode material Lix[Mn1.96Li0.04]O4 studied by muon spin depolarisation.* Phys. Rev. B 64, 9236-9239 (2000).

G.J. Kearley, H.G. Büttner, P.Schiebel. *Lattice-parameter dependence of translational/rotational coupling potentials* Physica B 276-278, 258-259 (2000).

M.B. Line, G.J. Kearley. *An inelastic incoherent neutron scattering study of water in small poared zeolites and other water bearing minerals.* J. Chem. Phys. 112, 9058-9067 (2000).

W. van der Lugt , P. Verkerk. *Anionic superstructures in liquid Zintl-phases.* Plasmas and Ions 3, 59-71 (2000).

V.W.J. Verhoeven, F.M. Mulder, I.M. de Schepper. *Influence of Mn by Li substitution on the Jahn-Teller distortion in LiMn2O4.* Physica B, 276-278, 950-951 (2000).

Author index

A
Álvarez, M. 60
Amato, A. 42

B
Backendorf, C. 8
Balakrishnan, G. 32
Bastiaansen, C. 50
Berghmans, H. 52
Bermejo, F.J. 60
Bessière, A. 18
Blake, G. R. 28
Bodin, A. 58
Bouwman, W.G. 16, 20, 48, 58
Brück, E. 24
Buschow, K.H.J. 42

C
Chung, E.M.L. 32
Cohen Stuart, M.A. 54
Combes, C.M. 18
Cottrell, S.P. 44
Currie, E.P.K. 54

D
Dalmas de Réotier, P. 42, 44
Dijk, N.H. van 56, 58
Dijkstra, B.W. 10
Dorenbos, P. 18

E
Egelhaaf, S.U. 8
Eijk, C.W.E. van 18

F
Feyerherm, R. 26
Fredrikze, H. 22
Fu, W.T. 40

G
Galli, F. 26
Graaf, M.A. de 50
Grigoriev, S.V. 16
Gubbens, P.C.M. 42, 44
Gygax, F.N. 42

H
Haas, J.T.M. de 18
Heenan, R.K. 58
Hendrikx, R.W.A. 26
Hirschberg, K. 46
Hollander, R.W. 18

I
IJdo, D.J.W. 40

J
Jesse, W. 8
Jong, K.P. de 36

K
Kaiser, C.T. 42, 44
Kearley, G.J. 34, 36, 38
Kelder, E.M. 44
Keller, T. 20
Kouwer, P.H.J. 38
Kraan, W.H. 16, 20
Kremer, R.K. 30
Kreuger, R. 18
Krouglov, T.V. 16, 48
Kruglova, O.V. 38
Kruif, C.G. de 6, 12
Kruijs, R.W.E. van de 22
Kulda, J. 30

L
Langridge, S. 22
Lapp, A. 8
Lees, M.R. 32
Loozen, E. 52

M
Maarel, J.R.C. van der 8
McIntyre, G.J. 32
Meijer, B. 46
Menowsky, A.A. 42
Moskvin, E. 30
Mulder, F.M. 34, 36, 38, 44
Mulders, A.M. 42

N

Nies, E.L.F. 50, 52
Nieuwenhuys, G.J. 26
Nugroho, A. 28

O

Offerman, S.E. 56, 58
Ohms, C. 14

P

Palstra, T.T.M. 28
Paul, D.McK. 32
Petukhov, A.V. 48
Picken, S.J. 38
Plakhty, V. P. 30
Pleshanov, N.K. 22
Plomp, J. 16, 48
Pusenkov, V.M. 22

R

Ramzi, A. 46, 50, 52
Rekveldt, M.Th. 16, 20, 22, 48, 56, 58
Ren, Y. 28
Roessli, B. 60

S

Schebetov, A.F. 22
Schenck, A. 42
Schepper, I.M. de 44
Schimmel, H.G. 36
Schoonman, J. 44
Sietsma, J. 56, 58
Sijbesma, R. 46
Snijder, H.J. 10
Stride, J. 38
Syromyatnikov, V.G. 22

T

Thies-Weesie, D.M.E. 48
Tromp, R.H. 6
Tuinier, R. 12

U

Ul'yanov, V.A. 22

V

Verhoeven, V.W.J. 44
Verkerk, P. 60
Visser, D. 30, 32, 40
Vroege, G.J. 48
Vuure, T. van 18

W

Wagemaker, M. 34, 54
Well, A.A. van 34, 54
Wilderen, L.J.G.W. van 56
Wilkinson, C. 32
Wosnitza, J. 30

Y

Yaouanc, A. 42, 44
Youtsos, A.G. 14

Z

Zakharova, S.S. 8
Zwaag, S. van der 56, 58